Peripheral Nerve Regeneration through Collagen Devices with Different In Vivo Degradation Characteristics

by

Brendan A. Harley

S.B., Engineering Sciences
Harvard College, 2000

Submitted to the Department of Mechanical Engineering
in Partial Fulfillment of the Requirements for the Degree of

Master of Science in Mechanical Engineering

at the

Massachusetts Institute of Technology
June 2002

Signature of Author _____
Department of Mechanical Engineering
May 10, 2002

Certified by _____
Ioannis V. Yannas
Professor of Polymer Science and Engineering
Thesis Supervisor

Accepted by _____
Ain A. Sonin
Professor of Mechanical Engineering
Chairman, Department Committee on Graduate Students

Peripheral Nerve Regeneration through Collagen Devices with Different In Vivo Degradation Characteristics

by

Brendan A. Harley

Submitted to the Department of Mechanical Engineering
on May 10, 2002, in Partial Fulfilment of the
Requirements for the Degree of
Master of Science in Mechanical Engineering

ABSTRACT

In the United States more than 200,000 people are treated each year for peripheral nerve injuries that require surgery. Functional recovery of motor and sensory capability is limited following autograft, the most common procedure for peripheral nerve repair. Tubulation repair of a transected peripheral nerve presents an alternative to autograft, but has not yet shown the ability to satisfactorily restore lost function. A variety of degradable and non-degradable materials have been used to fabricate the tubes used to bridge the stumps of a transected nerve, and collagen tubes have been specifically shown to improve the quality of regeneration. The optimal characteristics for the tube have yet to be identified, and a collagen device that can be manipulated and optimized to improve functional peripheral nerve recovery is needed. The overall goal of this thesis was to fabricate and characterize a new collagen tube such that the tube characteristics and their effects on peripheral nerve regeneration can be closely studied, manipulated, and optimized.

Following characterization of a homologous series of collagen tubes, each produced with a different density of crosslinks, the regenerative capacity of each member of the series of tubes was studied to determine the effects of device permeability, crosslink density, and *in vivo* tube degradation rate on peripheral nerve regeneration. It was first observed that the device permeability to cells and large soluble regulators significantly affected the quality of peripheral nerve regeneration, with the more permeable device (pore diameter 80 - 100 μm) showing significantly improved regenerative capacity compared to a semi-permeable tube (pore diameter ~ 22 nm). It was then observed that the quality of nerve regeneration increases with an increase in tube degradation rate; however, after reaching a maximum at an intermediate degradation rate, the quality of nerve regeneration decreases gradually at increasingly higher tube degradation rates. The data indicate that the morphologic properties of the regenerated axons can be optimized by varying the *in vivo* degradation rate of the tube, and that tube degradation has a powerful effect on peripheral nerve regeneration.

Thesis Supervisor: *Ioannis V. Yannas*
Title: *Professor of Polymer Science and Engineering*

Acknowledgments

There are many people who have contributed a great deal toward the completion of this degree. I would first like to thank Prof. Yannas for serving as my research advisor. It has been a pleasure working in your laboratory, and you have taught me a great deal about how to properly organize, conduct, and document research. Your insight has been invaluable in my development as a scientist. In addition, I would like to thank Dr. Spector for his genuine enthusiasm for my research and for the wealth of knowledge he brings to any conversation.

I owe a great deal of gratitude to Dr. Hu-Ping Hsu. Without your surgical talents and graciousness in always taking the extra time to help get the job done, all of the surgeries and this work would not have been possible. You have taught me a great deal, provided wise advice, and become a friend. I would also like to thank Mark Spilker for all of his assistance. When I arrived, Mark laid the groundwork for my research and has been a valuable resource throughout, providing technical assistance, advice, and guidance from someone who has been there.

I would like to thank all of the members, past and present, of the Fiber and Polymers Laboratory at MIT and the Orthopedic Research Laboratory at Brigham and Women's Hospital for being part of this research experience. In particular I would like to thank Ricardo Brau and Julie Rioux for their wealth of knowledge and all the assistance they offered along the way.

On a more personal note, I would like to thank my family for sparking my interest in learning, encouraging my desire to continue developing as an academic, and providing so much support through all the ups and downs. I also want to thank Kathryn and Cormac. You have added so much to my experience, through your support and advice, and especially through your friendship.

Table of Contents

List of Figures

List of Tables

Chapter 1

Introduction and Background

1.1. Clinical Treatment of Peripheral Nerve Injury

Observations in nature show us that lizards have the ability to regenerate their tail when lost and that an earthworm cut in half will develop into two separate, viable earthworms. The mammalian fetus has the ability to regenerate damaged organs and tissue spontaneously through the third trimester of gestation; however, adult mammals do not exhibit spontaneous regeneration of most lost or damaged organs or tissues (Yannas, 2001). The normal mammalian response to acute or chronic trauma is closure of the wound by contraction and formation of scar, a process termed repair. Contraction of the wound and the formation of scar tissue has been studied in severe wounds in the skin (Yannas et al., 1989; Yannas 2001), conjunctiva (Hsu et al., 2000), and in peripheral nerves (Jenq et al., 1985; Chamberlain et al., 1998b; Yannas, 2001).

Severe chronic and acute injuries to the peripheral nervous system result in the formation of a neural scar at the wound site and a loss of functionality at the point of innervation. It has been estimated that each year in the United States, approximately 200,000 patients are treated for peripheral nerve injuries requiring surgical procedures (Madison et al., 1992). If not repaired, peripheral nerve injury will result in partial or total paralysis in the affected tissue.

The most significant peripheral nerve injury treated clinically is the complete transection of the peripheral nerve where the nerve trunk is completely severed, leaving two opposing stumps. Clinical treatment of this injury relies primarily on two methods: direct suturing or autografting techniques. Recovery of functional motor and sensory capability is usually limited following both of these procedures. Direct suturing is employed when the gap between the two opposing stumps is small enough that the two ends can be directly opposed without putting undo tension on the suture line (Madison et al., 1992). Recovery of full motor function is observed in 25% of patients, and recovery of full sensory function is observed in only 3% of patients following direct suturing of median nerve transection (Mackinnon and Dellon, 1988).

When the gap between the two stumps is longer than approximately 5 mm, direct suturing

is no longer possible due to the added tension that is applied to the suture line; the added tension leads to neural degeneration. Autografting is the current clinical treatment for larger gaps. The autograft procedure requires a functional nerve be harvested for implantation between the two opposing stumps. Usually the sural nerve, a sensory nerve in the leg, serves as the autograft tissue. There are a number of difficulties relating to the use of the autograft technique. The first is that the potential autograft tissue is not abundantly available for transplantion. Additionally, the autograft procedure requires the creation of a secondary wound site and the loss of sensory function at that site. Only 20% of patients recovered full motor function while no patients recovered full sensory function following autografting (Mackinnon and Dellon, 1988).

These two clinical treatments for peripheral nerve injury have been largely unsatisfactory for functional nerve recovery; the use of tubular devices presents a third option for exploration. The two transected ends of the nerve are inserted into opposite ends of a tubular implant and sutured in place. This technique allows reattachment of the transected ends of the nerve through the implant for a variety of gap lengths. Tubular implants grant a greater deal of freedom for clinical treatment; the device ends the requirement for autograft tissue as well as the second surgical site. In addition, the device parameters can be readily modified to improve performance.

A search of the literature reveals a wide variety of studies that have examined many different tube parameters and their affect on peripheral nerve regeneration. These parameters include tube dimensions (Ducker and Hayes, 1968), chemical composition (Fields et al., 1989), molecular permeability (Aebischer et al., 1988; Jenq et al., 1987; Li et al., 1990; Li et al., 1992), and degradation characteristics (Aldini et al., 1996; den Dunnen et al., 1993a; Robinson et al., 1991; Tountas et al., 1993). In addition to these physical characteristics of the tube, a number of substrate materials have been used inside the tube as filling to affect performance; materials such as extracellular matrix (ECM) proteins (Bailey et al., 1993; Bryan et al., 1993; Chang et al., 1990; Glasby et al., 1986; Madison et al., 1988; Ohbayashi et al., 1996; Rosen et al., 1990; Yannas et al., 1987; Yoshii et al., 1987), and Schwann cells (Guenard et al., 1992; Morrissey et al., 1991; Kim et al., 1994) have all been implanted for study. While there have been a large number of studies investigating many different device designs, few have been shown to perform as well as the autograft, and none have been able to improve over the autograft for cases where the gap is larger than 10 mm (Chamberlain, 1998a).

1.2. Regeneration versus Repair

There are two potential endpoints of the mammalian healing process following both acute and chronic injuries; these responses are mediated by either regeneration or repair processes. Regeneration results in formation of replacement tissue with structurally and functionally similar to the original tissue, while repair does not. Regeneration is characterized by the replacement of tissue lost through injury by synthesis of the missing tissue in the anatomical wound site. Repair is characterized by synthesis of scar tissue (non-physiological tissue) without replacing the normal tissue lost through injury.

The defect closure rule describes the healing response to injury; healing involves closure of the wound by any of three processes: contraction (C), scar formation (S), and regeneration (R). The closure of the wound site can be represented by the relation: $A_C + A_S + A_R = 100$ ($A_X \equiv$ percentage wound area closed by process X), where these three processes are the only processes that work to close the wound. In adult mammals, both chronic and acute injuries show a common clinical outcome due to repair mechanisms (not regeneration) that act to close the wound through contraction and scar formation ($A_C + A_S = 100$; $A_R = 0$). The ability to regenerate tissues and organs is lost in mammalian adults, with the exception of a certain class of injuries. Spontaneous regeneration (without external stimulation) occurs in some adult mammalian tissues following minor injuries, *i.e.* a small skin scape or a first or second degree burn, while a more severe injury results in repair and scar formation, *i.e.* deep skin wound or third degree burn.

1.3. The Tissue Triad and Response to Injury

Extracellular matrix (ECM) analogs have been studied for use in a variety of tissue engineering related disciplines, and have been used to regenerate tissues lost due to severe injury in cases where the body would normally respond to injury through repair. The mammalian adult responds to severe wounds by contraction of the wound site and repair processes resulting in the formation of scar ($A_C + A_S = 100$; $A_R = 0$), while the mammalian fetus is able to regenerate the lost tissue ($A_C, A_S << A_R$). The causes for transformation of the mammalian response to injury from the fetus to the adult are not known, but adult mammalians are unable to regenerate tissue lost by severe injury (Yannas, 2001). Specific analogs of the ECM have been shown to have a high degree of

bioactivity and a high regenerative capacity for healing lesions in a variety of anatomical sites. Three specific wounds and the appropriate ECM analogs have been studied in our laboratory: the skin and the DRT (dermal regeneration template), peripheral nerves and the NRT (nerve regeneration template), and the conjunctiva and the DRT (the dermal regeneration template was used to test the gross regenerative capacity of the conjunctiva) (Skin: Yannas et al., 1989; Orgill et al., 1996; Yannas, 2001; Nerve: Chang et al., 1990; Yannas, 1995; Chamberlain et al., 1998a, 1998b, 1998c, 2000a, 2000b; Yannas, 2001; Conjunctiva: Hsu et al., 2000).

The adult mammalian skin is made up of three distinct tissue layers (Figure 1.1). The epidermis (epithelial layer) is a non-vascularized, cell-continuous tissue that is exposed to the outside environment. The basement membrane (basal lamina layer) is a very thin acellulr layer of type IV collagen that serves as an attachment layer between the epidermis and the dermis. The dermis (stromal layer) is the vascularized, matrix-continuous tissue that sits between the upper tissue layers of the skin and the underlying musculature. The dermis provides nutrients to the epidermis and basement membranes via capillary loops through rete ridges, villi protruding into the upper tissue layers and that anchors the skin to the underlying submucosal fat layer (Fig. 1.2). The epidermis and the basement membrane layers of the adult mammalian skin have the ability to regenerate spontaneously following injury, provided that the dermal layer remains intact (Fig. 1.3) (Yannas, 2001). However, the dermis of the adult mammal does not regenerate spontaneously following injury; instead contraction of the wound and repair processes result in the formation of scar (Figures 1.3, 1.4) (Billingham and Medawar, 1951; Billingham and Medawar, 1955; Yannas, 2001).

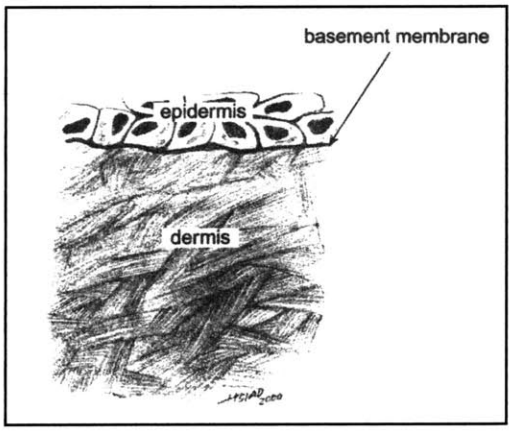

Figure 1.1. Triad of tissue present in mammalian skin (Yannas, 2001).

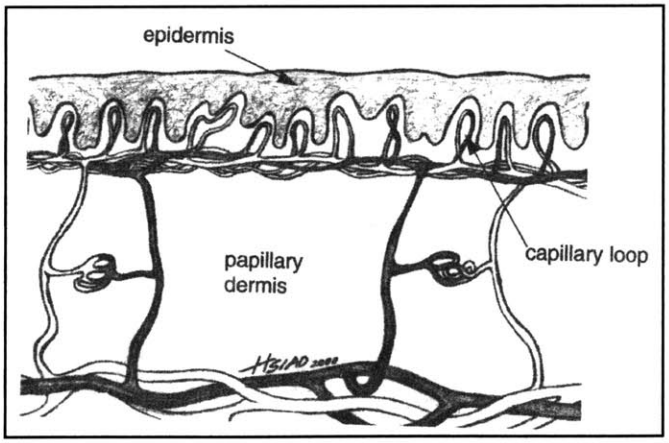

Figure 1.2. Diagram showing the vascular network in the subepidermal region of the skin (Yannas, 2001).

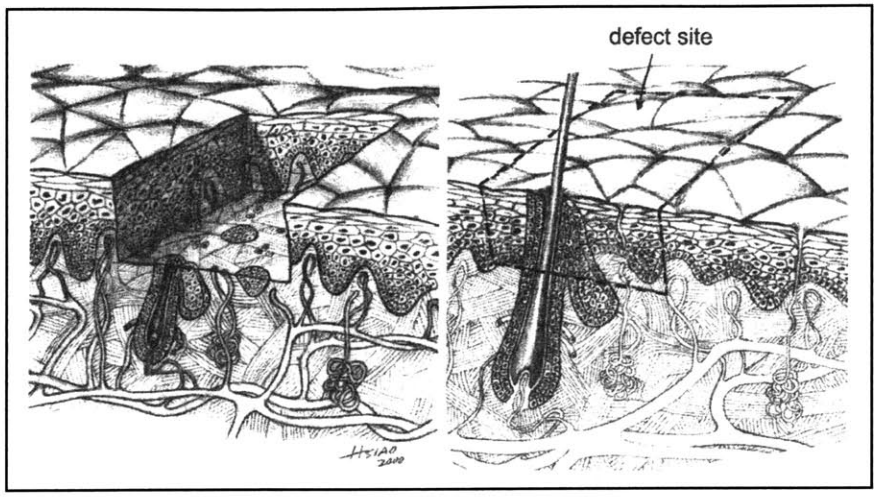

Figure 1.3. The epidermis and basement membrane are regenerative tissues. Spontaneous regeneration of epidermis and basement membrane is observed following injuries that keep the dermis intact (Yannas, 2001).

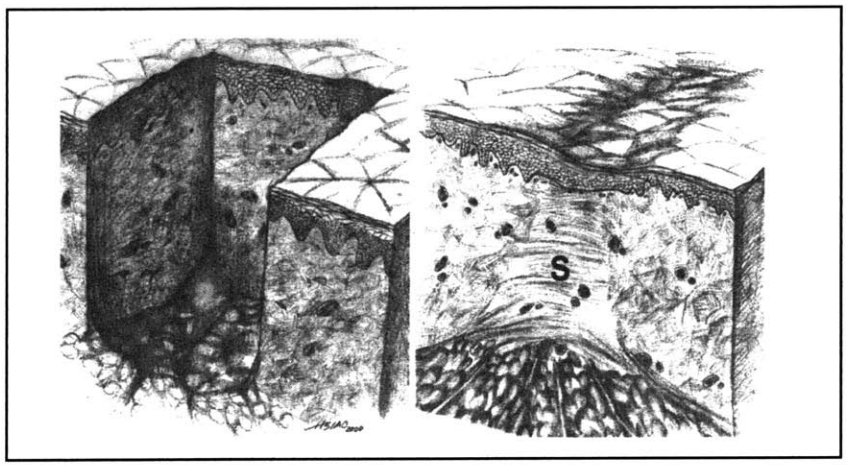

Figure 1.4. The dermis is a non-regenerative tissue. Contraction of the skin wound and repair follows severe injury to epidermis, basement membrane, and dermis (Yannas, 2001).

The mammalian peripheral nervous system consists grossly of three layers of tissue as well. An individual axon is surrounded sequentially by an epithelial, basement membrane, and stromal layer. Schwann cells wrap around the individual axon, forming the myelin sheath that constitutes the epithelial layer of the peripheral nerve. Surrounding the epithelial layer is the basement membrane, the acellular extracellular matrix connecting the myelin sheath and the stromal layer (Figure 1.5). The endoneurium forms the stromal layer of cells and extracellular matrix that surrounds all axons (Martinez-Hernandez, 1998; Yannas, 2001). The myelin sheath and basement

membrane have the ability to regenerate following severe injury (Figure 1.6) (Yannas, 2001). However, the endoneurium, like the dermis, does not regenerate spontaneously following injury. As a result of severe injury, the peripheral nervous system heals by the formation of a neural scar (neuroma) made up of tissue with contractile properties (Chamberlain, 1998a; Yannas, 2001).

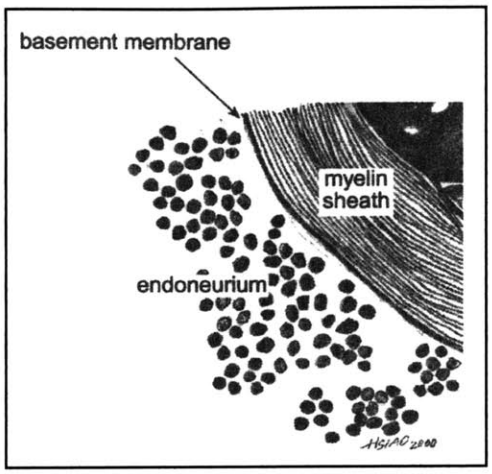

Figure 1.5. Triad of tissues present in mammalian peripheral nerve (Yannas, 2001).

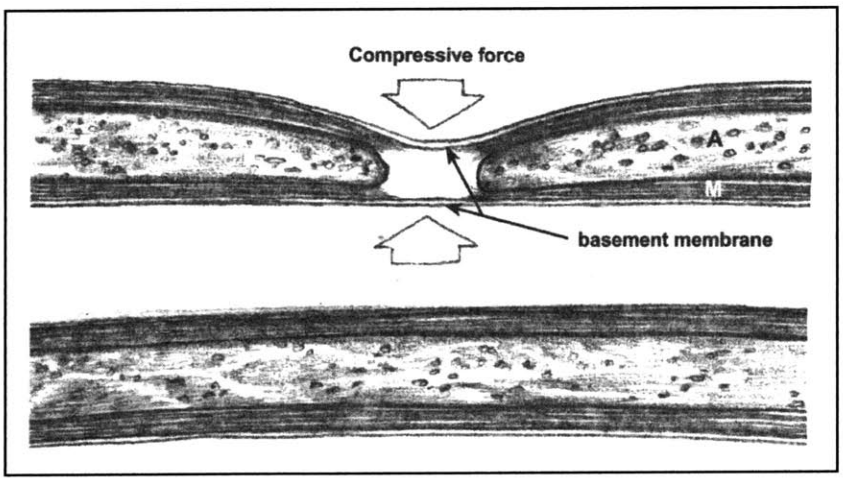

Figure 1.6. Axons and myelin sheath inside a nerve fiber are regenerative. Spontaneous peripheral nerve regeneration can occur following injury to the axoplasm and/or the epithelial layers (Yannas, 2001).

The mammalian conjunctiva is the tissue that covers the inside of the eyelid and consists of three specific tissue layers as well: the conjunctival epithelium, the conjunctival basement membrane layer, and the Substantia Propria. The substantia propria is the conjunctival stromal layer extending from the Tenon's capsule to the surface of the Sclera. Small conjunctival wounds (wound to conjunctival epithelia and basement membrane) result in re-epithelialization of the wound site and regeneration (Geggel, et al., 1984). However, a severe injury to the conjunctival tissue (disruption

of the epithelia, basement membrane, and the Substantia Propria) results in wound site inflammation, followed by re-epithelialization, wound contraction, and the formation of conjunctival fibrous scar (Cordeiro et al., 1997; Hsu et al., 2000). While the epithelia and basement membranes undergo regeneration following injury, the Substantia Propria does not regenerate spontaneously.

A basic pattern can be observed when examining the structure and response to injury of the skin, peripheral nerve, and conjunctiva. There are three tissue layers that are grouped together in sequence in all organs, not only the three briefly mentioned above. They are the epithelia, the basement membrane, and the stroma (Martinez-Hernandez, 1988; Yannas, 2001). This sequence has been termed the tissue triad, and understanding the response of each member of the tissue triad to injury will aid in understanding the process of regeneration and how to induce regeneration in normally non-regenerative tissues. The epithelial layer covers all of the surfaces, tubes, and cavities of the body. The epithelial is completely cellular and is the only member of the tissue triad that does not contain an extracellular matrix (Yannas, 2001). The basement membrane (also termed basal lamina) is a continuous layer of tissue separating the epithelial layer from the stroma. The basement membrane layer is acellular in all tissues; no blood vessels pass through the basement membrane layer from the stroma to the epithelial. The stroma contains connective tissues as well as the blood supply, and is responsible for regulating nutrient uptake to and waste removal from the basement membrane and epithelial. Figure 1.7 provides a basic diagram of the organization of the tissue triad in the adult mammalian system.

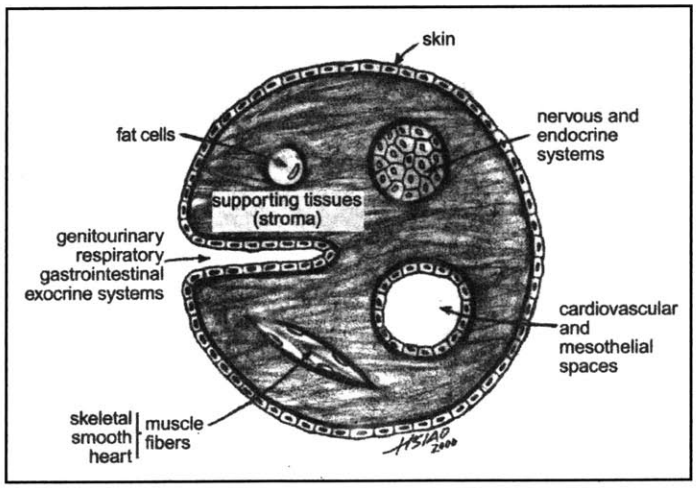

Figure 1.7. General organization of the tissue triad in mammals (Yannas, 2001).

Using the tissue triad as a guide, we can identify similarities between the three tissues previously discussed. In skin, peripheral nerves, and the conjunctiva, there are tissues that spontaneously regenerate (the epithelial and basement membrane) and a tissue that do not spontaneously regenerate (the stroma) in response to injury. A number of studies have observed the regenerative capacity of epithelial tissue (Stenn and Malhotra, 1992; Fu and Gordon, 1997; Yannas, 2001) and the basement membrane (Haber et al., 1985; Fu and Gordon, 1997; Ikeda, 1989) in both the skin and peripheral nerve, while observing the irreversible nature of stromal wound healing (Uitto et al., 1996; Yannas, 2001). The stromal layer has been observed repeatedly to be non-regenerative in the skin (Yannas et al., 1989; Ferdman et al., 1993), peripheral nerves (Yannas, 2001), blood vessels (Stemerman et al., 1977), the lung (Vracko, 1972), the kidney (Oliver, 1953) and the pancreas (Lehv and Fitzgerald, 1968).

It has been suggested that the mechanism for the irreversibility of injury (non-regenerative response) is not dependent on the epithelial tissue at all, and is instead fully dependent on disruption of the stromal architecture (Vracko, 1974; Yannas, 2001). In addition, a parallel between the cell types in the epithelial layers of skin and peripheral nerves (keratinocytes and Schwann cells) has been noted indicating developmental and functional similarities between the tissues (Yannas, 2001)., further supporting the constancy of the tissue triad.

1.4. Active Extracellular Matrix Analogs

Active extracellular matrix (ECM) analogs have been used to induce regeneration of normally non-regenerative tissues following severe injury (Yannas, 2001). The biological activity of the ECM analogs has previously been shown to be significantly affected by the variation of three device parameters: the composition of the matrix, the density of the ligands, and the degradation rate of the material (Yannas, 2001). The composition of the matrix defines the ligands on the ECM available for cell-matrix binding and interactions through integrins on the cell surface. The density of these ligands can be controlled by varying the pore volume fraction and the pore size of the porous ECMs. The pore volume fraction and pore diameter define the surface area of the ECM analog available for cell-ligand interactions, where decreasing the pore diameter and increasing the pore volume fraction increase the total surface area of the pores and the number of ligand binding sites.

The degradation rate of the material defines the length of time that the particular matrix ligands are available for binding. Previous optimization of ECM analogs for skin and nerve regeneration have required specific adjustment of all three criteria to maximize the biological activity of the matrix (Yannas, 2001).

The dermal regeneration template (DRT) has induced the regeneration of dermis (leading to the regeneration of the basement membrane and reepithelialization consistent with normal skin) in full-thickness skin wounds in the guinea pig model (Yannas et al., 1981; Yannas et al., 1982; Yannas et al., 1989; Murphy et al., 1990), the porcine model (Orgill et al., 1996), and in humans (Burke et al., 1981; Yannas et al., 1981; Heimbach et al., 1988; Stern et al., 1990). The DRT can be seeded with keratinocytes to increase the regenerative capacity (Orgill et al., 1996). When unseeded, the DRT induces sequential regeneration of the skin, where the dermis is first regenerated, and then the basement membrane and epithelial layers are regenerated by keratinocytes that migrate from the wound edges over the top of the newly synthesized dermis (Yannas et al., 1989; Yannas, 2001). When seeded with keratinocytes, the DRT displays the ability to simultaneously regenerate the dermal, basement membrane, and epidermal layers, resulting in a faster completion of regeneration (Orgill et al., 1996; Yannas et al., 1989; Yannas, 2001) (Figure 1.8). Immunohistochemistry as well as light scattering analysis of the regenerated tissue has confirmed that regeneration of a tissue consistent with normal mammalian skin has occurred, and that the regenerated tissue maintains the mechanical properties of skin (Yannas et al., 1989; Ferdman et al., 1993; Compton et al., 1996; Yannas, 2001). An unseeded DRT is currently used as a dermal regeneration template for patients who have sustained severe burns (third degree burns) or deep mechanical trauma, that compromises the epidermal, basement membrane, and dermal layers. The DRT actively induces regeneration of partial skin; this partial skin is vascularized, has the same mechanical

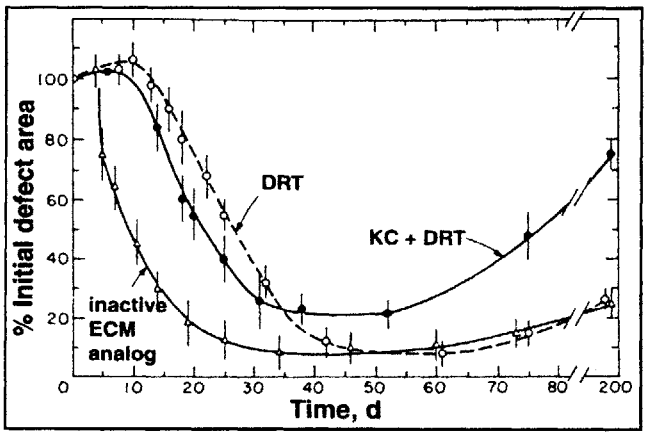

Figure 1.8. Contraction kinetics following grafting of a dermis free defect in the guinea pig. The functional performance of ECM analogs varies considerably between the bioactive (DRT), the inactive, and the cell-seeded matrices. The keratinocyte (KC) seeded matrix resulted in the highest quality of regeneration. (Yannas, 2001).

properties of normal skin, and shows similar tissue morphology to normal skin when analyzed using both histological and immunohistochemical methods, but lacks pores and hair follicles (Heimbach et al., 1988; Yannas, 2001).

The bioactivity of the DRT is closely related to specific physical parameters of the ECM analog. The pore diameter (Figure 1.9) chemical composition, and the pore volume fraction of the ECM analog have all been shown to have a significant affect on the quality of skin regeneration (Yannas, et al., 1989; Yannas, 2001). In addition, the degradation rate of the ECM analog significantly affects the process of skin regeneration (Figure 1.10). There only exists a narrow range of bioactivity for each of these criteria. It has been hypothesized that the ECM analog induces skin

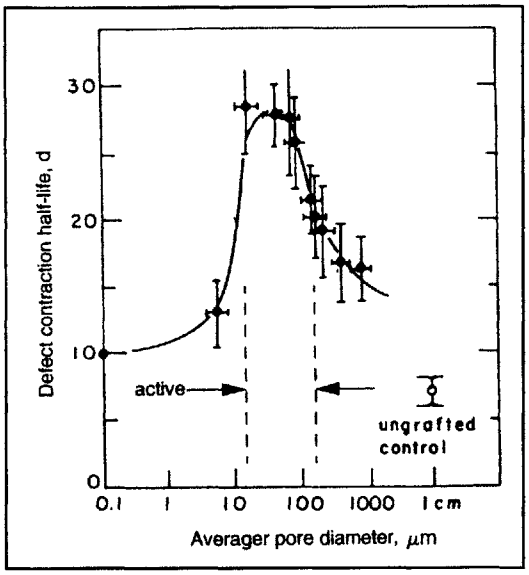

Figure 1.9. Bioactivity of ECM analog variants for skin regeneration with respect to average pore diameter (Yannas, 1989)

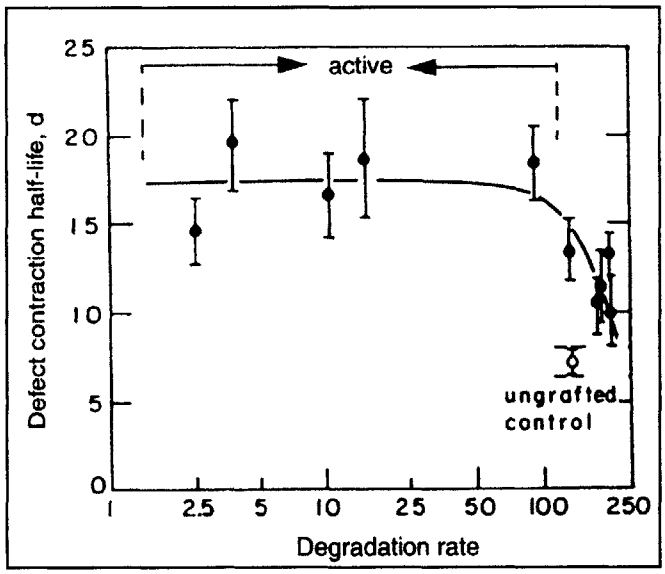

Figure 1.10. Bioactivity of ECM analog variants for skin regeneration with respect to degradation rate (Yannas, 1989)

regeneration by establishing an environment that selectively inhibits wound contraction by preventing the organization of the contractile response that normally closes a skin wound through contraction and scar formation following severe injury (Yannas, 2001). Without wound contraction taking place, the fundamental (fetal) response to injury - regeneration - occurs. An ECM analog with the proper ligands for integrin-mediated cell binding is required for the selective inhibition of contraction, thus defining the chemical composition and pore structure of the bioactive matrix. The contractile response in a skin wound becomes active shortly after the injury and lasts for 2 - 3 weeks,

thus defining the length of time that the ECM analog needs to remain in the wound site and consequently defining the optimal degradation rate. ECM analogs that degrade too rapidly do not retain structural integrity or present the proper ligands long enough to affect the wound healing response, while those that degrade too slowly interfere with the wound healing response and long-term establishment of new skin. Two competing requirements therefore affect skin regeneration: a requirement for an ECM analog to prevent organized contraction of the wound site, and a requirement that the device not interfere with the synthesis of new extracellular matrix and skin.

The nerve regeneration template (NRT) has induced regeneration of a functional peripheral nerve across gaps varying from 10 to 25 mm in the rat sciatic nerve (Yannas et al., 1985; Yannas et al., 1987; Chamberlain, 1998a; Chamberlain et al., 1998b; Chamberlain et al., 1998c; Spilker, 2000). Using this approach, the ECM analog fills the empty lumen of a tubular device made from either silicon (non-degradable polymer) or collagen (degradable polymer). The nerve stumps are inserted into either end of the tube, butted against the ECM analog inside the tube, and sutured into place. The structure of the NRT results in maximal nerve regeneration activity and recovery of functionality in a rat sciatic nerve wound (Chang et al., 1990; Chang and Yannas, 1992). The use of different designs and materials in the tube portion of the device has been studied, and the choice of tube significantly affects the quality of peripheral nerve regeneration (Lundborg et al., 1982; Fields et al., 1989; Archibald et al., 1995; Chamberlain, 1998; Yannas, 2001). The use of an NRT has been tested extensively in the rat sciatic nerve model (Yannas, 2001), but the collagen tubes that have recently been approved by the FDA for clinical use as a treatment for total transection of peripheral nerves do not use a NRT inside of the tube. The functional recovery of a peripheral nerve following injury depends significantly on the structural properties of the extracellular matrix analog, particularly the average pore diameter and the degradation rate (Figure 1.11). ECM analogs that degraded too rapidly or too slowly led to significantly poorer functional recovery (Chang et al., 1990; Yannas, 2001).

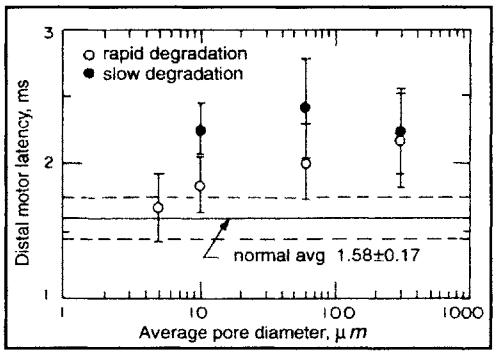

Figure 1.11. Functional performance of collagen-GAG ECM analog for peripheral nerve regeneration varies with degradation rate (Chang and Yannas, 1992).

A dermal regeneration template (DRT) has recently been tested to assess the regenerative capacity of the device in conjunctival wounds. An ECM analog was implanted into a full-thickness wound of the conjunctiva in the New Zealand White Rabbit, and was shown to prevent wound contraction and induce the closure of the wound with tissue that is dissimilar to scar and similar in structure to normal conjunctiva (Hsu et al., 2000; Yannas, 2001). While initial work has shown that an ECM analog can induce closure of a severe defect in a manner consistent with regeneration of conjunctiva future optimization of an ECM analog specifically for the conjunctiva has not occurred.

1.5. Peripheral Nervous System

Conductive and non-conductive tissues in the peripheral nervous system form the structure that transmits afferent (from the periphery) and efferent (to the periphery) signals between the central nervous system (the brain and spinal cord) and the motor and sensory receptors throughout the body. The structure of the conducting portion of a peripheral nerve is divided into three separate sections: the neuron cell body that is located in the ventral gray matter of the spinal cord, the nerve terminal (synapse) located at the distal target organ, and the elongated cylindrical process, the axon (nerve cell process), that connects the cell body and terminal without interruption. A single nerve trunk is made up of thousands of individual axons, surrounded by a series of non-conducting tissues: the epineurium, perineurium, and the endoneurium.

The conducting tissue of the peripheral nerve fibers is comprised of both afferent and efferent axons. Efferent fibers (motor neurons) transfer electrical signals and information from the CNS to the muscles (smooth, skeletal, and cardiac) and glands (Kandel et al., 1991). The individual efferent fibers carry signals from a variety of input sources: CNS neurons carrying signals from the brain, interneurons and motor neurons in the spinal cord, and sensory neurons. The peripheral nerve cell body gathers the input signals, and fires an action potential down the axon to the innervation point (Aidley, 1971; Kandel et al., 1991). The afferent system innervates the sensory organs in the periphery, carrying afferent information from the sensory organs back to the sensory neuron cells bodies located in the dorsal root ganglia. The sensory neuron cell body transmits the signal received from the periphery to the CNS, in particular to other neuron cell bodies such as motor neurons, interneurons in the spinal cord, and spinal cord neurons which take the signal through the CNS to

the brain (Kandel et al., 1991).

The individual axon, efferent or afferent, is comprised of a series of tissue structures: the center core of the axon, or the conducting portion, is made up of cytoplasm containing neurofilaments, microtubules, and other cellular structures, and is termed the axoplasm (Madison et al., 1992). There are two types of axons found in the peripheral nervous system: myelinated and unmyelinated. All peripheral nerve axons, myelinated and unmyelinated, are surrounded by Schwann cells. In a myelinated axon, an individual axon is surrounded by a fatty sheath termed myelin. Electron microscopy has shown that the myelin is formed from closely packed layers of the Schwann cell membrane that are wrapped around the axon to act as an insulator (Geren, 1954; Robertson, 1960; Aidley, 1971). Each Schwann cell is associated with a single axon (Figure 1.12), where the Schwann cell ensheathes a 1 - 2 mm length of the individual axon. The thickness of a myelin sheath varies between axons and depends on the axon diameter. The ratio of axoplasm diameter to total fiber diameter (the axoplasm plus the myelin sheath) is termed the G-Ratio and ranges from 0.65 - 0.8 (Fields et al., 1989). The myelin sheath is interrupted by gaps of approximately 2 μm at points between adjacent Schwann cells along the axial length of the axon, forming the nodes of Ranvier (Figure 1.13) (Kandel et al., 1991). The nodes of Ranvier are responsible for the process of saltatory conduction of action potentials that only occurs in myelinated axons.

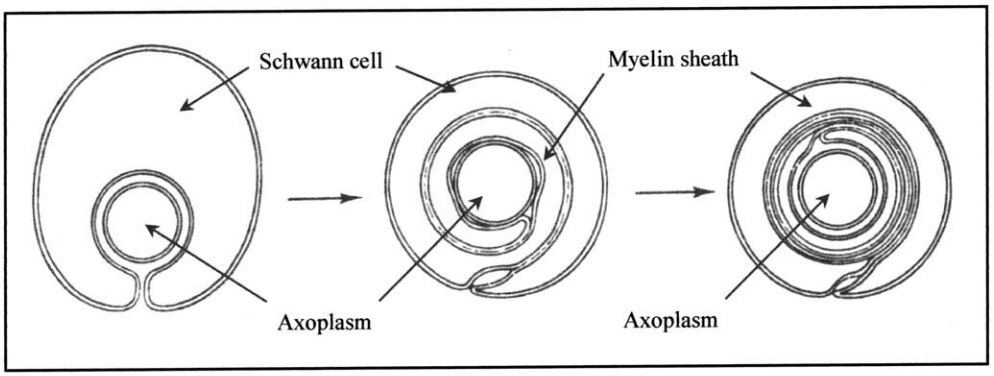

Figure 1.12. Myelination of a motor axon occurs when Schwann cell wraps itself repeatedly around the axon (Robertson, 1960).

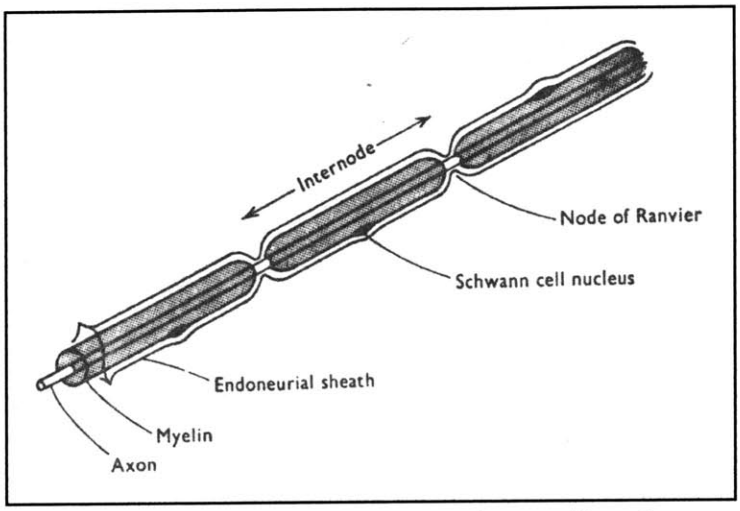

Figure 1.13. Structure of a myelinated nerve fiber: the axon, myelin and endoneurial sheaths, the nodes of Ranvier, and the internode spacing (Aidley, 1971).

The myelin sheath allows for rapid transmission of action potentials without significant attenuation. Unmyelinated axons are not insulated (there is no myelin sheath wrapped around the axon) and do not have the same functional capabilities as myelinated axons. They are smaller in diameter, and many axons are surrounded by a single Schwann cell. In unmyelinated axons, the axon is separated from the Schwann cell by a space of approximately 150 μm that allows for communication between the axon and the extracellular fluid via passages termed mesaxons (Figure 1.14) (Aidley, 1971).

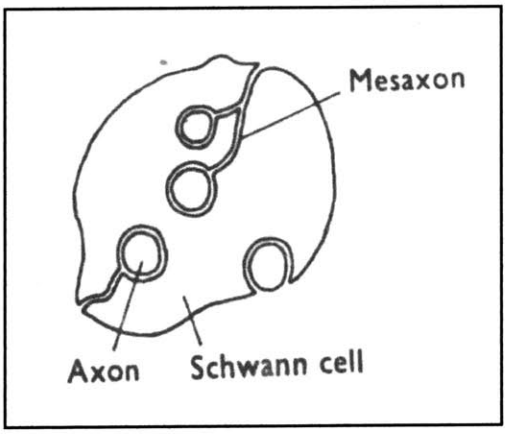

Figure 1.14. Arrangement of Schwann cells around unmyelinated axons (Hodgkin, 1964).

The presence of a myelin sheath significantly affects the electrical properties of the individual axon. The Schwann cell membranes act as resistors and capacitors in series, giving the myelin sheath a much higher transverse resistance and a lower transverse capacitance than the normal cell membrane (Aidley, 1971). As a result, current flow through the axon membrane at the node is greater than that through the membrane at the internode, and conduction of an electrical signal down the axon is discontinuous, or saltatory (Aidley, 1971).

Myelinated axons are responsible for motor activity and some sensory activity. Myelinated axons range in size from 1 to 16 μm in diameter and are grouped in two separate classes: A-fibers and B-fibers. The unmyelinated fibers are known as C-fibers. A-fibers are the largest in diameter, with diameters greater than 6 μm; A-fibers carry impulses from the CNS to the muscles and proprioceptive information from the muscles and joints (i.e. limb position and movement) back to the spinal cord (Strichartz and Covino, 1990). It has been shown that the conduction velocity of a myelinated axon is proportional to axonal size, where the A-fiber has the highest signal conduction velocity (See Figure 1.15 and Tables 1.1 and 1.2) (Hursh, 1939; Rushton, 1951; Arbuthnott et al., 1980).

Fiber Group	Conduction Velocity [m/s]
A α	41
A β	22
A γ	15
B	4
C	0.7

Table 1.1. Typical conduction velocities of fiber groups in bullfrog sciatic nerve. The shaded groups are myelinated motor axons, while the unshaded are unmyelinated sensory axons (Erlanger and Gasser, 1937).

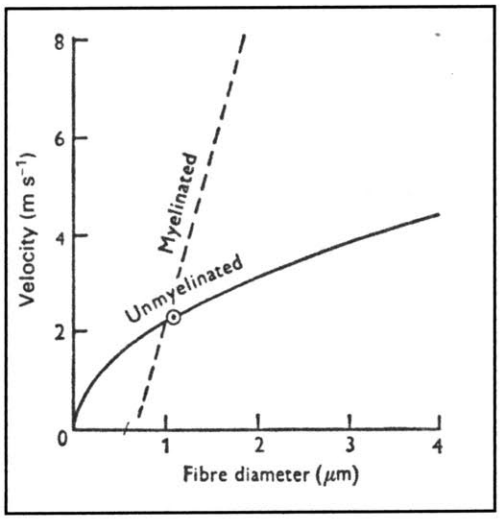

Figure 1.15. Theoretical relationship between axon diameter and conduction velocity for myelinated and unmyelinated axons (Rushton, 1951).

Group	Diameter [μm]	Conduction velocity [m/s]	Sensory Endings
Ia	12-20	72-120	Primary endings on muscle spindles
Ib	12-20	72-120	Golgi tendon organs
II	4-12	24-27	Secondary endings on muscle spindles
III	1-4	6-24	Pressure/Pain receptors
IV	Non-myelinated fiber		Pain

Table 1.2. Relationship between axon diameter, function, and conduction velocity of action potentials. The shaded axons represent motor neurons, while the unshaded groups are sensory neurons (Hunt, 1954).

Myelinated B-fibers are smaller in diameter than A-fibers, usually 1 - 3 μm in diameter and carry predominantly autonomic system information. The smallest of the axons are the unmyelinated C-fibers; C-fibers are responsible for carrying the majority of the sensory signals such as information relating to touch, pain, and temperature (Strichartz and Covino, 1990). C-fibers are usually 0.3 - 1.2 μm in diameter and have very poor conduction properties as a result of a lack of insulation (no myelination) and a high resistance (due to the small fiber diameter). In the rat sciatic nerve there is one myelinated axon for every 1.9-2.5 unmyelinated axons, and in general there are more unmyelinated than myelinated axons in a nerve trunk. The ratio of myelinated to unmyelinated axons is between 1:2 and 1:5 for rats, while humans show a ratio of 1:3 (Lisney, 1989).

The primary function of the axons is the transmission of information in the form of changes in the electrical potential across the cell membrane known as nerve impulses or action potentials. At rest, the environment inside the axon is negatively charged (approximately -60 mV) while the environment outside the axon is positively charged. The electrical performance of the axon is due to changes in the ionic permeability of the axon membrane, particularly permeability to sodium and potassium. Concentration gradients of the ions act as a battery; the Nernst equation determines the electromotive force due to each ion where the electromotive force (E_X) is a function of the concentrations of a particular ion ([X]) inside (i) and outside (o) of the cell membrane:

$$E_X = \frac{RT}{F} \log_e \frac{[X]_o}{[X]_i}$$

In axons at rest, there is a greater concentration of potassium inside the axon (E_K = -75 mV) and a greater concentration of sodium outside of the axon (E_{Na} = +55 mV) (Aidley, 1971), establishing the negative resting potential inside of the axon. The concentrations of ions in the axoplasm is markedly different than the ionic make-up of other physiological tissues and fluids (Table 1.3) (Aidley, 1971); rapid changes in ionic concentrations in the axon precipitate the transmission of an action potential along the length of the axon.

Ion	Axoplasm Concentration [mM]	Blood Concentration [mM]
K	400	20
Na	50	440
Cl	40-150	560
Ca	0.4	10
Mg	10	54

Table 1.3. Ionic concentration in squid axoplasm and blood. The shaded sections are those ions that most significantly affect action potential transmission along an axon. Hodgkin, 1958.

When an impulse is generated for transmission down the axon, the potential of the axon is observed to rise dramatically to approximately +40 mV from the resting potential of -60 mV as a result of sodium and potassium channels opening, allowing the sodium ions to rush into the axon and the potassium ions to rush out of the axon at the site of the action potential (Fig. 1.X) (Aidley, 1971). As the membrane begins to depolarize, more ion channels are recruited, and the depolarization zone propagates along the axon as more channels are affected by the initial local depolarization event. The membrane does not immediately settle back to the resting phase after the action potential. The action potential is followed by a series of overshoots (positive phase, negative after-potential, positive after-potential) as the membrane potential stabilizes back at the resting potential (Figures 1.16 and 1.17). This behavior comes as a result of the rapid changes in the concentrations of sodium and potassium inside and outside the axon. For unmyelinated axons, this behavior can take place along the entire length of the axon, allowing for a smooth conduction of an action potential along the length of the axonal process. The myelin sheath present in myelinated

axons prevents the influx and efflux of ions except at the nodes of Ranvier. There is a very high concentration of sodium and potassium channels at the nodes, ensuring that the amplitude of the signal is not lost. Since the transport of ions can only take place at the nodes of Ranvier, the action potential jumps from one node to the next node in a process termed saltatory conduction (Aidley, 1971; Vander et al., 1990).

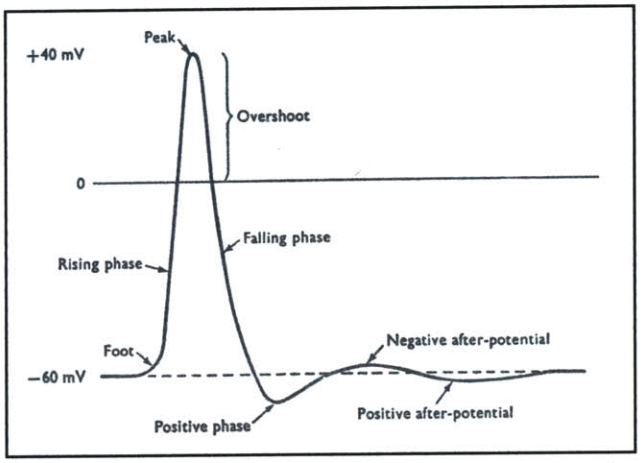

Figure 1.16. Characteristics and nomenclature of axonal action potential (Aidley, 1971).

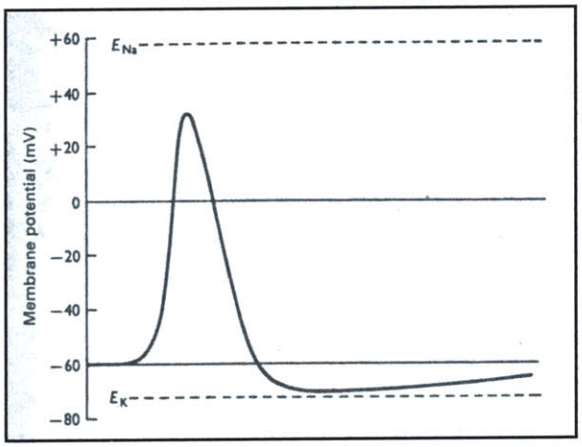

Figure 1.17. Changes in membrane potential during transmission of action potential. Also displayed are the equlibrium potentials of sodium and potassium (Hodgkin and Huxley, 1952).

The final step in the transmission of an action potential from the nerve cell body to the target organ is the synapse at the axon terminus (i.e. a muscle fiber for a motor neuron and the CNS for a sensory neuron) where the action potential must jump across a non-conductive gap. The synapse has been shown by electron microscopy to be a zone where the axon terminus and the target organ are separated by a very small distance, as small as 2 nm, that is known as the gap junction or synaptic cleft (Aidley, 1971). When the action potential reaches the axon terminus, the synapse depolarizes, leading to the release of a chemical neurotransmitter such as acetylcholine in the case of a motor neuron, into the gap junction. Across the gap, transmitter-gated ion channels on the post-synaptic membrane (target organ) bind to the neurotransmitter. This causes the depolarization of the target organ (i.e. muscle fiber), generating the action potential inside the target organ. The transfer of electrical to chemical back to electrical potential allows for efficient and rapid transmission of the action potential across the non-conductive synapse.

A large nerve trunk such as the sciatic nerve is filled with thousands of individual axons, each with different target organs (Chamberlain, 1998a). The complex structure of the individual axon (both myelinated surrounded by myelin sheath and unmyelinated surrounded by Schwann cells) is enclosed within a larger structure of non-conducting tissue. This connective tissue provides additional insulation characteristics in addition to providing support and protection. Immediately surrounding the individual axon is the basement membrane, a thin layer of extracellular matrix (acellular) which serves to connect the Schwann cells with the underlying stroma surrounding the axons. Surrounding the basement membrane is the endoneurium. The endoneurium is composed of loosely packed type III collagen fibers and fibroblasts (Rosen et al., 1983; Madison et al., 1992; Bradley et al., 1998). The endoneurium serves to support individual axonal pathways (Rosen et al., 1983), provides electrical insulation between axons (Bradley et al., 2000), and provides packing between fibers (Thomas and Olsson, 1975).

The axons and endoneurial tissue are packed into fascicles that can range in size from 0.1 to 1 mm in diameter; a single nerve trunk can have many fascicles inside of it, and the fascicles themselves are constantly changing in size and orientation along the length of the nerve trunk (Sunderland, 1990). Each fascicle is surrounded by a sheath of connective tissue known as the perineurium. The perineurium is made up of layers of perineurial cells forming a cell-continuous membrane, surrounded by a basement membrane layer and an outer layer of collagen III fibers. The

perineurium provides strength and elasticity to the individual fascicle and acts as a diffusion barrier (Rosen et al., 1983; Sunderland, 1990; Madison et al., 1992). The fascicles form nerve branches that separate from the main nerve trunk at distal locations, allowing an individual axon to innervate a wider range of anatomical locations.

A loose layer of connective tissue made up of type I collagen fibers and fibroblasts forms the epineurium that surrounds all of the individual fascicles; the epineurial tissue forms the outer surface of the nerve trunk that is seen through gross anatomical observation of a nerve. The epineurium provides protection from compressive trauma and holds the nerve trunk together (Rosen et al., 1983; Madison et al., 1992).

Like the epidermis, the axons do not have an individual blood supply to provide necessary nutrients. Instead, there is a complex system of intrafascicular blood vessels, made up of small capillaries running parallel to the axons, and extrafascicular blood vessels made up of larger blood vessels in the epineurium that provides the proper nutrient environment. Similar to the blood-brain barrier, the characteristics of the intrafascicular blood vessels prevent the transmission of many molecules from the extrafascicular blood vessels, reducing the possibility of neural tissue infection (Madison et al., 1992).

1.6. Requirements for Peripheral Nerve Regeneration

The adult mammalian peripheral nerve fiber can be divided into three major components: the neuron cell body, the axon, and the nerve terminus at the synapse. Regeneration of the peripheral nervous system requires functional reconnection of these three elements. Additionally, the nerve fiber must show the electrophysiological and functional characteristics of the normal nerve. The majority of peripheral nerve injuries involve damage to the axon, rather than damage to the terminus or neuron cell body. Regeneration of a peripheral nerve requires the survival of the neuron cell body following injury, regrowth of functional (i.e. myelinated in the case of motor nerves) axons from the proximal stump of the injured axon through the distal stump, and axonal reconnection with the appropriate terminus to innervate the correct distal target. Damage to a nerve usually does not involve damage to a single axon, so many axons are seen extending across the gap and into the distal stump. Regeneration requires reconnection of the proximal stump with the appropriate distal target

(Madison et al., 1992). For successful regeneration, all three requirements (survival of the neuron cell body, axonal elongation, and reinnervation) must be met. In order to properly design a device to regenerate peripheral nerves, it is first necessary to understand the level of survival seen in the three sections of a PNS axon following transection injury (axotomy).

Previous studies have shown that most of the motor neurons in the spinal cord survive a transection injury to the peripheral nervous system. However, neuron cell death increases in frequency with increasing proximity to the spinal cord (Lisney, 1989; Fu and Gordon, 1997). In addition, it has been reported that the sensory neuron cell bodies are far more susceptible to cell death following axonal injury; as many as 50% of the sensory neuron cell bodies die in response to axotomy (Lisney, 1989; Fu and Gordon, 1997). It is therefore important to standardize the distance from the CNS where an *in vivo* test of regenerative capacity is performed, and important to separate between motor and sensory neurons in assessing recovery of nerve functionality. The design of the surgical protocol used for all of the *in vivo* nerve regeneration studies included in this work has been appropriately standardized and is discussed in Chapter 3 and in Appendix B.

Following axotomy, it is important for the injured axons to grow across the gap that is created from the proximal stump through the injury site, and into the distal stump of the injured nerve. After the axon reconnects with the distal stump, it is important for the regenerated axons to reenter the distal nerve trunk fascicles. The small diameter axons that do bridge the gap must also grow in diameter and regain their myeline sheath in order to become functional. The environment in the wound site is critical in either allowing or preventing extension of the axons across the gap. If the axons are unable to reach the distal stump, regeneration is a failure and there is no recovery of functional capacity. Tubular devices and autografts play a critical role in establishing the correct environment for regeneration and it has been previously shown that the characteristics of the tubular devices critically impact regeneration (Chamberlain, 1998a; Chamberlain, et al., 1998b; Spilker, 2000; Yannas, 2001). It is in this step that tubular devices play the largest role in affecting peripheral nerve regeneration following axotomy.

The formation of functional connections between the axons and the appropriate distal target organs is the final critical requirement for regeneration of peripheral nerves following injury. This requirement necessitates that each regenerating axon reach an appropriate target - sensory or motor - and form a functional synapse with that organ. Motor and sensory axons must not only form a motor

or sensory synapse, respectively, with the correct target, but the connection must be made to the appropriate muscle (for a motor neuron) so that there is a functional connection that can be properly utilized by signals from the brain and in a feedback loop involving afferent and efferent peripheral nerves and interneurons. It has been shown in the literature that sensory neurons have the affinity to innervate sensory targets such as muscle spindles and stretch receptors in the muscle, and that motor neurons have demonstrated an ability to preferentially innervate muscle endpoints (Brushart, 1988; Madison, et al., 1996).

The critical point of regeneration that can be affected by the implantation of tubular devices or the use of an autograft is the reconnection of the proximal and distal stumps of the injured peripheral nerve. I will focus on the development of such devices that causes maximal reconnection of the proximal and distal stumps determined by the morphology of the regenerated axons.

1.7. Peripheral Nerve Injury Wound Models

1.7.1. Animal Model

Many species have been used as experimental models for peripheral nerve injury and regeneration, specifically the rabbit (Fawcett and Keynes, 1986; Whitworth, et al., 1995), cat (Noback et al., 1958; Rosen et al., 1983), mouse (Navarro et al., 1995; Buti et al., 1996), non-human primate (Dellon and Mackinnon, 1988; Archibald et al., 1995), and rat (Fields et al., 1989; Yannas, 2001). The rat is most commonly used due to the less complex nature of the surgical procedure and its high resistance to post-operative infection. A significant problem with the rat that needs to be carefully prevented is autotomy, or self-mutilation of the affected limb. Various rat strains show more or less resistance to autotomy. In severe cases of autotomy, pain and infection of the limb can result, excluding the animal from experimental analysis (Wall et al., 1979). Resistance to autotomy has been studied to identify the species that most effectively resist autotomous behavior; Sprague-Dawley rats exhibited 100% and 71% of autotomy for cases of nerve transection without repair and direct suturing, respectively. Lewis rats displayed no autotomy in the same study (Carr et al., 1992), leading to the adoption of Lewis rat as a primary animal model for peripheral nerve regeneration research, and the only animal model used for this thesis research.

1.7.2. Injury Mode and Wound Site

Severe wound injury comes as a result of injury to both the axon and the surrounding myelin sheath and endoneurium; the primary modes for severe peripheral nerve injury are either compression of the nerve tissue or total transection of the nerve trunk. The compression wound model has been studied by a number of investigators (Haftek and Thomas, 1968; Walker et al., 1994; Korompilias et al., 1999), but this wound model does not easily lend itself to the use of a tubular device, and allows the connective and support tissue surrounding the axons to remain grossly intact. In addition, regeneration is difficult to quantify because axons found in the wound site could exist as a result of regeneration or could be fibers that were not damaged by the crush. Transection imitates a severe class of clinical injury where the continuity between the proximal and distal ends of the nerve is lost. The transection wound lends itself to the use of tubular devices to study regeneration, and all axons found in the wound site can be definitively identified as regenerated fibers. As a result, transection of the nerve is the most common wound model used for the study of peripheral nerve injury (Fields et al., 1989; Fu and Gordon, 1997; Yannas, 2001); sciatic nerve transection was used in this research due to the ability to create a reproducible wound and due to the large body of research involving sciatic nerve transection that can be found in the literature for purposes of comparison.

Nerve transection wound studies in the rat are most commonly performed on the sciatic nerve due to the ease of surgical manipulation and due to a well-defined pattern of innervation following injury (Spilker, 2000). The sciatic nerve is transected at the mid-point of the nerve, with either end placed into a tubular device. The finite length of the sciatic nerve trunk and the femur restrict the dimensions of the gap and device that can be tested. For single leg anastomosis, the gap lengths that can be studied range between 2 and 15 mm (Fields, et al., 1989). To study gap lengths greater than 15 mm, a cross-anastomosis wound model is used where the proximal stump of the transected sciatic nerve in one leg is bridged over the back of the animal to the distal stump of the other transected sciatic nerve (Lundborg, et al, 1982; Yannas, et al., 1987; Spilker, 2000; Yannas, 2001).

1.8. Tubular Devices for Peripheral Nerve Regeneration

1.8.1. Tube-Assisted Regeneration

Tubulation repair of peripheral nerve injury has been studied for over 100 years and presents an alternative to the autograft procedure used commonly as a clinical treatment for nerve injury (Fields et al., 1989). The two ends of a transected nerve are inserted into either end of a tube; the tube is involved with a number of functions relevant for peripheral nerve regeneration. Following total transection of a nerve, regeneration is not observed in the absence of a tubular device if the gap between the two cut ends is more than a few millimeters (Yannas, 2001). A tube is sufficient to induce regeneration (Chamberlain, 1998a; Yannas, 2001); however the physical parameters of the tube significantly affect the kinetics and quality of regeneration (Chamberlain, 1998a; Yannas, 2001). It has been suggested that tubulation can induce peripheral nerve regeneration by a number of mechanisms: (1) accumulation of regulatory factors and cells from both the proximal and distal stumps in the wound site, (2) isolation of the wound site from the pathological processes in the surrounding connective tissue, and (3) providing directional guidance for the cells and axons elongating across the gap (Madison et al., 1992).

1.8.2. Tube Materials

A wide variety of natural and synthetic polymers have been used to create tubular devices for peripheral nerve regeneration (Archibald et al., 1991; Robinson et al., 1991; den Dunnen et al., 1993a; Tountas et al., 1993; Archibald et al., 1995; Aldini et al., 1996; Chamberlain, 1998a; Yannas, 2001). The earliest devices were composed of naturally occurring materials that could be easily harvested and implanted in the wound site, specifically bone, dura, perineurium, and bone. More recent devices have relied upon nondegradable, synthetic materials such as stainless steel, rayon, silicone, tantalum, and magnesium, as well as degradable synthetic (polyester, polyglactin, and polylactate) and natural (collagen, laminin, fibronectin) polymers (Fields et al., 1989).

Silicone tubes have been widely used by many investigators, and there is a substantial amount of data available in the literature about silicone tube mediated regeneration (Ducker and Hayes, 1968; Lundborg et al., 1982; Williams et al., 1983; Jenq and Coggeshall, 1984; Williams et al., 1985; Fields and Ellisman, 1986; LeBeau et al., 1988; Williams et al., 1993; Buti et al., 1996). The

silicone tube creates a nondegradable wound chamber that has been tested in human models (Lundborg et al., 1991; Janecka et al., 1993) and more recently has been used as a well characterized experimental standard.

Components of the extracellular matrix, specifically collagen, fibronectin, and laminin, have been shown to enhance the regeneration of axons across tubulated nerve gaps (Madison et al., 1985; Glasby et al., 1986; Yoshii et al., 1987; Madison et al., 1988; Gulati et al., 1988; Chang et al., 1990; Rosen et al., 1990; Chang and Yannas, 1992; Bailey et al., 1993; Bryan et al., 1993; Ohbayashi, et al., 1996; Chamberlain, 1998b; Yannas, 2001). Collagen tubes in particular have been observed to induce the highest quality of regeneration, as characterized by both morphological and electrophysiological methods (Archibald et al., 1995; Chamberlain, 1998a; Yannas, 2001). Collagen contains inherent binding sites (ligands) for attachment and migration of various cell types, and can be manufactured in such a way that the tube walls contains small pores that will allow passage of soluble agents such as molecules and proteins, as well as cells. In addition to the use of a tube, specific ECM analogs have been shown to significantly increase the maximal gap that can be bridged by axonal tissue (Yannas et al., 1987; Madison et al., 1988; Yannas, 2001), the speed of axonal bridging (Madison et al., 1985; Ohbayashi et al., 1996), and the quality of regeneration (Chang et al., 1990; Chang and Yannas, 1992; Chamberlain, 1998a; Yannas, 2001).

1.8.3. Critical Length for Peripheral Nerve Regeneration

The critical length (L_c) is a single quantitative parameter that describes the effectiveness of a given nerve repair device in promoting nerve regeneration across gaps of various lengths (Spilker, 2000; Yannas, 2001). The critical gap length can be identified by a curve-fitting exercise from experimental data describing percent reinnervation at the gap midpoint versus gap length. Reinnervation was assessed as presence or absence of axons at the gap midpoint, with percent reinnervation calculated using innervation information collected from all animals treated with the same device. The percent reinnervation data is fitted with the sigmoidal equation, and (L_c) calculated as the length where the particular device results in 50% reinnervation (and 50% formation of neuroma). Percent reinnervation is observed to drop abruptly with only a small increase in the gap length (Lundborg, et al., 1982), leading to the calculation of a fairly reliable L_c value for 50% reinnervation.

Reinnervation at the midpoint is used rather than reinnervation at the distal stump because elongating axons reach the midpoint at earlier times than the distal stump, and thus the midpoint data reach a time-independent state before the distal stump data. For the rat sciatic nerve model, the midpoint data reached an apparent time-independent state after 6 weeks, and when fitted to the sigmoidal equation, yielded the critical length (Spilker, 2000).

The experimental data indicate that for the silicone tube device, the value of L_c reached a plateau with time before 9 weeks, and the standard error was less than 5 percent of the critical gap length value observed in two different peripheral nerve repair models (sciatic nerve single-leg and cross-anastomosis). The data suggest that statistically significant differences between the silicone tube device and a collagen-based device (the CG device) are obtainable during short-term (12-week) studies (Spilker, 2000). The critical length has a use as a quantitative measure of effectiveness of various nerve repair devices (Yannas, 2001); devices can be effectively ranked to compare regenerative capacity using the critical length.

1.9. Permeable and Degradable Devices for Regeneration

The permeability of a tubular device used to induce peripheral nerve regeneration following injury has the potential to significantly affect the mechanism of regeneration. Previous observations have identified a contractile response to peripheral nerve injury, and that the process of neuroma formation is marked by contraction and cellular expression of α-Smooth Muscle Actin (SMA) (Chamberlain, 1998a). It has been hypothesized that SMA mediated contraction leads to the formation of a contractile capsule surrounding the nerve stumps and the regenerating axons, and that this capsule attempts to close the wound site: the pressure cuff hypothesis. SMA expression, however, is also observed in the case of successful peripheral nerve regeneration, and the thickness of the contractile capsule surrounding the regenerated nerve trunk has been observed to vary significantly between a silicone versus a collagen tube, and vary significantly between a regenerated and a normal nerve (Chamberlain, 1998a). Non-permeable tubes, such as the silicone tube, exhibit a significantly smaller critical length and significantly inferior regeneration, while also exhibiting increased contraction. Device permeability may play a significant role in reducing the contractile response following peripheral nerve injury. It is hypothesized that device permeability can affect the

environment of the wound by allowing binding or migration of the contractile cells, mediated by cell-mediated binding to the ECM.

Device permeability can come as a result of increased porosity or increased degradation rate, and the affects of both will be studied in this thesis. Both of these variations will lead to devices that allow increased movement of cells and soluble regulators into and out of the wound site.

1.10. Research Aim

The work for this thesis involved three distinct studies with specific objectives:

1. Fabricate and characterize a high solids-content collagen tube for peripheral nerve regeneration
2. Evaluate the regenerative capacity of the new high solids-content collagen tube and the effect of implant crosslink density on the quality of peripheral nerve regeneration.
3. Determine the percent remaining mass and degradation characteristics of the collagen tubes, and determine the affect of device degradation rate on the process of peripheral nerve regeneration.

Six different device groups were tested over a 15 mm gap length (3-6 animals per device group). Type I collagen tubes (high solids-content tubes) fabricated in the laboratory and crosslinked using variable dehydrothermal and EDAC treatments, as well as the Integra LifeSciences NeuraGen collagen tube were tested without and ECM analog filling inside the tube over a 15 mm gap, single anastomosis wound model. Implantation into a rat sciatic nerve was used for an experimental model, and an untreated gap was used as the control. The collagen tubes was fabricated using type I collagen and a molding technique for the high solids-content mixture, followed by freeze-drying. The biodegradability of these devices varied with crosslinking density (intensity of crosslinking treatment), and a variable amount of tube was retained over the 9 week implantation period for the different devices. The Integra NeuraGen devices were also biodegradable, but degraded at a much lower rate so the devices retained their structural integrity and the majority of their mass over the

length of the experiment, as has been previously observed by others (Chamberlain, 1998; Archibald, et al., 1995).

Following nine weeks of implantation, the regenerated tissue and any remaining devices were retrieved for histological and immunohistochemical evaluation. Quantitative measurements of the remaining mass of the tubular devices and of the regenerated myelinated axons (number, diameter, density, N-Ratio) were made through analysis of digital images of regenerate cross-section.

The experimental findings are organized into Chapters 2-4 according to the objective of each study. Each chapter is a self-contained unit, expressing a particular introduction, materials and methods, results, and discussion. In Chapter 2, I present the fabrication and characterization of a new class of collagen devices for peripheral nerve regeneration: the high solids-content collagen tube. In Chapter 3, I present the work studying the effects of the high solids-content collagen tubes on the quality of peripheral nerve regeneration compared to the NeuraGen (control) over a long gap (15 mm) at an early time point (9 weeks). In Chapter 4, I will present work studying the effects of implant degradation on the quality of regeneration. In Chapter 5, I restate the conclusions from each chapter in order to bring together this body of work, highlight and make particular conclusions based upon the sum of all data, and make recommendations for future study and experimentation based upon this work.

Chapter 2

Fabrication and Characterization of High Solids-Content Collagen Tubes

2.1. Introduction

2.1.1. Tubular Devices For Peripheral Nerve Regeneration

Fabrication of an effective tubular device for regeneration of peripheral nerves requires an understanding of why tubulation works. Without the use of a tube, regeneration of the sciatic nerve is not observed when the gap between the abstracted stumps is greater than 5 mm (Chamberlain, 1998a; Yannas, 2001). A number of hypotheses have been extended to explain the use of tubulation in peripheral nerve regeneration. The contact guidance hypothesis suggests that regenerating axons require physical guidance by the appropriate solid-like surface that is present inside the tube, while the neurotrophic hypothesis suggests that a concentration gradient of growth factors inside the closed chamber signals the axons to elongate is required for regeneration of axons (Yannas, 2001). The contraction hypothesis has its origin in the study of regeneration in other tissues (Yannas, et al., 1989; Yannas, 2001), but has been used to explain regeneration of peripheral nerves by tubulation, or more specifically the formation of neuroma in cases of nonregeneration, stating that regeneration is possible when wound site contraction is inhibited. The discovery of a dermal regeneration template in our laboratory initiated research in the field of fabricating active extracellular matrices (AECM), porous structures made using a collagen-glycosaminoglycan copolymer with the specific characteristics necessary to maximize inhibition of contraction in a given organ. It has been hypothesized that introducing a highly porous scaffold disturbs the intercellular organization process that normally takes place in an open wound and that leads to contraction; cells lose the ability to coordinate a contractile response when the ECM analog is introduced, allowing regeneration - the fundamental fetal response - to occur (Yannas, 2001). A number of different materials and device configurations have been tested, showing that the tube characteristics play a significant role in determining the success of regeneration (Chamberlain, 1998a; Spilker, 2000; Yannas, 2001).

2.1.2. Permeable Devices for Peripheral Nerve Regeneration

It has been suggested in the literature (Li et al., 1992; Aebischer et al., 1998; Chamberlain, 1998a; Yannas, 2001) that permeability of the tube to cells or regulators has a significant affect on peripheral nerve regenerative capacity. Permeability can be incorporated into a tubular device either directly or indirectly.

Direct introduction of permeability can be made by varying the average pore size of the tube during fabrication. Non-porous devices, or those devices with a very small pore diameter, do not allow cells or soluble regulators to pass into or out of the wound site. As the pore size gets larger, the device becomes permeable to increasingly larger proteins and soluble regulators, and eventually becomes permeable to cells when the pore size becomes larger than about 10 μm, the approximate length scale of a cell. Cellular permeability is strongly affected by the porous structure, specifically the pore diameter and the pore volume fraction. For a given pore volume fraction, larger pores present a lower surface area (area of pore walls) for cellular binding compared to smaller diameter pores. As the pore diameter gets smaller, more cells can attach to and migrate through the matrix. This trend has a lower limit, however, due to the dimensions of the cell because the cells need to be able to fit into the pore spaces. Direct regulation of device permeability can be obtained by varying either the pore volume fraction or the pore diameter.

Indirect introduction of permeability can be accomplished by varying the crosslink density of otherwise identical devices. Increasing the density of crosslinks decreases the *in vivo* degradation rate of the device (Yannas et al., 1975); degradation introduces artificial permeability by breaking down the tube walls. Device degradation is not a uniform process; degradation develops local areas of relative permeability, and these areas of permeability grow over time. The areas increase in dimension and porosity, serving to increase the total device permeability.

Both of these techniques (direct and indirect introduction of permeability) have been utilized in this study to fabricate homologous series of five experimental devices that are identical except for a variable crosslink density.

2.1.3. Tube Manufacturing Methods

A variety of manufacturing techniques have been employed to fabricate tubular devices for peripheral nerve injury. The earliest tubular devices utilized naturally occurring structures and

materials from the body such as bone, dura, and blood vessels (Fields et al., 1989). More recently synthetic (*i.e.* polylactic acid, silicon) and natural (*i.e.* collagen, laminin) polymers have been used to fabricate devices what have shown regenerative capacities similar to autograft over a relatively small gap length (< 10 mm) in rats (Yannas, 2001). In particular, collagen tubes have been shown to provide an improved environment for regeneration. Two specific techniques that have been previously used to produce collagen tubes are cross flow filtration molding and spinning extrusion.

Cross flow filtration molding was an early method developed in this laboratory to fabricate complicated geometries (not only tubes) from dispersions of solids (*i.e.* collagen) in a liquid medium. In this device (U.S. Patent No. 4252759) the dispersion medium was pumped though a central mold with porous walls; under a high enough hydrostatic pressure the liquid portion of the dispersion is pumped through the porous walls, leaving the solid phase deposited on the walls of the mold to form the shaped article. This technique provided the ability to form complicated shapes or simple tubular geometries using a variety of solid-liquid dispersions.

A second method for producing collagen tubes is currently used by Integra Lifesciences Corp. to fabricate the FDA-approved NeuraGen device that is used as a control for these experiments. This process involves spinning of collagen fibers around a central mandrel (mold) to form the tubular geometry. The spinning technique results in a very small pore diameter (22nm; Li et al., 1992; Chamberlain, 1998a), where a cross-sectional micrograph of the device walls show layers of collagen wrapped around the inner core of the device. Even with such small pores, cellular infiltration of the tube walls is eventually observed, most likely due to local degradation effects.

The collagen tubes used for peripheral nerve regeneration have previously been supplied to our laboratory by outside manufacturing agents (i.e. Integra LifeSciences Corp. NeuraGen device). Previous experience in fabricating active ECM analogs for skin and nerve regeneration has shown that device bioactivity is closely linked to the characteristics (materials, pore volume fraction, pore diameter, degradation rate) of the matrix. In order to more closely study the individual effects of all of these criteria, it is necessary to develop a technique for fabricating high solids-content collagen tubes that will be used in the series of *in vivo* regeneration experiments studying peripheral nerve regeneration that is presented in this thesis. This new fabrication technique will call upon the wide range of technical knowledge in the literature and our laboratory for producing polymeric tubes.

2.1.4. Project Goal

Previous *in vivo* experiments testing the peripheral nerve regenerative capacity of a number of different devices have identified a collagen tube with improved regenerative capabilities (Chamberlain, 1998a). This device (NeuraGen, Integra Lifesciences Corp., Plainsboro, NJ) currently has FDA approval for clinical use to treat peripheral nerve injuries. Since this device is manufactured as part of a standardized industrial process, it is not convenient to control the degradation rate during the period when healing processes are most active (< 1 year post-injury). In order to gain more control over specific tube characteristics, a high solids-content collagen tube was developed in this laboratory to serve as an alternative peripheral nerve regeneration device. The fabrication of this device allows the degradation characteristics of the device to be varied so that it can degrade slowly (device half like on the order of years), rapidly (half life on the order of days), or over a range of intermediate speeds (half life on the order of weeks or months).

The objective of this study was to fabricate and characterize a new high solids-content (5% w/w) collagen tube with variable degradation rate for peripheral nerve regeneration. The chemical composition of the tube was chosen based upon previous work identifying type I collagen tubes as having superior regenerative capabilities (Archibald, et al., 1995; Chamberlain, 1998a; Yannas, 2001). Both the pore structure and the swelling characteristics of the new tube were assayed. The pore structure of the tube is important for establishing a density of ligands available for integrin-mediated cell binding, contraction, and motility and for defining initial device permeability. These cell processes have been identified to play a significant role in skin regeneration (Yannas et al., 1989; Orgill et al., 1996) and may have an effect on peripheral nerve regeneration (Madison et al., 1988; Madison et al., 1992; Chamberlain, 1998a; Yannas, 2001). Serial sections of the the tubes were generated and the corresponding images of pore structure were analyzed using a linear intercept method to calculate the tube pore size and to determine the homogeneity of the porous structure throughout the device. The swelling characteristics of the collagen tube were calculated to be used as a method to assay the relative crosslinking densities of the porous collagen devices (Methods described in Yannas et al., 1967; Yannas, 1975). The devices with lower crosslink densities have collagen fibers less tightly bound together and show a more rapid in vivo degradation rate; when hydrated, these matrices swell (measures by a mass or volumetric change) to a much greater degree than those devices with higher crosslinking densities. In addition, information pertaining to the

swollen density of the collagen tubes was used to ascertain the remaining mass of the collagen tube following surgical implantation (to be detailed in Chapter 4).

Characterization of the high solids-content collagen tubes is critical for interpreting the regenerative capacity of the device. The bioactivity of peripheral nerve regeneration templates is closely linked to specific physical characteristics - chemical composition, pore size, pore volume fraction, and degradation rate - so it is important to understand these characteristics in order to compare this new device and its regenerative capacity with those previously tested.

2.2. Materials and Methods

2.2.1. Fabrication of a High Solids-Content Collagen Tube

The high solids-content collagen tube was fabricated from microfibrillar, type I bovine tendon collagen (Integra LifeSciences Corp., Plainsboro, NJ). Detailed description of the procedure used for molding and fabricating these tubes is included in Appendix A. There are many technologies that have been utilized to fabricate tubes, mold collagen, and form high solids-content polymers. Briefly, fabrication of the high solids-content tubes involved the use of a mandrel (a solid insert) surrounded by a suspension of collagen polymer within an outer mold to form the tubular geometry. The process used to fabricate the new class of high solids-content collagen tubes in this study is a synthesis of four techniques.

The first step in the process is the formation of a high solids-content collagen suspension (5% w/w collagen solution). Previous work has shown that collagen denatures when heated in solution at temperatures above 30°C (Yannas, 2001), so temperature-induced solubility is not viable to create this mixture. A plasticating extruder was used to form the high solid suspension (Rodriguez, 1996). To fabricate the tubes, a high solids-content mixture of collagen, distilled water, and glacial acetic acid was mixed using a plasticating extruder; the extruder was formed by connecting two syringes together with a luer-lock coupling, and mechanical power was used to mix the collagen and liquid. After forming the suspension, the collagen fibers swelled in the acetic environment. The process of pumping the suspension between the two syringes allowed a higher solid content than with conventional mixing techniques. The high solids-content was critical for formation of a device with

enough rigidity to act as an experimental chamber in the wound site. The mixture was degassed via centrifugation to remove the air content introduced by the plasticating extruder. Vacuum degassing is not possible due to the high viscosity of the mixture, and sonication-mediated degassing would damage the collagen fibers. High-speed centrifugation drives the air content to the surface of the collagen mixture,

The second step of the process took the degassed collagen mixture, now a highly viscous liquid, formed in the first step, and molded it into the desired tubular shape using a two-leaf aluminum and Teflon mold. Thin wire inserts were covered with Teflon tubing and used as the mandrels to be inserted into the center of the mold to form the tubular geometry. The final dimensions of the mold channel with mandrel were outer diameter 3.0 mm and inner diameter 1.5 mm, dimensions that were consistent with the animal model to be used and with previous tubes used for nerve regeneration (NeuraGen device: I.D. 1.5 mm, O.D. 2.8 mm). The viscous collagen mixture was injected directly from the syringe (no needle is used) into the individual channels formed by the mold. The Teflon mandrel was then inserted into the center of each mold channel to form the tubular geometry.

The third step in tube fabrication was the freezing process. The completed molds were placed in a freeze-drier at a temperature of –40°C, and the molds were frozen for 1 hour. After freezing, the mold was split open, and the newly frozen tubes and their mandrels were removed in one piece from the mold and kept at –40°C in the freeze-drier. The freezing process allows the tubes to be removed from the molds in a solid state without damage.

The fourth and final step of the fabrication process was lyophilization. Sublimation of ice crystals by freeze-drying (Pressure: <100 mTorr, Temperature: 0°C, Time: 17 hours) transformed the frozen collagen injection into a highly porous collagen tube surrounding the Teflon mandrel. After sublimation, the mandrel could be easily removed, leaving a porous collagen (5% w/w) tube. These tubes were then crosslinked using a variety of techniques enumerated in section 2.2.3.

2.2.2. Peripheral Nerve Devices

Two types of collagen tubes were used throughout this experiment: a control device and the high solid-content collagen tube fabricated in this laboratory (See Section 2.2.1). The control device (NeuraGen Integra Lifesciences Corp., Plainsboro, NJ) was a tube fabricated from type I bovine

tendon collagen, with an inner diameter of 1.5 mm. The walls of this device were approximately 650 μm thick and were comprised of collagen fibers loosely packed and in a laminar arrangement. The tube walls have a maximum pore diameter of 22 nm, making the tubes initially impermeable to cells or proteins with a molecular weight greater than 540 kD, either into or out of the inner chamber (Li et al., 1992). The fabrication techniques have previously been described (Archibald et al., 195; Li et al., 1990; Li et al., 1992). Following production, the collagen tubes were crosslinked by gaseous formaldehyde in order to decrease the *in vivo* degradation rate following implantation (Archibald et al., 1995).

The high solid-content collagen tubes (5% type I bovine microfibrillar collagen, by mass) had an inner diameter of 1.5 mm and a wall thickness of 500 μm. These tubes were crosslinked for varying periods of time using either dehydrothermal or chemical (1 ethyl 3-(3dimenthyl aminopropyl)carbodiimide) methods. Dehydrothermal treatment of the devices established conditions that also yielded a sterilized collagen tube; those not treated dehydrothermally were sterilized using 100% ethanol.

The collagen-glycosaminoglycan (CG) matrix copolymer was prepared as previously described to fabricate the nerve regeneration template (NRT), a tube filling (Chang et al., 190; Loree et al., 1989; Yannas et al., 1989). Previous fabrication methods did not allow for consistent, efficient production of CG copolymers with consistency, and a variation of the original protocol has been developed and is presented here. The new technique is treated in greater detail in Appendix A.

The CG copolymer is comprised of three major components: microfibrillar, type I collagen from bovine tendon (Integra Lifesciences Corp., Plainsboro, NJ), the glycosaminoglycan chondroitin-6-sulfate (Sigma Chemical Corp., St. Louis, MO), and 0.05M acetic acid (Catalog No. UN2789, Mallinckrodt Chemical Corp.). These components are combined to result in a 98/2 w/w relationship between collagen and GAG that results in a pore volume fraction of 0.95 for the finalized ECM analog. To prepare this matrix, the CG suspension was injected into silicone processing tubes (O.D.: 1.96 mm, I..D. 1.47 mm, Catalog No. 60-011-06, Dow Corning Silastic Q7-4750, Helix Medical Corp.) that were inserted inside of a PVC sleeve (O.D.: 0.25", I.D.: 0.125", Catalog No. 60985-512, VWR Scientific) to create the mold structure. Previous fabrication techniques dictated that the slurry was injected directly into the tube though a knot tied in the tubing, giving little room for error; the new technique employed a locking luer adapter fitting with a re-

sealable membrane linked to the silicone tube. This technique allows for easier injection of the slurry without the danger of damaging the silicone molding tube.

The pressurized silicone-PVC molds were frozen under conditions that resulted in the production of an ECM analog that has previously been reported as having the optimal pore characteristics for inducing regeneration of peripheral nerves, as measured through a 40 week electrophysiological study of nerve regeneration (Chang et al., 1990; Chang and Yannas, 1992). The silicone processing tube with frozen CG slurry is removed from the PVC jacket; freeze-drying results in the production of an ECM analog inside the silicone tube with axially oriented pore channels with an average pore diameter of 35 μm (Chamberlain, 1998a). The ECM analog was then dehydrothermally crosslinked at 105°C for 24 hours under vacuum (Fisher Isotemp 201 Vacuum Oven, Fisher Scientific, Boston, MA) in order to both crosslink and sterilize the devices. The ECM analog has an *in vivo* half-life of approximately 4 - 6 weeks in the rat sciatic nerve (Chamberlain, 1998a).

While the ECM analog devices were not used in this preliminary experiment, the development of an improved method for analog fabrication greatly increased the speed and consistency of the fabrication process. The NRT is a critical component of the complete device for peripheral nerve regeneration, and will be included in future experiments.

2.2.3. Collagen Tube Crosslinking Treatment

In order to test the effects of device degradation on the quality of nerve regeneration, a homologous series of devices must be fabricated, varying only in density of crosslinks (and hence degradation rate). A chemical and a physical crosslinking technique was utilized to achieve a gradient in crosslinking density across five separate experimental groups. Specifically dehydrothermal (physical) and carbodiimide (EDAC, chemical) crosslinking was utilized. 1-ethyl-3-(3-dimethylaminopropyl)carbodiimide acts as a chemical crosslinking agent by catalyzing the crosslinking reaction between collagen fibers (Lee, et al., 2001). Carbodiimide crosslinking has an advantage over other chemical crosslinking methods because the carbodiimide is not bound to the collagen during the crosslinking process. When a chemical compound is physically bound to the collagen during crosslinking, the chemical species remains bound to the matrix and is released in the wound site as the ECM analog degrades, with cytotoxic affects. Acting only as a catalyst, the

cytotoxic carbodiimide can be completely rinsed from the matrix following the crosslinking reaction. Carbodiimide crosslinking also has an advantage over other chemical crosslinking agents because it forms collagen-collagen and collagen-GAG crosslinks, while many other chemical crosslinkers form only collagen-collagen crosslinks (resulting in a lower density of crosslinks compared to EDAC). The carbodiimide crosslinking results in a high density of crosslinks (Lee et al., 2001) and low degradation rate.

Dehydrothermal crosslinking of a collagen matrix does not involve introduction of a physical agent. DHT treatment shifts the equilibrium point of the crosslinking reaction; a product of collagen crosslinking is water. By exposing the matrix to an environment of high heat while under a vacuum, evaporation pulls water from the matrix, the crosslinking reaction is driven towards the product as dictated by Le Châtelier's Principle. Varying the temperature and length of exposure to a dehydrothermal environment (vacuum, high temperature) affects the strength of crosslinking, where higher temperatures and longer exposures create a greater density of crosslinks (Yannas et al., 1967; Yannas, 1972; Yannas et al., 1975; Yannas et al., 1980). Dehydrothermal crosslinking took place in a vacuum oven (Fisher Isotemp 201 Vacuum Oven, Fisher Scientific, Boston, MA) at a variety of temperature set-points and durations (Table 2.1). Dehydrothermal treatment leaves the helical structure of collagen intact, provided that the moisture content of collagen prior to heat treatment is less than 1% by weight (Yannas, 1972; Yannas et al., 1989). Dehydrothermal crosslinking (a physical process) is not as powerful a crosslinking agent as carbodiimide crosslinking (a chemical process), and results in a much lower density of crosslinks and a faster expected degradation rate in the wound site.

Using both carbodiimide (EDAC) and dehydrothermal (DHT) treatments of varying magnitude, a series of five experimental groups with different crosslink densities were created (Table 2.1). A control device, an FDA approved, type I collagen tube crosslinked via gaseous formaldehyde and supplied by Integra LifeSciences Corporation (NeuraGen, tube), was also tested. The formaldeyde crosslinking treatment results in a tube with a large crosslink density (Chamberlain, 1998a; Yannas, 2001). It is not possible to directly compare the crosslink densities of the DHT, EDAC, and Integra device, but the EDAC and Integra devices were much more strongly crosslinked. A crosslink density gradient was established between the experimental devices due to the DHT and EDAC treatments:

Device Identifier	Tube Type	Crosslinking Technique
A	5% Collagen	Not crosslinked
B	5% Collagen	DHT crosslinked, 90°C, 24 hours
C	5% Collagen	DHT crosslinked, 90°C, 48 hours
D	5% Collagen	DHT crosslinked, 120°C, 48 hours
E	5% Collagen	EDAC crosslinked, Room temperature, 24 hours
F	Integra	Gaseous formaldehyde

Table 2.1. Crosslinking treatment and intensity for each of the experimental group (A - E) and for the control (F).

Expected Density of Crosslinks: A < B < C < D < E, F

Expected Device Degradation Rate: A > B > C > D > E, F

The dehydrothermal treatment serves additionally to sterilize the collagen matrices prior to implantation due to the high temperature and vacuum. Experimental devices that were not dehydrothermally crosslinked (devices A and E) were sterilized with 100% ethanol prior to implantation. The NeuraGen tube (Integra Lifesciences Corp.) was sterilized prior to shipment and was kept sterile at all times. All devices were stored in a desiccator (in sterile containers) after fabrication in order to prevent rehydration of the collagen matrix.

2.2.4. Pore Size Analysis Procedures

Following fabrication and crosslinking of the high solids-content collagen tube, the average pore size for each device was determined. A 3-5 mm length of each type of tube was embedded in JB-4 resin (Catalog No.00221-1, Polysciences, Inc., Warrington, PA). Sections suitable for morphological analysis were prepared by sectioning the JB-4 samples at a 5 μm thickness and mounting the sections onto standard slides. Histological sections were taken from two levels of the tube, near the inner surface and near the outer surface of the tube wall, in order to determine whether there was a uniform pore structure through the thickness of the tube wall. The sections were stained with Aniline Blue stain (Catalog No.02570, Polysciences, Inc., Warrington, PA) to enhance the contrast between the pore and collagen strut, and then mounted and cover slipped using Cytoseal 60 mounting medium (Cat. No. 8310-16, Stephens Scientific, Kalamazoo, MI). The stained sections

were digitized into a personal computer using a digital camera (Digital camera and interface, Catalog No. DEI-750, Optronics Engineering, Goleta, CA) connected to a light microscope (Nikon E600 with Nikon objectives). Low magnification (4x, 10x) images were captured using Snappy (Video Capture Board) in order to obtain an image with a large number of pores for analysis.

The pore structure (average pore diameter) for each digital image was determined using the public domain software Scion Image, downloadable at www.scioncorp.com. Pore size was determined using a linear intercept method. This technique and the linear intercept macro used are further specified in Appendix A. The average distance between collagen struts along on a series of lines at 5° intervals emanating from the center of the image was determined; from these measurements, the linear intercept coefficients and a best-fit ellipse describing average pore orientation were calculated. The average pore diameter and the pore aspect ratio were calculated for each matrix using the relations described in Appendix A. The average pore diameter for each matrix was compared to determine if crosslinking technique had an affect on the pore structure and the pore structure near the outer and inner surfaces was compared within each tube to determine the level of structural homology.

2.2.5. Swelling Characteristics Analysis Procedure

Both the kinetics of swelling and the steady-state swelling ratios of the devices are significant for characterizing the crosslinked collagen tubes. Device swelling can be defined as either mass change, which is more common, or a volume change of the porous matrix when it is exposed to a liquid environment, such as a wound site. A qualitative understanding of relative crosslink density can be determined using an assay of matrix swelling. This qualitative comparison is possible because collagen matrix crosslinking plays a significant role in swelling; collagen matrices with high density crosslinks swell less than those with a much lower density of crosslinks (Yannas et al., 1967). Besides its use as a tool to help understand the relative crosslink density of all of the device, the swelling ratio of the devices is also important in understanding the degradation of the collagen tubes *in vivo*.

Following animal sacrifice, the regenerated tissue (nerve) and any remaining tube were removed together. The remaining device and the regenerated tissue had become interconnected, so it is impossible to remove the tube to determine its remaining mass and degradation characteristics.

It is possible, through optical methods (See Chapter 4 Methods Section and Appendix A for a more detailed protocol), to determine the volume of the remaining tube. The collagen tube swells once implanted in the wound site (liquid environment at 37°C), so the volume of the remaining tube that is optically observed is in terms of a swollen volume. The remaining mass of the devices and the degradation characteristics of each tube are determined using the swelling characteristics of each separate device (swollen collagen densities) and a measurement of the volume of the tube remaining after the nine week implantation period.

An assay of device swelling was performed on each of the five experimental devices and on the Integra NeuraGen control. Prior to the start of the swelling test, the mass and volume of each tested tube were determined. The tubes were individually labeled and kept separately for the entire experiment to track changes in individual tubes. Sections of the tube were placed into a simulated wound site environment; the devices were placed into sterile Phosphate Buffered Saline (Catalog No. P-3813, Sigma Aldrich Chemical Corp., St. Louis, MO) and kept at 37°C in a cell-culture incubator (Revco Ultima, VWR Scientific). During the course of the experiment, measurements of the swollen volume and mass of each tube were taken at 24 hour intervals for a period of 9 days in order to get an understanding of the kinetics of the swelling process. Once the kinetics were understood, an experiment involving a larger sample size was performed to obtain more accurate swollen mass and volume characteristics of each crosslink variant; the swollen density of each device was calculated and used for the histological analysis of the devices removed following *in vivo* nerve regeneration. In addition, the swelling ratio results were also used to help characterize the relative density of crosslinks in each device.

2.2.6. Statistical Analysis Methods

One-factor analyses of variance (ANOVA) were performed to determine the effect of crosslinking treatment on either average tube pore diameter or tube swelling characteristics. If ANOVA indicated statistical significance, subsequent multiple comparisons were made using the Fisher's PLSD post-hoc test to determine the differences between pairs of experimental groups. Students' T-test was used to determine if there were changes in pore structure within individual groups by comparing the pore diameters calculations made of the pore structures near the inner and outer diameter of the tube. The StatView v5.0 (SAS Institute, Inc.) statistical software package was

used for all analyses. For all analyses, statistical significance was accepted for $p < 0.05$. All graphical representations are presented with the average value of the data for each group ± the standard error of the means (SEM).

2.3. Results

2.3.1. Collagen Tube Pore Size

The porous structure of the ECM analogs significantly affects the quality of regeneration of peripheral nerves and skin (Yannas et al., 1989; Chang et al., 1990; Yannas, 2001). Determining the pore structure of the collagen tubes, specifically the pore diameter is critical to understanding the experimental results observed for peripheral nerve regeneration. The pore diameter is essential to define the specific surface area of the matrix, important in influencing integrin-mediated cell binding and interaction with the matrix. Fabrication of the collagen tube involves nucleation of ice crystals followed by sublimation to produce a random porous structure; freeze-drying has been previously been observed to result in pore structures that are uniform throughout the matrix (Yannas et al., 1989). Crosslinking increases the structural stability and the resistance to degradation of the matrix, but crosslinking does not affect the pore diameter of the ECM. The average pore diameter was determined for three of the experimental devices (B, C, and D) as well as for the Integra NeuraGen control. The pore size analysis of device E was not performed because this chemical crosslinking procedure hydrates the matrix, a process that change the pore geometry due to the swelling of collagen fibers. The non-crosslinked tube was also not initially analyzed because a range of DHT crosslinked devices were being tested. If a significant variation in pore size was noted between the three DHT variants tested, the pore diameter of device A was to be analyzed.

Device Pore Characterization

The average pore diameter of the Integra NeuraGen devices is 22 nm and is uniform throughout the tube wall; this pore structure has pores small enough such that the tubes remain impermeable to proteins with a molecular weight greater than 540 kDa (Li et al., 1992). This size is significant in affecting cellular processes following peripheral nerve injury; the average cell, 10

μm in diameter, is able to interact with only the surface of the tube, and cellular migration into or out of the wound site is impossible until *in vivo* degradation increases device permeability. Sublimation-based technologies for the fabrication of porous ECM analogs (skin, peripheral nerve) have resulted in pore sizes significantly larger than that of the Integra device (Yannas et al., 1989;Chang et al., 1990; Yannas, 2001). These pores (30 - 500 μm) have previously been shown to allow cellular binding inside of the porous material and allow for cellular migration through the matrix (Yannas, 2001).

The average pore diameter was determined for three experimental devices (B, C, D) in order to determine the pore characteristics of the new collagen tube design, and to determine whether there was any variation in pore structure as a result of crosslinking treatment. The three devices had average pore diameters ranging from 76 - 102 μm (Table 2.2, Figure 2.1). One-way ANOVA revealed a significant difference between groups ($p < 0.0001$), and post-hoc testing revealed a significant difference between the mean pore diameter of each of the devices ($p < 0.0001$).

Device	Pore Diameter (Mean ± SEM)
B	86.7 ± 0.9
C	101.9 ± 1.6
D	76.5 ± 1.3

Table 2.2. Average pore size for three experimental devices (DHT crosslinking).

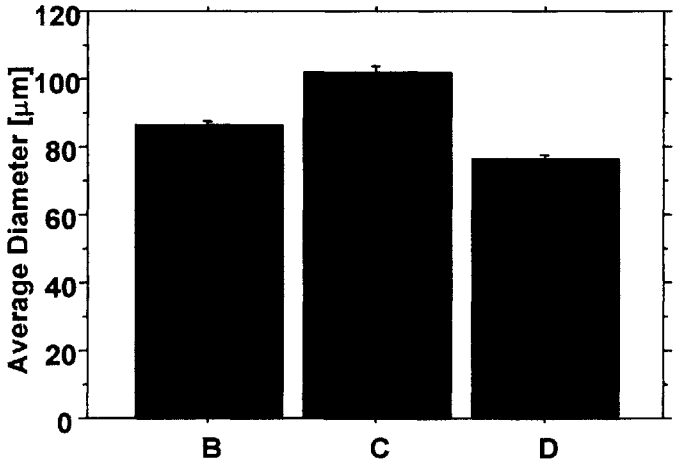

Figure 2.1. Average pore size (Mean ± SEM) for three variants of the experimental device (variable DHT crosslinking treatment, increasing from left to right).

Post-hoc testing revealed significant differences between each group; however, these devices were part of a homologous series of devices, where the tubes were identical except for their crosslinking treatment. No observable pattern existed between the groups to correlate the variation in pore structure to the changing crosslink density, suggesting that the devices in fact had similar

pore diameters and any variation observed is a result of the linear intercept method used for determining pore diameter. The pores in this matrix are not perfectly spherical nor entirely separate from all other pores and the structure is such that the pores are randomly oriented and interconnected, making accurate, statistical comparison of the data very difficult.

Homogeneity of High-Solids Content Collagen Tube

The homogeneity of the collagen tube is also important. For this experiment, a series of cross-sectional images of tube sections taken from near the inner and outer tube walls were analyzed to determine whether there was a variation in the average pore diameter between the inner and outer tube wall. Such a change could have a significant affect on the direction of cellular migration. The pore structure of the device (80 - 100 μm) is large enough to allow cellular attachment to the pore walls and cellular migration through the device by integrin-mediated binding and migration. However, if the device has significantly larger pores along the inner tube wall compared to the outer tube wall, more cells will be able to start migrating out of the device at an earlier time, and vice versa for devices with larger pore diameters near that outer tube wall. The effects of variable cell migration have yet to be observed, but it is a significant factor to keep in mind.

The Integra NeuraGen device shows a consistent pore diameter throughout the tube wall as a result of the spinning fabrication methods. The pore structure near the tube outer wall (O.D.) and near the inner tube wall (I.D.) was compared for the individual devices (B, C, and D) in particular and for the entire population of high solids-content collagen tubes as a whole (O.D. vs. I.D.). This last comparison was made as a result of the conclusion that while the pore diameters of the three devices showed statistically significant difference, these differences were likely caused by slight variations in the fabrication of the devices or due to the linear intercept method itself, and difference in pore diameter were not a description of differences caused by the crosslinking density. The results are presented below for the comparison of the pore size at the inner and outer tube wall for all devices (Table 2.3, Figure 2.2) and then for the comparison of inner versus outer tube wall for all the devices together (Table 2,4, Figure 2.3).

Device	Location	Pore Size (Mean ± SEM)
B	OD	87.5 ± 1.1
B	ID	85.9 ± 6.0
C	OD	93.2 ± 0.7
C	ID	105.4 ± 1.8
D	OD	75.2 ± 1.6
D	ID	80.2 ± 1.4

Table 2.3. Average pore diameter at the inner and outer wall tube surfaces. for all devices

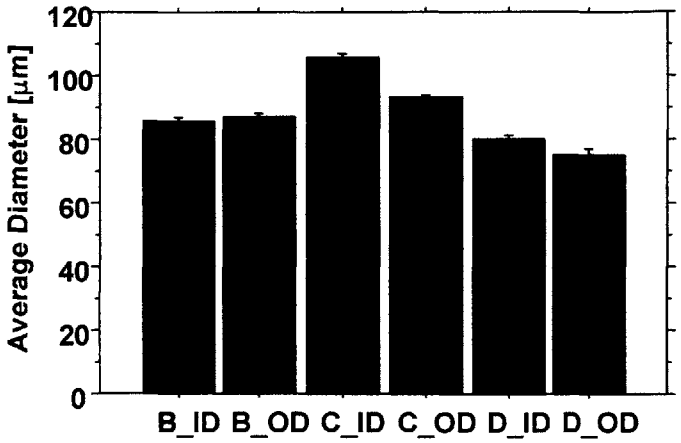

Figure 2.2. Average pore diameter (Mean ± SEM) at the inner and outer tube wall surfaces for three devices with variable crosslinking density (DHT mediated).

One-way ANOVA revealed a significant difference between the groups ($p < 0.0001$), but post-hoc testing did not indicate a difference between the pore diameter at the inner and outer tube wall of devices B or D ($p < 0.536$, 0.140, respectively), but did indicate a difference in the pore diameter for device C ($p < 0.0001$).

Histology Location	Pore Size (Mean ± SEM) [μm]
OD	84.7 ± 1.2
ID	94.9 ± 1.8

Table 2.4. Comparison of pore diameter at the inner versus the outer tube wall for the newly fabricated collagen tubes.

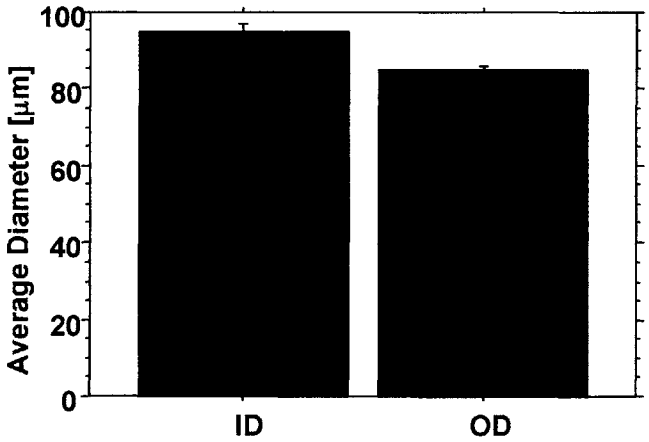

Figure 2.3. Comparison of pore diameter near the inner and outer tube wall surface (Mean ± SEM)

Comparison of the pore diameter between the inner and outer tube wall for all of the experimental devices combined showed a significant difference ($p < 0.0001$) between the two locations. The differences between the inner and outer diameter of all of the devices was shown to

be approximately 10 μm. Because the fabrication of each individual device is dictated by a random process of ice nucleation, and because the linear intercept method is not meant to give an exact value for pore diameter, it is more reasonable to conclude that there is no significant difference in the pore geometries through the thickness of the device.

The structure of the mold suggests that it is possible, however, to vary the pore geometries at the inner and outer tube surfaces. The mold features solid aluminum leaves covered in Teflon around the outside of the tube, while a Teflon tube covering a stainless steel wire formed the mandrel that was inserted down the central axis, forming the tube. The mold leaves are in direct contact with the freeze-drier shelf, while the mandrel is made out of a different material that is not directly connected to the cold shelf. Conductive heat transfer could lead to a colder freezing temperature at the outer surface of the tube than at the inner surface, leading to a smaller pore diameter at the outer surface. This technique may have great significance in fabrication of a new generation of tubular devices to test more thoroughly the effects of cellular migration versus binding on the process of peripheral nerve regeneration. Varying the mold and mandrel materials could lead to the formation of larger or smaller pores at either the inner or outer surface, significantly affecting cellular binding and migration either towards or away from the wound site. However for the homologous series of devices (high solids-content collagen tube), the pore structure was found to be relatively uniform throughout the device wall thickness.

Device Porosity

Comparisons between the porous structure of the collagen tube with different crosslinking densities and between the pore structure of the collagen tubes near the outer and inner the wall have been made. A clear determination concerning any significant differences between groups is impossible, due to the linear intercept method used for analysis. The errors describing the measurements of pore diameter for the different groups is much larger than that which is determined statistically due to the linear intercept method. The average pore diameter is a characteristic that is very difficult to determine due to the random process of nucleation of ice crystals used to form the pore structure and the high degree of interconnection between the pores throughout the matrix. The methods used for determining pore diameter do not give an exact definition for pore size, but do allow basic characterization. Based upon this work, there were no differences between groups that

were large enough to suggest that there was in fact a significant difference between the pore structure of devices with different densities of crosslinks (DHT mediated), or to suggest that the tube wall was not relatively homogenous. What is significant, however, is the difference between the pore structure of the new collagen devices and the Integra NeuraGen control.

The collagen devices have an average pore diameter of approximately 80 - 100 μm throughout the wall thickness, for all crosslink densities. This pore diameter is significantly larger than that of the Integra NeuraGen device (≈22 nm pore diameter). While the Integra device is only permeable to proteins with a molecular weight of less than 540 kDa until degradation affects the device, the new collagen devices are immediately cell permeable, allowing cells along with small and large proteins to migrate in both directions (from outside to inside and inside to outside of the wound environment). Prior devices (i.e. Integra NeuraGen and impermeable silicone tubing) have not been cell-permeable, so these high solids-content collagen tube present a significantly different environment for regeneration. Cell binding and migration significantly affect skin regeneration (Yannas, 2001); these conclusions suggest that there will be significant differences in the regenerative capacity of the new collagen device compared to previous controls.

2.3.2. Density of the Collagen Tube

The swelling characteristics of the devices provide an indication of their relative crosslink density. In order to properly compare the swollen density of the tubes, the dry density of the collagen tubes needs to be determined. The density of the collagen tubes is not expected to differ significantly between the members of the homologous series of experimental devices. The variable crosslinking density does not affect the density of the device at large. EDAC crosslinking (Device E) is a chemical process where the dry collagen tube is crosslinked in a chemical solution; this process is expected to lead to a significantly denser device due to hydration (a by-product of crosslinking). The density of the experimental and control devices was calculated using a technique described in more detail in Appendix A. The weight and volume of a number of tubes from each experiment and control group was measured, and the dry density calculated. The dry density of each device is presented below (Table 2.5, Figures 2.4 and 2.5):

Device	Density [g/mm^3]
A	$0.00011 \pm 4x10^{-6}$
B	$0.000098 \pm 2x10^{-6}$
C	$0.0001 \pm 4x10^{-6}$
D	$0.000093 \pm 4x10^{-6}$
E	$0.00087 \pm 6x10^{-5}$
F	$0.00014 \pm 8x10^{-6}$

Table 2.5. Unswollen density for all experimental and control devices, Mean ± SEM.

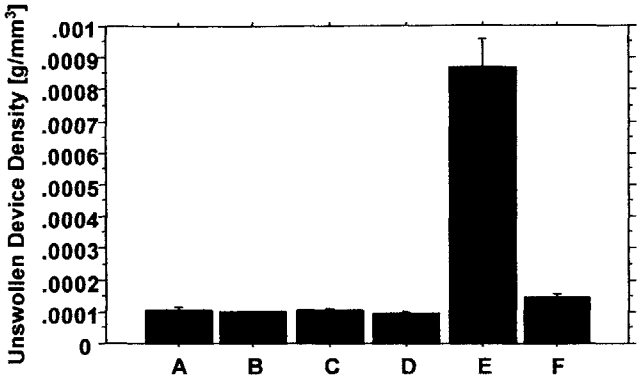

Figure 2.4. Unswollen density of all of the crosslinked devices (Mean ± SEM), including the EDAC crosslinked device.

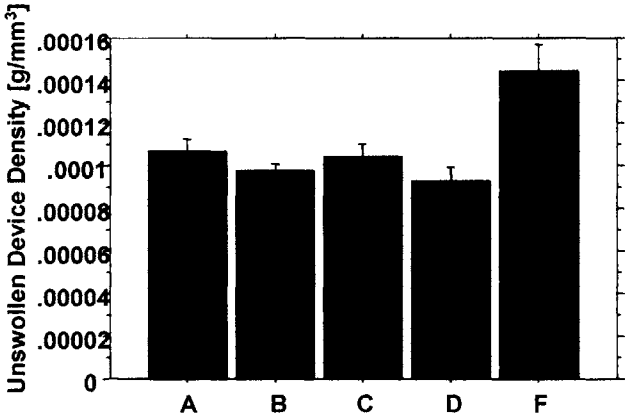

Figure 2.5. Unswollen density of all of the crosslinked devices (Mean ± SEM), excluding the EDAC crosslinked device.

One-factor ANOVA revealed significant differences ($p < 0.0001$) between the groups, and pos-hoc testing indicated that the EDAC crosslinked device was significantly denser than all other devices ($p < 0.0001$). Further comparison between the five dry devices (A, B, C, D, F) revealed that the Integra NeuraGen device was significantly denser ($p \leq 0.0004$ for all comparisons) than the other devices, and that no significant difference exists in device density between any of the dehydrothermally crosslinked devices ($p \geq 0.133$). This finding is consistent with the expectations that variable dehydrothermal treatment will not significantly alter the device density, and that the EDAC crosslinking process will result in a significantly denser device than other "dry" crosslinking techniques.

2.3.3. Pore Volume Fraction

The density of the dry high solids-content collagen tubes fabricated in the laboratory was determined to be approximately $1x10^{-4}$ g/mm^3 (Table 2.5). The pore volume fraction can be determined using this density and the known density of non-porous proteins in their dry state. A nonporous protein in it's dry state has a density of approximately 1.3 g/cm^3 (Yannas et al, 1967; Yannas et al., 1980). The density of a non-porous protein ($1.3x10^{-3}$ g/mm^3) is 10 times greater than that observed for the collagen tube, indicating that only 10% of the tube volume is collagen, and that the tube has a pore volume fraction of 90%. This compares favorably with the porous ECM analogs fabricated in our laboratory that have a pore volume fraction $\geq$90%.

2.3.4. Collagen Tube Swelling Kinetics

Prior to implantation, the collagen tubes are placed in sterile saline solution (See Appendix B for a detailed surgical description) in order to partially hydrate the device to allow for easier surgical manipulation. This hydration lasts for only an hour or two, and when the collagen device is placed in the wound, it will continue to hydrate and swell, eventually reaching a steady-state value. The kinetics of swelling can be used to understand the time scale during which the devices will swell in the *in vivo* wound environment.

The dry density of the experimental and control devices was determined; the devices were then placed in sterile PBS and kept in an incubator at 37°C in order to mimic the wound environment for swelling. The weight and volume of each device was measured at 24 hour intervals for a period of nine days to determine the kinetics of swelling. The kinetics of swelling are presented as either swelling mass or swelling volume ratios, where the swelling ratio for a particular time point is the ratio of either the mass or volume at that given time to the dry mass or volume:

$$MassRatio = \frac{Mass(t)}{Mass(t=0)}$$

$$VolumeRatio = \frac{Volume(t)}{Volume(t=0)}$$

Both the mas and volume ratio kinetics are presented in this section. The first chart in this series presents the kinetics of the swelling mass ratio for all 6 experimental and control groups (Figure 2.6).

The second graph (Figure 2.7) in the series presents the kinetics of the swelling volume ratio for all six of the experimental and control devices.

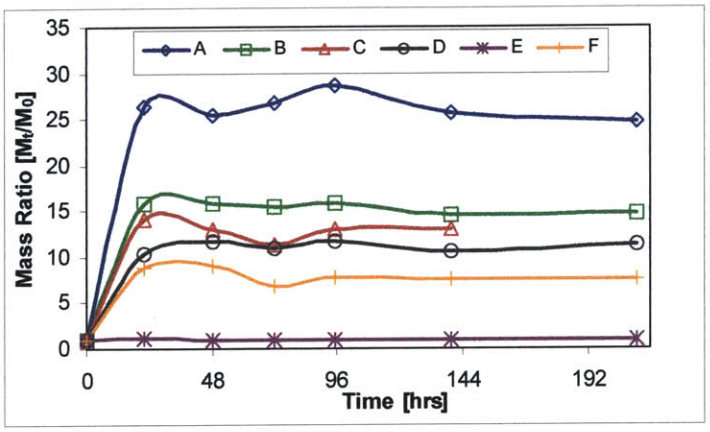

Figure 2.6. Swelling kinetics (mass ratio) for the control and experimental groups.

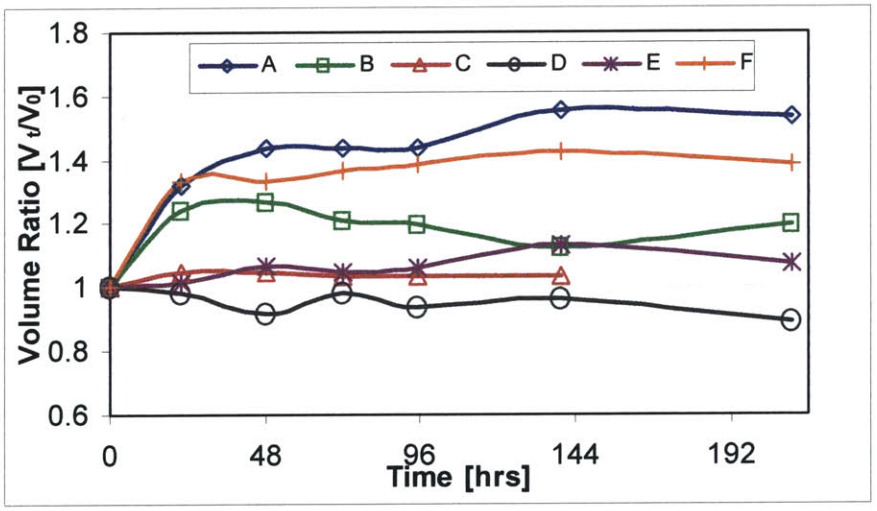

Figure 2.7. Swelling kinetics (volume ratio) for the control and experimental groups.

The kinetics of device swelling are most clearly described by the mass ratio chart. Device swelling is dependent upon swelling of individual fibers that make up the device in a liquid environment. These results show an asymptotic increase in device mass towards a steady state value that is different for each device. This increase is very rapid ($\tau < 24$ hours), and the resulting mass

ratios correspond to expectations based upon the crosslink density of the devices, where the devices with the lowest crosslink densities (A and B) showed the greatest swelling. Of the experimental devices, the EDAC crosslinked tube showed the smallest swelling ratio; this is to be expected as the EDAC process also hydrates (and hence swells) the matrix prior to the start of the swelling experiment. Resistance to degradation (Yannas et al., 1975) and stiffness of collagen matrices is positively correlated to matrix crosslink density; in addition, matrix swelling is negatively correlated with crosslink density. The steady state mass ratios for the devices were observed to be negatively correlated with the density of crosslinks.

The experimental and control devices showed a similar relationship for the volume ratio kinetics graph (Figure 2.7) although these ratios were neither as well defined nor as large as the mass ratio asymptotes. Within the homologous series, device A had the largest steady-state volume ratio while device D had the smallest.

Confirmation of the variable crosslink densities in the experimental and control devices can be observed by comparing the steady state mass swelling ratio (Table, 2.6, Figure 2.8).

Device	Swelling Mass Ratio $[M_t/M_0]$
A	25.5
B	14.5
C	13.0
D	10.5
E	0.93
F	7.5

Table 2.6. Swelling mass ratio for experimental and control devices.

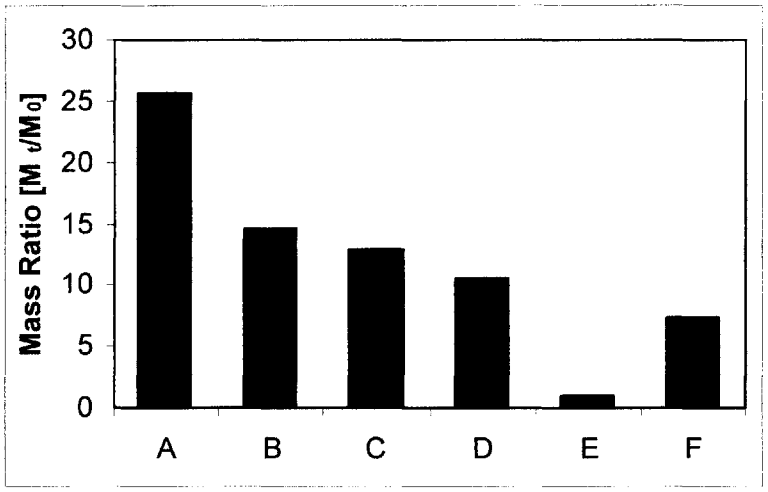

Figure 2.8. Steady-state swelling mass ratios (day six) of experimental and control devices.

Collagen matrix crosslink density is negatively correlated to swelling; there is a decreasing swelling (mass) ratio observed from device A to E of the homologous series, indicating increasing quantity of crosslinks. Additionally, device F was observed to have a smaller swelling ratio than devices A, B, C, and D. It is impossible, however, to compare the swelling ratio of this control

device to the other experimental devices to any conclusion about relative crosslink density because of the difference in fabrication methods and pore structure.

2.3.5. Steady-State Density of Swollen Collagen Tube

The swollen density of the collagen tube is an important characteristic for calculating the remaining mass of each device following the nine week *in vivo* peripheral nerve regeneration assay described in Chapter 3. Further description of the remaining mass analysis and calculation of the degradation characteristics of each device will be addressed in Chapter 4. The density of the collagen devices was determined after a minimum of 96 hours in swelling conditions (sterile PBS, 37°C). This time was established based on the observations made during the swelling kinetics study (2.3.4) so as to get the steady-state swollen density of each device.

The density of the swollen collagen devices varied from 6.68×10^{-4} g/mm^3 to 1.33×10^{-3} g/mm^3 (Table 2.7, Figure 2.9). One-factor ANOVA analysis indicated a significant difference between the swollen density of the experimental and control devices ($p < 0.0001$). While no significant difference was found between the unswollen densities of the experimental groups A - D, post-hoc testing indicated a significant increase in the swollen device density with increasing device crosslink density for devices A, B, C, and D. Devices E and F showed different swelling characteristics as a result of either differences in fabrication or crosslinking treatment compared to the other four devices. The ratio of swollen density to unswollen density increased from device A through D as well (Table 2.7).

Device	Unswollen Density [g/mm^3]	Swollen Density [g/mm^3]	Ratio
A	$0.00011 \pm 3.91 \times 10^{-6}$	$0.00067 \pm 5.3 \times 10^{-5}$	6.27
B	$0.000098 \pm 2.44 \times 10^{-6}$	$0.0010 \pm 2.5 \times 10^{-5}$	10.68
C	$0.00010 \pm 4.39 \times 10^{-6}$	$0.0011 \pm 3.7 \times 10^{-6}$	10.84
D	$0.000093 \pm 4.48 \times 10^{-6}$	$0.0013 \pm 3.89 \times 10^{-5}$	14.37
E	$0.00087 \pm 6.02 \times 10^{-5}$	$0.00095 \pm 4.87 \times 10^{-5}$	1.09
F	$0.00014 \pm 8.11 \times 10^{-6}$	$0.0012 \pm 8.25 \times 10^{-6}$	8.84

Table 2.7. Unswollen and swollen density of the five experimental devices and one control device (Mean ± SEM), along with ratio of swollen to unswollen density.

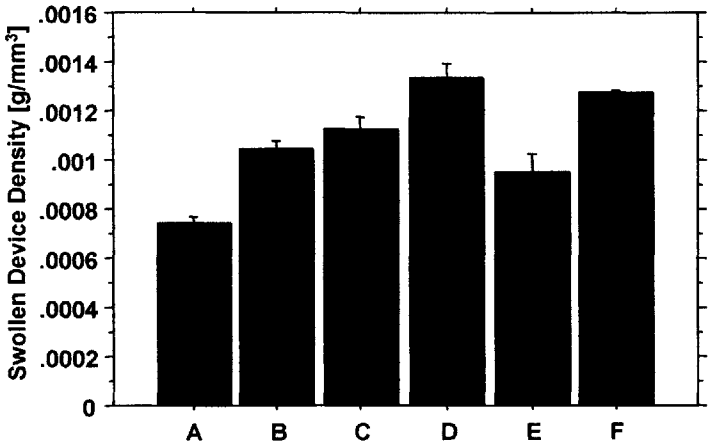

Figure 2.9.. Swollen device density, Mean ± SEM.

The swollen density of the collagen tubes increased with crosslinking density, due to the increase in device mass as a result of fiber swelling coupled with a less significant volume change as a result of the added stiffness with greater crosslink density (Figures 2.10, 2.11). Those devices with a higher density of crosslinks remained relatively constant in volume while those with low crosslink density expanded by greater than 50%.

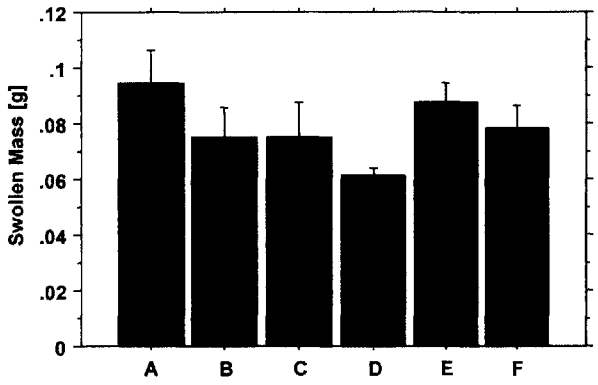

Figure 2.10. Swollen mass steady-state characteristics of the collagen devices (Mean ± SEM)

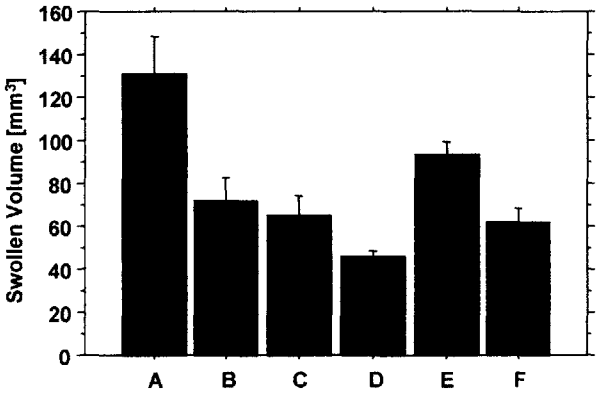

Figure 2.11. Swollen volume steady-state characteristics of collagen devices (Mean ± SEM).

The swollen density was significantly larger than the unswollen density for all devices ($p < 0.0001$) except for device E (EDAC crosslinking, $p > 0.185$) (Figure 2.12); this finding is consistent with previous observations indicating that collagen devices swell significantly except for those

treated with chemical crosslinking agent that swells the matrix during crosslinking.

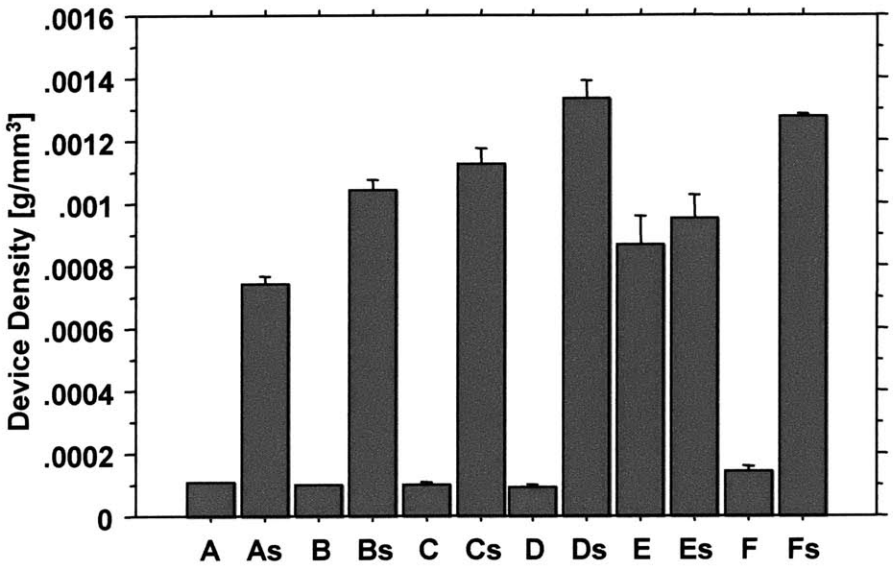

Figure 2.12.. Swollen vs. unswollen density of experimental and control devices (Mean ± SEM). Data presented as a comparison between unswollen tube (X) and swollen device (Xs).

2.4. Discussion

A variety of tubular devices have been tested as regenerative templates for peripheral nerves following transection. Previous studies have identified a collagen tube, impermeable to cells or proteins greater than 540 kDa in size, that resulted in improved regeneration of peripheral nerves. A series of new collagen tubes was developed in this laboratory for use in order to test the effect of device permeability and degradation rate on the quality of peripheral nerve regeneration. Characterization of this new high solid-content collagen tube for peripheral nerve regeneration is critical in understanding device performance *in vivo*. A homologous series of devices, varying only by crosslink density, were created for *in vitro* characterization (Chapter 2) and *in vivo* functionality assays (Chapters 3 and 4). The five experimental devices had a variable density of crosslinks; these devices were not crosslinked (device A), crosslinked using increasing intensity dehydrothermal treatment (devices B, C, and D), or crosslinked via EDAC (device E). In addition, the Integra NeuraGen tube (control, device F) was included in all of the characterization and *in vivo* assays.

The pore diameter of the experimental devices was observed to be consistent for a variety

of dehydrothermal treatments, with an average pore diameter of 80 - 100 μm, significantly larger than the average pore diameter of the Integra tube: < 22 nm. In addition, the tube wall was observed to have a relatively uniform pore diameter distribution throughout its thickness. The new collagen tubes are permeable not only to small proteins, but larger proteins and cells as well. This characteristic may have a significant impact on the *in vivo* functionality of the tube, as the wound site will no longer be isolated from the surrounding tissue; the effect of this change is discussed in Chapters 3 and 4.

Both the collagen experimental devices and the control device show similar swelling kinetics; all devices reached steady-state asymptotes for mass and volume with a time constant of less than 24 hours. In addition, those devices with higher densities of crosslinks swelled less (lower mass and volume ratios) relative to those tubes with a lower density of crosslinks, provided that the tubes differ only in crosslink density. These mass and volume swelling relationships confirm the variable crosslink density created through variable chemical (EDAC) and physical (dehydrothermal) crosslinking treatments (Device crosslink density: A < B < C < D < E, F). The steady-state swollen density was calculated for later use in Chapter 4, and significant differences between device density was observed. The device density increased significantly with increasing crosslink density.

These observations provide the critical framework for better understanding the fabrication process as well as the *in vivo* performance of these devices that is described in the following chapters. The affect of the different experimental and control devices on peripheral nerve regeneration will be addressed next in Chapter 3, followed by an analysis of the affect of device degradation on the regenerative process in Chapter 4.

Chapter 3

Effects of High Solids-Content Collagen Tube and Crosslink Density on Nerve Regeneration

3.1. Introduction

3.1.1. Short-term Assays of Peripheral Nerve Regeneration

Analysis of the functional recovery of a transected peripheral nerve, via either electrophysiological or functional (i.e. SFI) assays, does not yield significant information regarding quality of regeneration until 30 weeks post-implantation; extensive remodeling of the regenerated tissue is required before axonal functional performance is observed (den Dunnen et al., 1996; Chamberlain, 1998a; Yannas, 2001). A long-term experiment yields significant functional information critical to understanding clinical outcomes for peripheral nerve injuries, but a short-term assay of the quality of regeneration is necessary for rapid comparison of devices. A nine week implantation period is not long enough for recovery of nerve functionality; morphological analysis of the regenerate (number, size, and structure of the axons) at nine weeks can be used however to determine differences between the regenerative capacity of experimental groups that could be observed through electrophysiological and functional tests at a much later time period (Chamberlain, 1998a; Spilker, 2000; Yannas, 2001). For short-term experiments of peripheral nerve regeneration, the critical gap length can be used to quantify the regenerative capacity of each device. In particular, silicone tubes without an ECM analog insert are a common device used to regenerate peripheral nerves but have a critical gap length of only 10 mm (Lundborg et al., 1982; Spilker, 2000; Yannas, 2001; Brau, 2002). Collagen tubes have shown improved quality of regeneration over similar gap lengths when compared to silicone tubes, and collagen tubes have also shown longer critical gap lengths (Spilker, 2000). In addition, the degradation rate of devices used for skin regeneration is a significant factor affecting the quality of regeneration (Yannas, et al., 1989; Yannas, 2001); a collagen device allows variation of the degradation rate by changing the device crosslink density (Yannas, 2001).

A homologous series of degradable collagen tubes and an Integra Lifesciences NeuraGen device were studied in order to assess the regenerative capacity of a new, high solid-content collagen tube (fabrication and characterization described in Chapter 2) in comparison with the previous laboratory standard (Integra NeuraGen device), and to observe any role played by device crosslink density and/or the degradation rate on the process of peripheral nerve regeneration.

3.1.2. Project Goal

The objective of this study was to evaluate the effects of a new tubular device on the process of peripheral nerve regeneration following severe sciatic nerve injury. The collagen tubes were produced with a variable density of crosslinks in order to degrade at different rates, and the effects of device degradation rate on the quality of peripheral nerve regeneration were studied. A homologous series of collagen tubes varying only by crosslinking density (varying in expected *in vivo* degradation rate) were implanted into a 15 mm gap in the sciatic nerve of a Lewis rat model; the devices were filled only with sterile saline and not the NRT developed previously that optimizes the regenerative capacity of a particular tube design (Chang et al., 1990). The crosslinking techniques and intensities were chosen to present a wide range of degradation rates for analysis. Histomorphometric analysis of cross-sections from the gap mid-point of each regenerate was performed at nine weeks to determine the effects of the new high solids-content collagen tube when compared to the NeuraGen control, and the effects of the different crosslink densities on the number and size distributions of axons regenerating across the gap midpoint (7.5 mm from the proximal stump). The length of the experiment was too short to be able to recover any functional information concerning reinnervation, but past work has shown that this early time point can be utilized for morphological comparison that will allow classification of the regenerative capacity of each device (Spilker, 2000; Yannas, 2001). A study of the effects of *in vivo* on degradation rate, where the degradation rate was assayed using information concerning the remaining mass of the collagen tubes upon explantation, will be reported in Chapter 4.

The most important morphological characteristics considered were the large diameter axons (A-fibers, diameter $\geq$ 6 μm) (Arbuthnott et al., 1980; Strichartz and Covino, 1990). This particular axon population plays a major role in the recovery of electrophysiological function as well as in efficient and rapid conduction of action potentials through motor neurons (Mackinnon et al., 1990;

Chamberlain, 1998a). In addition, those axons observed to be A-fibers have likely reached a distal target and can be considered a relatively permanent axon (Sanders and Young, 1944; Weiss et al., 1945; Sanders and Young, 1946; Aitken et al., 1947; Aitken, 1949). The number of A-fibers present in a regenerating nerve trunk is a significant measurement of the quality of regeneration. The N-ratio is an important measurement of the maturity of a regenerating nerve (den Dunnen et al., 1996), and this ratio was used as a second significant characteristic for device comparison. In addition, the total number of axons, the density of axons, and the average size of the axons will be considered to obtain a better understanding of the differences between experimental groups.

3.2. Materials and Methods

3.2.1. Peripheral Nerve Devices

The two types of collagen tubes used for this experiment were both fabricated from type I bovine tendon collagen, each with an inner diameter of 1.5 mm. The details of the fabrication of these two separate devices are detailed in sections 2.2.1 and 2.2.2. The control device, a collagen tube supplied by Integra Lifesciences (NeuraGen, Plainsboro, NJ) has been previously used for peripheral nerve regeneration in this laboratory and has recently received FDA approval for clinical use. The experimental devices are 5% (w/w) collagen tubes (high solids-content tube) fabricated in this laboratory (Section 2.2.1). Crosslinking density is negatively correlated with *in vivo* degradation rate (Yannas, et al., 1975); a homologous series of experimental devices, varying only in crosslink density, were prepared for *in vivo* experimentation. The high solid-content tubes were crosslinked via both physical (Dehydrothermal - DHT) and chemical (EDAC) processes (Table 3.1).

The devices were prepared for implantation in a sterile hood. The tubes were cut to a final length of 25 mm (15 mm gap plus 5 mm insertion zones on either end of the tube). Each implant was individually placed in sterile phosphate buffered saline (PBS, Sigma Aldrich Chemical Company, St. Louis, MO) one hour prior to implantation, and the lumen was considered to be at least partially filled with saline when implanted. The collagen tubes are stiff and relatively brittle as prepared, and need to be hydrated prior to implantation in order to provide the ductility required for implantation; hydration time prior to operation plays a significant role in the handling of the device during implantation. Short hydration periods ($t < 1$ hour) result in the device remaining too stiff to

properly manipulate in the wound site, and long hydration periods (t > 6 hours) result in devices that kink and crush too easily when handled with surgical instruments; observations made during surgery indicated that the optimal pre-surgery hydration time was approximately 2 hours.

Device Identifier	Tube Type	Crosslinking Technique
A	5% (w/w) Collagen	Not crosslinked
B	5% (w/w) Collagen	DHT crosslinked, 90°C, 24 hours
C	5% (w/w) Collagen	DHT crosslinked, 90°C, 48 hours
D	5% (w/w) Collagen	DHT crosslinked, 120°C, 48 hours
E	5% (w/w) Collagen	EDAC crosslinked, Room temperature, 24 hours
F	Integra	Gaseous formaldehyde

Table 3.1. Crosslinking treatment and intensity for each of the experimental group (A - E) and for the control (F). The control group is an FDA-approved device used clinically to treat peripheral nerve injury (Integra LifeSciences, and is additionally shaded).

3.2.2. Animal Model

Thirty-two female Lewis rats (Charles River Laboratories), 175-200 gm, were used for this study. The Lewis rat was chosen for this experiment as a result of past experimental observations that the Lewis strain of rat showed resistence to autotomy (self-mutilation) following sciatic nerve transection (Carr et al., 1992). Females were used because they do not display the same level of aggressiveness towards each other observed among males. The animals were divided into the six experimental groups previously described (Table 3.1) with the following group sizes: Table 3.2.

Device	n
A	6
B	6
C	6
D	6
E	3
F	5

Table 3.2. Experimental group size

A standardized wound was created in each animal by transecting the right sciatic nerve at the midpoint (*) between the sciatic notch, located at the proximal end of the femur, and the distal bifurcation, located just distal to the distal end of the femur (Figure 3.1 and Figure 3.2).

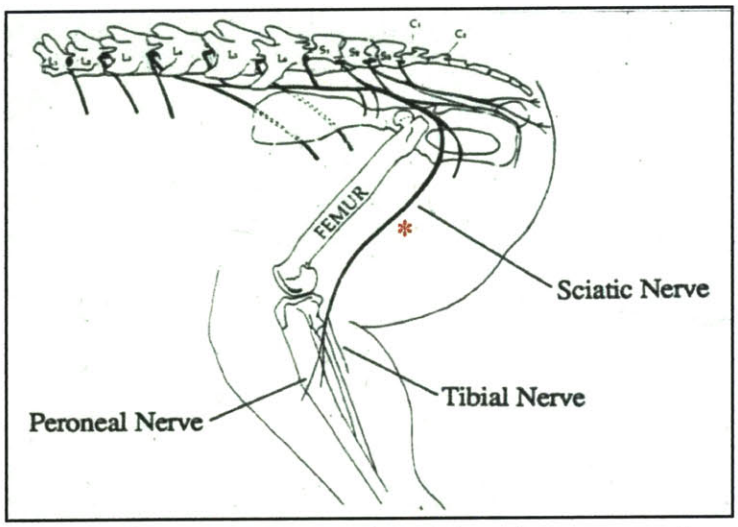

Figure 3.1. Anatomical location of the sciatic nerve and surgical wound site (Chamberlain, 1998a)

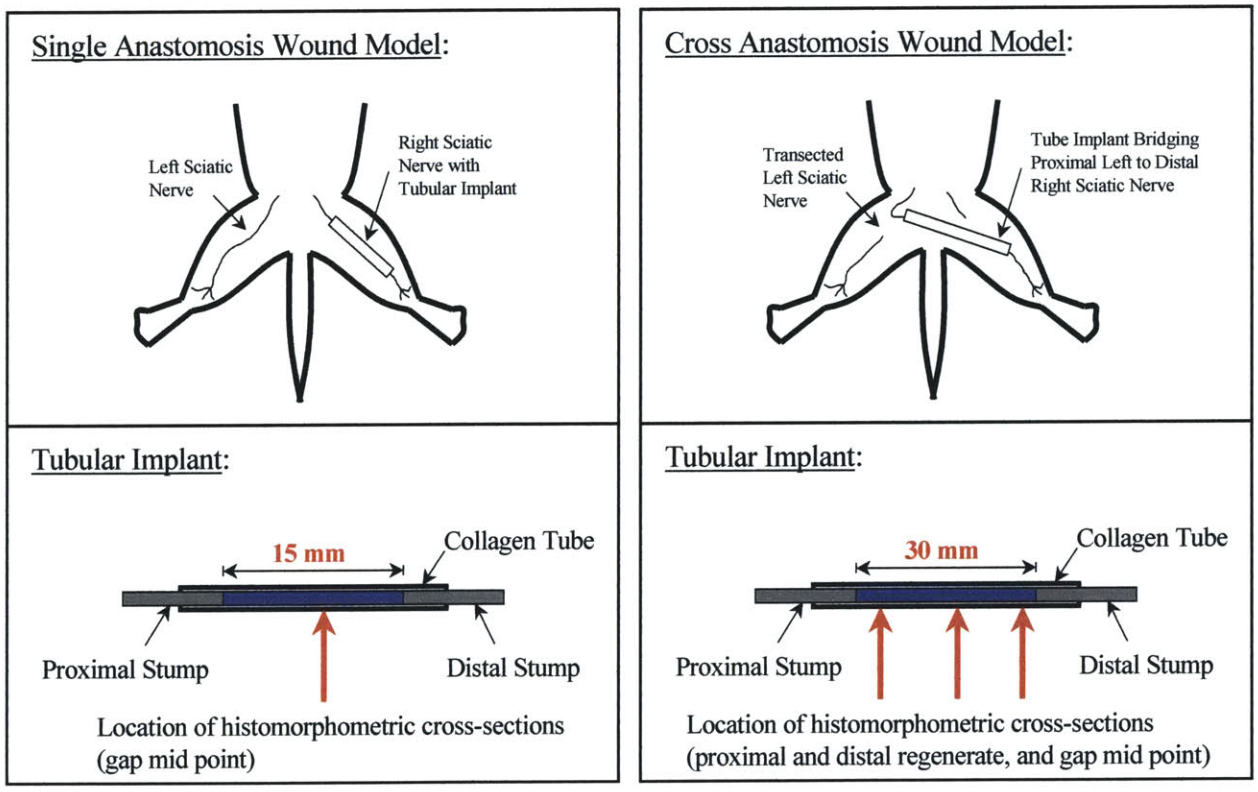

Figure 3.2. Schematic of single and cross anastomosis wound models, as well as the tubular implant.

A single-anastomosis surgical wound model was used for testing the experimental devices over a 15 mm gap where the right sciatic nerve was transected, and the tubular implant placed between the two stumps in order to induce regeneration from the proximal to the distal stump (Figure 3.2). A cross-anastomosis model requires connection of the proximal stump of the left sciatic nerve with the distal end of the right sciatic nerve with a device that runs posterior to the spinal column (Figure 3.2); this is a more stringent wound model for testing.

A 50 mg/kg intraperitoneal injection of sodium pentobarbital (Nembutal Sodium Solution, Parke-Davis, 50 mg/ml) was used to anesthetize each animal. The surgical area was shaved with animal clippers and cleansed with a providone-iodine sponge. Each animal was placed in a prone position on a surgical board with the limbs secured, with the hind legs additionally held in 30° abduction. A 4 cm incision was made parallel and posterior to the right femur. The muscle and fascia were dissected and cut away so that the nerve was completely exposed. After exposing the sciatic nerve, the nerve was anesthetized using a few drops of 1% Lidocaine directly on the nerve.

The sciatic nerve was transected midway between the distal bifurcation and the sciatic notch using microscissors. The tubular device, filled only with the sterile saline used to hydrate the device prior to implantation, was placed in the gap and the proximal and distal stumps of the nerve were inserted 5 mm into either end of the tube, leaving the 15 mm gap used for this experiment (Figure 3.2). The two stumps of the nerve were secured inside the tube using two 10-0 nylon sutures (Catalog No. 9002G, Ethicon Suture, Johnson & Johnson) at each end. The muscle and skin were closed using 4-0 vicryl sutures (Catalog No. J496, Ethicon Suture, Johnson & Johnson) and skin staples (Reflex 9 skin Staples, Catalog No. RS-9262, Roboz Surgical Instrument Co., Inc., Rockville, MD). Following surgery, the animals were housed in cages on their own and monitored until they were fully alert. Additionally, the animals were treated with subcutaneous injections of 1 mg/kg Buprenorphine (Cat. No. 40182C, Lyphomed, Deerfield, IL) as an analgesic twice a day for the first two days following surgery, and then as needed for the duration of the experiment. The animals were housed on wood chip bedding, one animal to a cage for the first 7 days after surgery and then two animals to a cage for the remainder of the experiment, with water and food available *ad libitum*. The animals were monitored daily for signs of abnormal activity such as aggression, lack of appetite, insufficient grooming, lack of mobility, and autotomy.

All animals were sacrificed at 9 weeks post-operatively by carbon dioxide inhalation, and the

regenerated tissue and any remaining portion of the device were removed together and prepared for histomorphometric analysis.

3.2.3. Histomorphometric Procedures

Following sacrifice, the regenerated nerve tissue and any portions of the tube that remained intact were removed along with the remaining sciatic nerve proximal to the tube through the sciatic notch and distal from the implant to the distal bifurcation; the tissue was placed into Yanoff's fixative and stored in 70% ethanol. A complete protocol for these histological analysis procedures are presented in Appendix C. A 2 - 3 mm segment of the regenerated nerve was removed from the gap midpoint, post-fixed in 1% osmium tetroxide (Catalog No. 251755, Sigma-Aldrich, St. Louis, MO), and embedded in Epon plastic (Catalog No. 08792, Polysciences, Inc., Warrington, PA). The tissue sections for histomorphological analysis were prepared by sectioning the Epon embedded tissue at a 1 μm thickness. The slides were additionally stained with Toluidine Blue (Catalog No. BP-107-10, Fisher Scientific, Boston, MA) to enhance the osmium tetroxide stain. The samples were then mounted and coverslipped with Permount (Catalog No. SP15-100, Fisher Scientific, Boston, MA).

The nerve sections were digitized into a personal computer using a digital video camera (Model No. DEI-750, Optronics Engineering, Goleta, CA) connected to a light microscope (Nikon Model E600, with Nikon objectives and optics). Low magnification images (4x, 10x objective) were captured in order to measure the cross-sectional area of the regenerated nerve. High magnification images (100x objective), representing at least 10% of the total cross-sectional area of the nerve trunk, were captured from a random distribution across the entire cross-section. These high magnification images were used for the morphological characterization of the regenerated axons.

The nerve trunk dimension and the morphological characteristics of the regenerated axons (number, density, and size of myelinated axons) were calculated using the public domain software Scion Image (available at www.scioncorp.com, see Appendix C for a more detailed protocol). The density of axons was multiplied by the total nerve trunk area to determine the number of total axons. Scion Image provides data describing the cross-sectional area and perimeter for every axon in each high magnification view; axon diameter is calculated using the relation $D = 4*A/L$ ($D \equiv$ axon diameter, $A \equiv$ axon cross sectional area, $L \equiv$ axon perimeter). This calculation allows for improved

accuracy in calculating the average diameter for axons that are not perfectly circular (compared to $D = L/\pi$ or $D = 2*(A/\pi)^{1/2}$). In addition, the total myelinated fiber area was determined by summing the areas of all myelinated action in the analyzed sections, and was used to calculate the N-Ratio for each nerve trunk:

$$N - Ratio = \frac{\sum MyelinatedAxonArea}{TotalNerveTrunkArea}$$

The N-Ratio has been used previously to provide valuable information regarding remodeling changes in peripheral nerves and is an important measure of the maturity of a regenerating nerve trunk (den Dunnen et al., 1996; Chamberlain, 1998a).

3.2.4. Statistical Methods

One-factor analyses of variance (ANOVA) were performed to determine the affect of crosslinking treatment on the morphology of the regenerated axons. If ANOVA indicated statistical significance, subsequent multiple comparisons were made using the Fisher's PLSD post-hoc test to determine the differences between pairs of experimental groups. The StatView v5.0 (SAS Institute, Inc.) statistical software package was used for all analyses. For all analyses, and statistical significance was accepted for $p < 0.05$. All graphical representations are presented with the average value of the data for each group ± the standard error of the means (SEM):

3.3. Results

3.3.1. General Observations

Following the surgical procedure, the animals did not exhibit outward signs of discomfort, and autotomy was not observed in any of the animals. During the 9 week experiment, two animals out of a total of 32 died prior to the completion of the experiment; one animal treated with device B died of unknown causes 3 weeks into the experiment ($n = 5$ for this group now) and the another animal treated with device F died of complications due to the implantation surgery ($n = 4$ for this group now). The remainder of the animals were included in the experimental analysis, and all experimental groups had large enough sample sizes for statistical analysis ($n \geq 3$).

In all animals sacrificed, tissue was observed to have bridged the 15mm gap between the proximal and distal stumps in both the Integra NeuraGen tube and in all five variants of the new high solids-content collagen tube. There was no significant difference (ANOVA, post-hoc testing, $0.0735 < p < 0.7674$) in the cross-sectional area of the regenerated tissue at the gap midpoint between all of the experimental groups (devices A - E), but there was a significant difference ($p < 0.008$) when the total area occupied by myelinated fibers was compared to the Integra device. The Integra tube showed a statistically greater total area occupied by myelinated fibers when compared to each of the experimental groups and the normal sciatic nerve (Table 3.3, Figure 3.3):

Device	Total Area Occupied by Myelinated Fibers [mm^2]
Normal	0.38 ± 0.03
A	0.20 ± 0.11
B	0.25 ± 0.05
C	0.12 ± 0.03
D	0.16 ± 0.01
E	0.41 ± 0.01
F	1.07 ± 0.24

Table 3.3. Morphological measurements (mean ± SEM) at 9 weeks post-implantation of the total area occupied by myelinated nerve fibers (total fascicle area). Normal nerve values based upon the work of Chamberlain, 1998a.

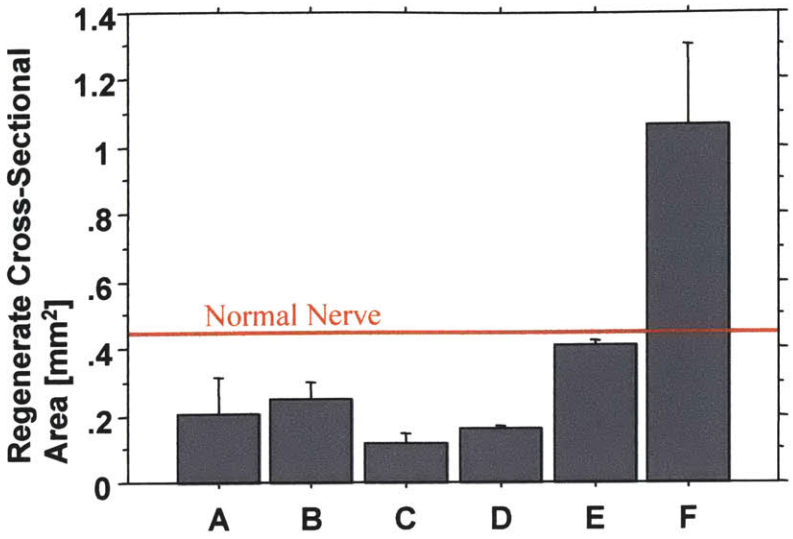

Figure 3.3. Morphological measurement of total cross-sectional area of tissue containing regenerated, myelinated axons (Mean ± SEM).

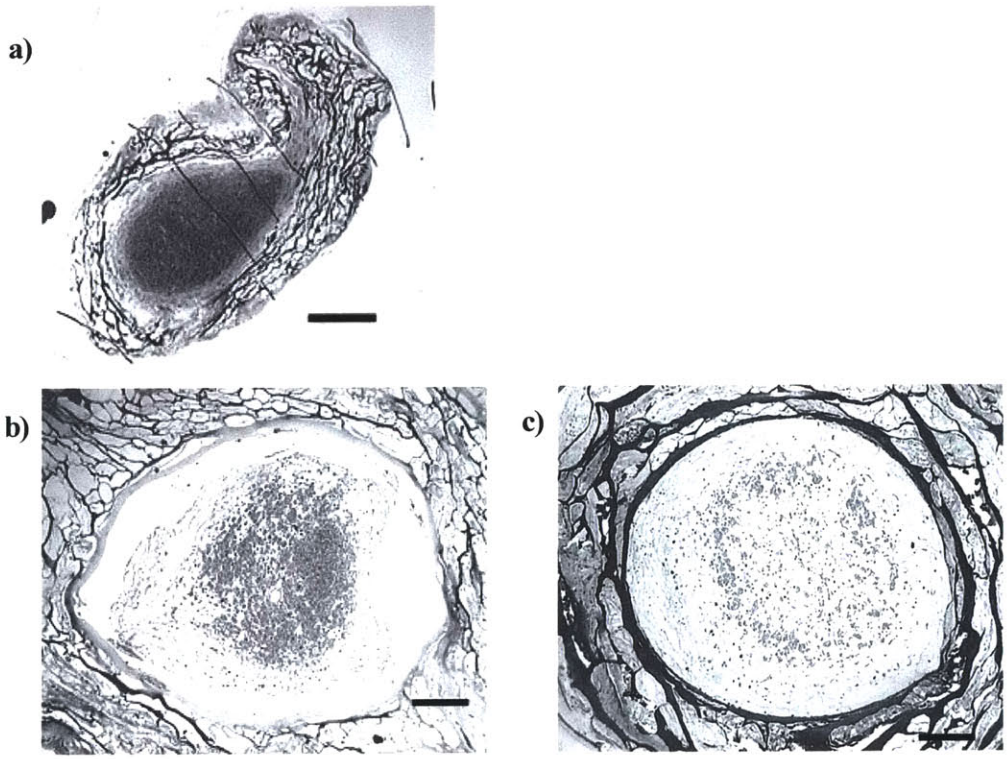

Figure 3.4. Low magnification images of three devices and the regenerated axons. (a) Device D, with a defined fascicle structure, (b) Device E with a defined fascicle structure, and (c) Device F where there is no defined fascicle structure and the axons fill the entire inner lumen of the tube. All images were taken with the same magnification and the scale bar = 0.25 mm.

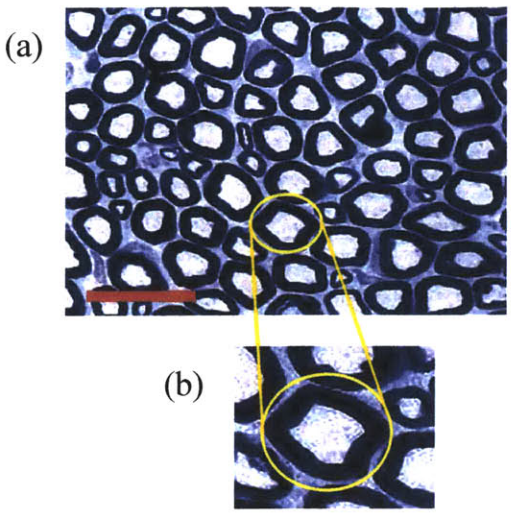

Figure 3.5. (a) Normal Lewis rat sciatic nerve cross-section image, scale bar = 25 μm. (b) Individual myelinated nerve fiber: axoplasm surrounded by a defined myelin sheath, separated from other axons by the endoneurium.

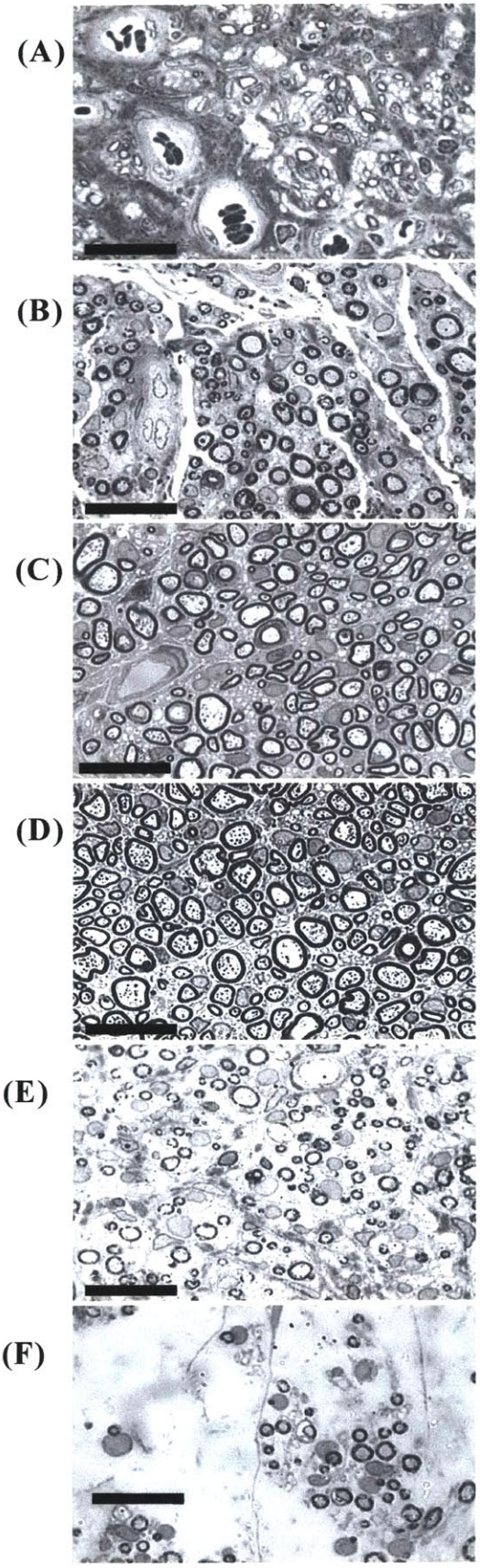

Figure 3.6. High magnification images of nerves regenerated with the five experimental devices (**A**: Non-crosslinked, **B**: DHT 90C, 24 hours, **C**: DHT 90C, 48 hours, **D**: DHT 120C, 48 hours, **E**: EDAC crosslinked) and one control device (**F**: Integra NeuraGen). The images are arranged in order from lowest to highest density of crosslinks (from the top image to the bottom). The magnification for each image is the same, with the scale bar = 25 μm.

Device **D** shows superior morphology of regenerated nerve, with significantly larger axons and a more defined myelin sheath.

There was a significant difference in the structure of the "fascicle" seen in the experimental devices and the Integra NeuraGen device (Figure 3.4). The term fascicle in this case describes the capsule of tissue that surrounds the regenerated axons. The tissue capsule containing regenerated axons is a well-defined structure that was readily apparent under light microscopy for the experimental devices (A - E). The experimental devices each showed a defined fascicle surrounding the myelinated fibers; however, the axons regenerated using the Integra device did not appear to be enclosed within a defined capsule of tissue. Instead, the axons were spread out throughout the lumen of the tube. Hence the area of the axons was significantly larger and th axonal density significantly smaller (Figure 3.7) for the Integra NeuraGen device; the inner wall of the tube defined the area filled with myelinated axons (Figure 3.4). Such tendencies were slightly apparent with the EDAC device, possibly indicating that tubes that remain relatively intact over long period in time destroy some of the fascicular architecture by introducing their own inner wall as the confining surface of the regenerating axons.

The number and size of the regenerated axons significantly affects the functional recovery of the nerve (Mackinnon et al., 1990). The number and size of the axons regenerated in the five experimental and one control group show a significant difference between the groups (Figure 3.6); this pattern is different from the relation observed for the total cross-sectional area of the nerve trunk. Grossly, the individual axons appear larger and their myelin sheath more well-defined for devices C and D, while those devices with lower (A and B) and higher (E and F) densities of crosslinks showed fewer myelinated axons with a smaller average diameter and with a less well-defined myelin sheath. This apparent difference in axonal structure is characterized and quantified in section 3.3.2. Not only are their significant structural differences in the nerve regenerates, but there appears to be a pattern describing this variation. Device performance (measure of size of the morphology of the regenerate) improves with increasing device crosslinking density (Device A → B → C → D → E); however, there is an optimal performance at some point or points because performance is also observed to decrease for very large crosslink densities (devices E and F).

Gross examination of the devices upon explantation indicates that the degradation characteristics of the differently crosslinked tubes are also significantly different. The Integra device (F) and the EDAC crosslinked collagen tube (E) did not appear to have degraded significantly after 9 weeks. There was a variable amount of collagen tube remaining for the three dehydrothermally

treated and the one non-crosslinked devices. The tube appeared completely degraded for the non-crosslinked tube (A) and the lightest crosslinked device (B); a small remainder of tube was visible for the other two collagen tubes (C, D). The results of a deeper analysis of the remaining masses of the devices at explantation and the effect of *in vivo* degradation rate on peripheral nerve regeneration is presented in Chapter 4.

3.3.2. Histomorphometry

Four criteria were used to assay the quality of peripheral nerve regeneration: the density and number of myelinated axons, the average axon diameter, the percentage and total number of large axon fibers, and the N-ratio of the nerve trunk. The criteria were all obtained from histological sections taken at the gap midpoint and help to describe either the speed with which axons are bridging the gap or the functional potential of the axons.

Number and Density of Myelinated Axons

Previous studies of the kinetics of peripheral nerve regeneration have revealed that a growth followed by a plateau region describe the number of myelinated axons that regenerate following nerve transection, where the plateau region was not reached until 20 - 30 weeks following injury (Chamberlain, 1998a). A nine week assay of the density and number of myelinated axons will not describe the characteristics of the fully regenerated nerve; however the 9 week time point will result in a better understanding of the speed of bridging that occurs with each group. The number of myelinated axons is positively correlated with the signal amplitude of the regenerated nerve (Mackinnon et al., 1990). (Experimental results presented below in Figures 3.7 and 3.8, Table 3.4).

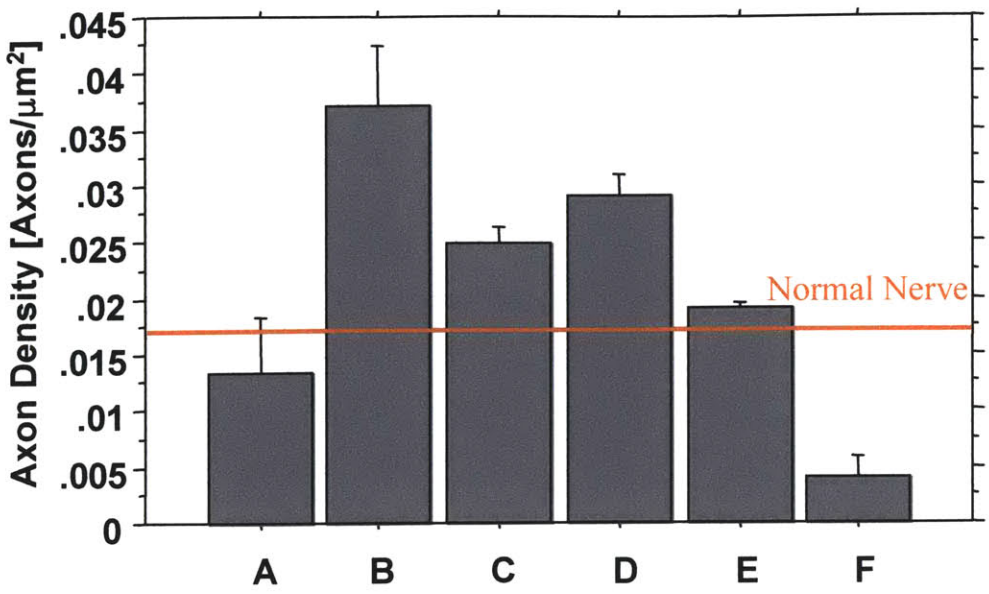

Figure 3.7. Density of myelinated axons for five experimental device (A - E) ad one control device (F). Normal sciatic axon density calculated using observations from Chamberlain, 1998a.

Device	Number of Myelinated Axons
Normal	6500
A	4670 ± 2870
B	8410 ± 1780
C	2970 ± 800
D	4760 ± 370
E	7790 ± 390
F	3480 ± 1310

Table 3.4. Number of myelinated axons (Mean ± SEM) per class of devices.

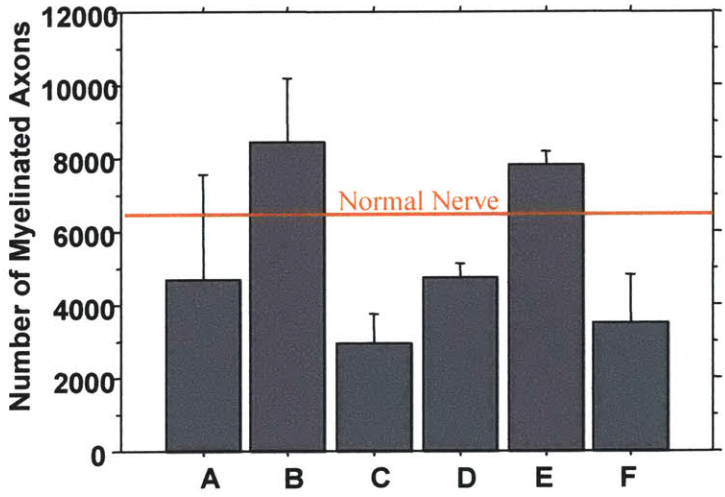

Figure 3.8. Average number of myelinated axons (Mean ± SEM) per regenerated nerve trunk.

At 9 weeks, there was a significantly higher density of myelinated axons in all groups ($p < 0.02$) when compared to the Integra NeuraGen device, with the exception of the non-crosslinked tube ($p = 0.075$). The regenerated axons in the Integra device, however, were not organized together and surrounded by a fascicle-like tissue. Instead, the axons were distributed throughout the inner area of the tube, making the density artificially low because the cross-sectional area of the regenerated

tissue was approximately 3 times of that seen in any other device or in the normal nerve. The devices with mid-value crosslink densities (Devices 1, 2, 3) appeared to have larger densities, but the more significant factor to use for comparison of the devices is the total number of myelinated axons, removing the variation in cross-sectional area of the regenerate.

All of the tubulated groups (experimental and control) showed a comparable or smaller number of regenerated, myelinated axons at the gap midpoint at 9 weeks when compared to the normal nerve. One-factor ANOVA, followed by post-hoc testing revealed a statistically significant difference between devices B and C ($p < 0.032$), but revealed no significant pattern between crosslinking treatments or between the high solids-content and the Integra tubes in the number of nerves bridging the wound gap. This observation fits well with past morphological observations made during a study of the kinetics of peripheral nerve regeneration (Chamberlain, 1998a; Chamberlain et al., 1998b; Chamberlain et al., 2000b). The total number of myelinated axons bridging the gap following complete sciatic nerve transection was observed to have a growth (before 30 weeks) and a plateau phase (after 30 weeks). During the growth phase, all of the devices showed bridging of the gap (10 mm gap) with a large number of axons; differences in number of axons between groups were not significant (ANOVA, $p > 0.3$). In this case, myelinated axons were observed to bridge a 15 mm gap via collagen tubes without an ECM analog insert, and the difference in cross-link treatment did not significantly affect the number of axons bridging the gap.

Average Axon Diameter

Normal axon diameter is observed to exhibit a slightly bimodal myelinated axon distribution with peaks at 3.5 μm and 8.5 μm, with a mean fiber diameter of 8.5 ± 0.2 μm (Chamberlain, 1998a). Nerve regeneration has been observed to first require successful bridging of the proximal and distal stumps; once bridging has occurred, the bridging axons are remodeled, resulting in increased axon diameter. These larger axons have the ability to conduct action potentials faster (Mackinnon et al., 1990), so average axon diameter is one method for quantifying the maturity of the regenerate. It has previously been observed that those devices that induce larger axons at an early time point have improved functional performance at an earlier time point (Chamberlain, 1998a). The distribution of axon diameter over the five experimental and one control devices showed a significant relationship between device performance (quality of peripheral nerve regeneration) and crosslinking

density (Table 3.5, Figure 3.9).

Normal sciatic nerve had a mean diameter of 8.5 ± 0.2 μm; at 9 weeks post-injury, the mean axon diameter at the gap mid-point for nerves regenerated with the six different devices ranged from 1.8 μm to 3.2 μm (Table 3.5, Figure 3.9), significantly lower than what is seen in the normal sciatic nerve. One-factor ANOVA revealed a significant affect of the differently crosslinked devices on the mean axon diameter of the regenerates ($p < 0.0001$). Post-hoc testing showed no statistical difference ($p > 0.79$) between the mean axon diameters for devices C and D. However, devices C and D showed significantly larger mean axon diameters when compared to all of the other devices: A ($p < 0.001$ (C), 0.001 (D)), B ($p < 0.0097$, 0.0072), E ($p < 0.0129$, 0.0095), and F ($p < 0.0441$, 0.0318). All of the mean axon diameter values were less than half that of normal sciatic nerve; however, studies of the kinetics of axon regeneration have revealed that axon diameter is observed to grow steadily over the course of more than one year following injury due to remodeling (den Dunnen et al., 1996; Chamberlain, 1998a).

Device	Mean Axon Diameter [μm]
Normal	8.5 ± 0.2
A	1.77 ± 0.35
B	2.38 ± 0.13
C	3.14 ± 0.09
D	3.21 ± 0.10
E	2.29 ± 0.04
F	2.53 ± 0.02

Table 3.5. Mean axon diameter (Mean ± SEM) for normal nerve, experimental device, and the Integra control device at 9 weeks.

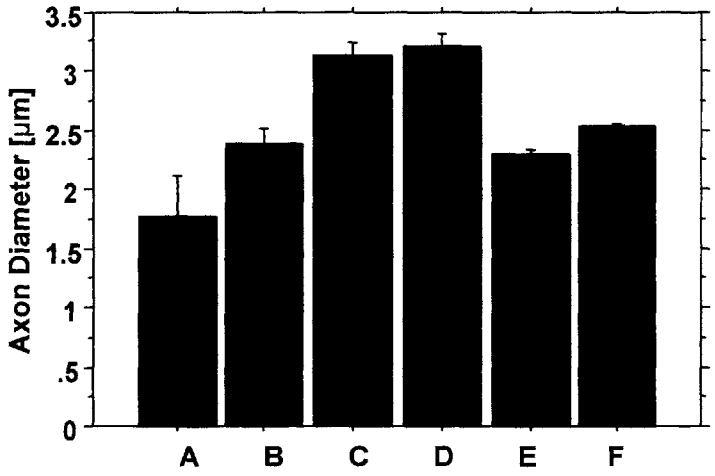

Figure 3.9. Mean axon diameter distribution (Mean ± SEM) for the experimental and control devices. While the number of regenerated axons remains relatively the same between experimental groups, there is a significant difference in the diameter of regenerated axons due to different crosslink densities.

Percentage of Large Diameter Fibers

The term "Large Diameter Fibers" describe the myelinated axons with fiber diameters greater than or equal to 6 μm; these axons are also termed 'A'-fibers and have been shown to have faster

conduction velocities and improved functional performance compared to smaller nerve fibers (See Chapter 1 for a more in-depth description). In contrast to the kinetics of axon formation (with growth and plateau regions), the total number of A-fibers increases at an relatively constant rate over a period of time greater than 1 year (Chamberlain, 1998a). An early time point such as 9 weeks can be used, however, for morphological comparison of the percentage of A-fibers in order to compare the quality of regeneration (Spilker, 2000). The relationship between the percentage of A fibers of each of the experimental and control devices show the same significant differences observed in the mean axon diameter analysis, where devices C and D performed significantly better than the other high solids-content tubes and the Integra control (Table 3.6, figure 3.10).

Device	Percentage of A-fibers [%]
Normal	68.4
A	0.07 ±0.05
B	0.19 ± 0.11
C	2.33 ± 0.68
D	2.25 ± 0.52
E	0.16 ± 0.11
F	0.09 ± 0.05

Table 3.6. Percentage of A-fibers (Mean ± SEM) for the experimental and control group. Percent A-fibers for a normal Lewis rat sciatic nerve was presented by Chamberlain, 1998a.

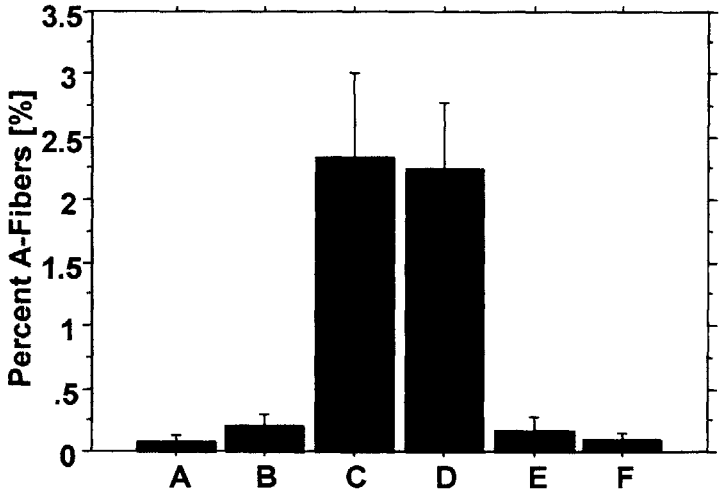

Figure 3.10. Percentage of A-fibers (Mean ± SEM) for the experimental and control devices. There is a significant effect of device crosslinking on the formation of A-fibers during early peripheral nerve regneration

There was a significant difference in the percentage of large diameter fibers observed between the experimental and control groups (ANOVA, $p = 0.003$). All devices showed significantly lower percentages of large diameter fibers when compared to a normal nerve, however. Post-hoc testing revealed that after 9 weeks, devices C and D again resulted in regenerates with superior morphology characteristics (significantly larger percentage of A-fibers) compared to all other devices ($p < 0.005$ for all groups). A significant difference between devices C and D was not observed ($p = 0.88$).

The total number of A-fibers was calculated from the total fascicle area containing myelinated axons, the density of myelinated axons, and the percentage of A-fibers (Table 3.7, Figure 3.11). One-factor ANOVA again revealed a significant difference between the devices ($p < 0.014$); post-hoc testing showed that devices C and D had a significantly larger number of A-fibers per regenerated nerve trunk than all of the other device groups ($p < 0.039$), with the exception of the comparison between devices C and E ($p = 0.055$). Even though the comparison between device C and E was not significant, the data distribution does suggest a difference between the two groups (Table 3.7, Figure 3.11). The total number of A-Fibers in all experimental groups is significantly less than the of number A-Fibers in the normal rat sciatic nerve.

Device	Number of A-fibers per trunk
Normal	4500
A	8.4 ± 5.8
B	17.3 ± 9.0
C	83.1 ± 39.48
D	100.8 ± 18.4
E	12.2 ± 9.0
F	4.0 ± 2.3

Table 3.7. Total number of myelinated A-fibers (Mean ± SEM)

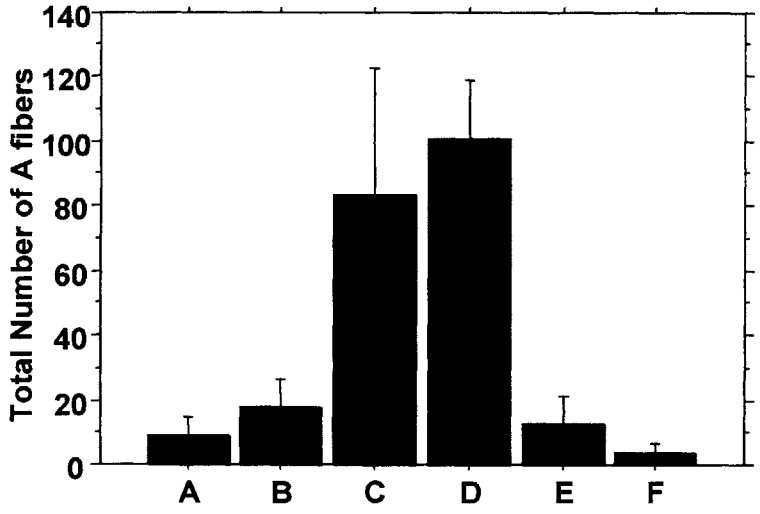

Figure 3.11. Total number of myelinated A-fibers (Mean ± SEM).

N-Ratio

The ratio between the total area of neural tissue (sum of the total axonal area of the nerve trunk) and the total nerve trunk area is the N-Ratio. The N-Ratio is an important measure of the maturity of the regenerating nerve (den Dunnen, et al., 1996). The normal sciatic nerve is densely packed with large, myelinated axons. This dense packing results in the functional characteristics (the amplitude and speed of signal transmission) of a normal nerve, and is described by a high N-Ratio. For the normal Lewis rat sciatic nerve, the N-Ratio is approximately 0.76 (Chamberlain, 1998a). For regenerating nerves, the N-Ratio, like the average axon diameter and the number of A-fibers per nerve trunk, increases continuously as time progresses due to remodeling; in addition the –Ratio at

the distal point of the gap is less than that at the proximal point of the gap for every time point (den Dunnen et al., 1996; Chamberlain, 1998a). The regenerates from the experimental devices displayed a range of N-Ratios at 9 weeks from 0.026 to 0.321, significantly lower than that of a normal nerve (Table 3.8, Figure 3.12).

Device	N-Ratio
Normal	0.76
A	0.07 ± 0.02
B	0.22 ± 0.012
C	0.27 ± 0.02
D	0.32 ± 0.02
E	0.10 ± 0.001
F	0.023 ± 0.01

Table 3.8. Results of N-Ratio calculations (Mean ± SEM) for the experimental device. Normal Lewis rat sciatic nerve N-Ratio courtesy of Chamberlain, 1998a.

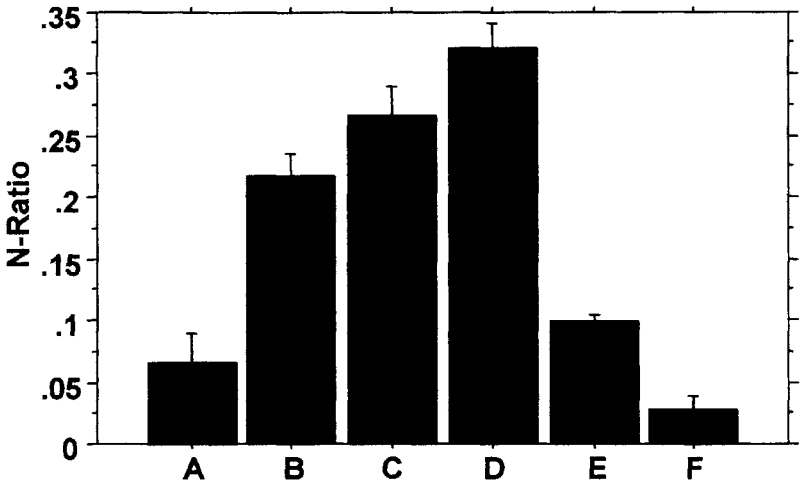

Figure 3.12. N-Ratio (Mean ± SEM) for the experimental and control groups. There is a significant effect of device crosslinking density on the N-Ratio of the regenerates.

One-factor ANOVA indicated a significant difference between the N-Ratio for each of the experimental groups ($p < 0.0001$). Post-hoc testing revealed that device D nerve regenerates showed significantly higher N-Ratios ($p \leq 0.015$) than all other devices except for device C. The data suggests a difference between the N-Ratios of devices C and D, with device D having a greater N-Ratio, but the difference is not significant ($p = 0.0627$).

3.4. Discussion

The degradation characteristics of ECM analogs significantly affects the quality of tissue regeneration (Yannas et al., 1989; Yannas, 2001). For regeneration of peripheral nerves, collagen tubes have been shown to result in improved quality of regeneration compared to other common tube materials such as silicone (Chamberlain, 1998a; Yannas, 2001). In this study, a new high solids-content type I collagen tube was fabricated and the regenerative capacity of a homologous series of

these tubes, each varying in crosslink density, was tested across a 15 mm gap over 9 weeks. Electrophysiology cannot be performed as early as 9 weeks post-implantation; histomorphometric analysis is required to compare the regenerative capacity of devices (Chamberlain, 1998a; Spilker, 2000; Yannas, 2001).

In all of the criteria studies, there was observed to e a large coefficient of variation (because the Standard deviation and hence the standard errors of the mean were large), suggesting the possibility of non-normally distributed data. Due to this, we need to be cautious while examining the results of ANOVA and post-hoc testing. Since the data is not necessarily normally distributed, it is more difficult to make conclusions based upon standard statistical analysis. After considering the variations, I have decided to include all of the statistical analysis above and use it to get a sense of the differences in data; since the differences between data groups were in many cases surprisingly large, we have been able to make conclusions based on this analysis.

Among the devices used for this experiment, the high solids-content collagen tubes with a median density of crosslinks (devices C, D) yielded the most favorable results, with the comparison of N-Ratios suggesting that device D induces a higher quality of regeneration. This collagen tube performed significantly better in a number of morphological assays than the same collagen with different crosslink densities (devices A, B, and E) and better than the experimental control: the Integra NeuraGen tube. Specifically, the measurement of average axon diameter, percentage and number of A-fibers, and the N-Ratio all exhibited the same statistical differences between groups, while the number of myelinated axons showed no significant difference across experimental groups.

The mean fiber diameter and number of large diameter fibers have previously been used in order to assess the quality of peripheral nerve regeneration (Aitken, 1949; Sanders and Young, 1944). In particular, measure of axon size (average diameter, percentage of large axons, N-Ratio) effectively differentiates between experimental groups, while simply the number of regenerated axons cannot (Chamberlain, 1998a; Yannas, 2001).

There are two major differences between the high solids-content tubes and the Integra control. The first difference is degradability, with the high solids-content collagen tubes showing significantly greater degradations rates (see Chapter 4 for this analysis). The other difference between these devices is the initial permeability of the tube walls; the high solids-content tubes were permeable to soluble regulators and cells from the beginning, while the Integra tube was permeable

to only a few small proteins. The high solids-content tubes showed significantly improved performance, compared to the Integra device, quantified by measurements of the average axon diameter, the N-Ratio, and the percentage and number of A-fibers in the regenerated nerves. This difference suggests that device permeability has a large affect on the quality of peripheral nerve regeneration and moreover, that increased permeability at earlier time points increases the quality of regeneration. There is obviously an upper bound to permeability, as an infinitely permeable device (no device) results in the formation of neuroma and a loss of regenerative capacity. Therefore, this analysis suggest that there is an optimum device permeability to maximize peripheral nerve regeneration. While the data suggest the presence of such a maximum, the value of the permeability that induces maximum regeneration is not known,

In addition, variation was observed between the groups of high solids-content devices that formed the homologous series. Since the homologous series varied only by crosslink density, these results suggest that crosslink density plays an important role in device performance. This variation suggested the existence of a specific crosslink density that maximizes the regenerative capacity. What is more likely, however, is that device degradability (mediated by crosslink density) significantly affects the regenerative process, and that there exists an optimum degradation rate that maximizes regeneration. This concept will be treated in greater detail in Chapter 4.

Although at 9 weeks post-implantation the structural characteristics of the regenerates were significantly inferior to that of a normal nerve, past studies of kinetics suggest that remodeling takes place for over a year post-injury, leading to significantly improved structural and functional characteristics. The exception to this monotonic increase in structural characteristics over time is the number of myelinated axons per nerve trunk. This criteria is observed to express both a rising and a plateau phase, where the number of axons per trunk has not been observed to be a statistically significant factor for determining the best quality of regeneration (Chamberlain, 1998a). At 9 weeks, it is possible to compare descriptions of axon size and N-Ratio, but not a description of the total number of myelinated axons per nerve trunk in order to assess the morphological quality of regeneration. Maturation of the regenerating axons has shown that beyond 6 months, even the N-Ratio reaches a plateau (Chamberlain, 1998a).

The gap length is a significant factor that affects peripheral nerve regeneration. The critical gap length for an unfilled silicone tube (a common control in peripheral nerve regeneration) is

approximately 10 mm. The gap length tested in this experiment was 15 mm; only a very small portion of silicone devices tested over this gap would show neural regeneration. However, reconnection of the proximal and distal stumps was observed in all collagen devices in this experiment, regardless of crosslinking treatment. This work identify the significance of device permeability in the process of peripheral nerve regeneration and indicate that the chemistry of the device, specifically the crosslink density and the degradation characteristics, is partially responsible for both the short term and long term ECM analog performance. The next chapter will deal specifically with device performance and the effects of the *in vivo* degradation characteristics of the specific devices.

Chapter 4

Effect of Tube Degradation on Nerve Regeneration

4.1. Introduction

4.1.1. Permeable Devices for Peripheral Nerve Regeneration

The degradation characteristics of ECM analogs used to induce regeneration of skin following severe injury significantly affect the quality of regeneration (Yannas et al., 1989; Yannas, 2001). The optimally degradable device selectively inhibits the contractile processes and works to close the wound through contraction and scar formation while inducing regeneration of new skin tissue to fill the wound (Yannas, 2001). In addition to a question of degradation rate, device permeability will begin to play a significant role in the process of peripheral nerve regeneration. Unlike the devices used to regenerate skin or the conjunctiva, the nerve regeneration template involves the use of a tube; many tubes are impermeable and nondegradable, forming a permanent reaction chamber where the process of regeneration can occur. The benefits of a closed versus an open ("permeable") experimental chamber and the timescale for any transition from impermeable to permeable is poorly understood; the significance of this transition must be better understood in order to design an optimal device for peripheral nerve regeneration. Early analysis concerning the effect of tube permeability on regeneration were resented in Chapter 3.

Previously, a collagen tube that is porous only to proteins smaller than 540 kDa (Integra NeuraGen) has shown the ability to induce regeneration of peripheral nerves over a 10 mm gap to the level achieved by autograft (Chamberlain, 1998). This device has been treated with gaseous formaldehyde as a crosslinking agent, resulting in a highly crosslinked device with a very slow *in vivo* degradation rate (Archibald et al., 1995; Chamberlain, 1998a; Spilker, 2000; Yannas, 2001). As the degradation rate of a crosslinked collagen matrix has been found to be inversely proportional to the density of crosslinks (Yannas et al., 1975), variation in the density of crosslinks of a collagen tube for peripheral nerve regeneration is a useful technique to significantly affect the degradation characteristics of the device.

The formation of a contractile capsule following injury has been implicated in the formation of a neuroma, or neural scar, that blocks the process of regeneration. Neuroma formation is an irreversible repair process that caps the nerve with nonphysiological tissue (scar); once a neuroma appears, peripheral nerve regeneration is no longer possible. In addition, contractile forces are observed at sites of severe wounding in the mammal; cells are observed contracting the ECM surrounding severe wounds in the skin (Yannas et al., 1989, Compton et al., 1996), the peripheral nerve (Chamberlain, 1998a; Brau, 2002), the conjunctiva (Hsu et al., 2000), and the kidney (Yannas et al., unpublished data). The contractile forces can have a significant affect on the process of tissue regeneration following injury.

Contractile forces, mediated by α-Smooth Muscle Actin (SMA) expressing myofibroblasts, appear in the peripheral nerve wound site as early as a few days post injury (Brau, 2002) and remain a significant factor for the first few weeks following injury (Yannas, 2001; Brau, 2002). The acute response to injury shows a large increase in the number and distribution of myofibroblasts, but the contractile phenotype is observed as a chronic response to injury and partial nerve regeneration as well (Chamberlain, 1998a). The appearance of SMA expressing myofibroblasts significantly affects the wound site; it has been hypothesized that in the case of severe peripheral nerve injury, these cells form a pressure cuff that surrounds the transected stumps and the tissue extending from the proximal stump toward the distal stump into the gap (Yannas, 2001). The pressure cuff hypothesis predicts that the contractile cells act to compress the stump and any regenerating tissue; if the contraction process is successful, a complete capsule of connective and contractile tissue (neuroma) forms around the transected stump. This hypothesis is currently being tested (Brau at al. 2002). Collagen tubes show a contractile capsule that is considerably thinner (fewer cell layers) when compared to a standard silicone tube (Chamberlain, 1998a; Chamberlain et al, 2000a; Yannas, 2001). In addition, collagen tubes have demonstrated the ability to bridge significantly longer gap lengths (larger L_C) as well as significantly improved regeneration over similar gap lengths when compared to the silicone tube (Archibald et al., 1995; Chamberlain, 1998a; Yannas, 2001).

Device permeability will affect the process of peripheral nerve regeneration by affecting the wound environment. A highly-permeable tube will allow both cells and proteins to flow into and out of the wound site through the tube walls, affecting the cells and growth factors surrounding the regenerating axons.

4.1.2. Permeability Characteristics Affecting Bioactivity

Device permeability can be either directly fabricated into the device (through changes in pore diameter), or introduced indirectly as a result of cellular processes such as degradation. Previous analysis of the new high solid-content collagen tubes fabricated in this laboratory has concentrated on direct methods of introducing permeability by increasing device porosity (Chapter 2). The indirect method of establishing device permeability, varying the degradation rate to change the device permeability over the length of an *in vivo* experiment, has been largely overlooked in the literature. Rapid degradation will lead to a substantial change in tube permeability over time, significantly affecting device functionality in the wound site. The results from Chapter 3 indicate that the new high solid-content collagen tubes significantly improve the quality of regeneration, determined by morphological analysis of the regenerate, compared to the control device during the first nine weeks following transection and that device permeability played a significant role in this difference. Examination of the two devices using the three most significant factors affecting bioactivity of ECM analogs - device material composition, pore volume fraction and diameter, and degradation rate - yields an important area for further investigation. Both the experimental (A, B, C, D, and E) and the control devices (F) are fabricated from type I bovine collagen supplied from Integra LifeSciences Corp. There are two significant differences between the experimental devices and the control device: the pore volume fraction and diameter and the device degradation rate.

The experimental collagen tubes had an average pore diameter of 80 - 100 μm while the Integra (control) device had an average pore diameter in the nanometer range. This difference can be described either as a direct difference in permeability or as a difference in device pore size. Studies of device performance, however, showed a significant difference between the control and the high solids-content collagen tube; there was a significant difference in the peripheral nerve regenerate morphology observed within groups of high solids-content tubes as well, suggesting that the difference in pore diameter and initial permeability is not the only factor affecting regeneration. The experimental groups were part of a homologous series of devices, where all components of the devices were constant except for the crosslink density and hence degradation rate. The degradation rate of the collagen devices is negatively correlated with crosslink density (Yannas et al., 1975); these observations suggest that the *in vivo* degradation rate of the devices may significantly affect the quality of peripheral nerve regeneration.

4.1.3. Project Goal

The objective of this study was to evaluate the affects of the device degradation characteristics and permeability on the process of peripheral nerve regeneration following severe injury (transection) to the sciatic nerve. A homologous series of collagen devices were fabricated in the laboratory according to procedures defined in Chapter 2 and Appendix A. This homologous series consisted of identically fabricated devices that different only in the density of crosslinks. These devices were assigned the labels A, B, C, D, and E, where device A had the lowest density of crosslinks (and highest theoretical degradation rate), and device E the highest density of crosslinks (and the lowest theoretical degradation rate). In addition, a control device, the Integra LifeSciences NeuraGen tube, was used due to prior experimental study that identified this device as having superior regenerative capabilities compared to most standard control devices such as a silicone tube (Chamberlain, 1998a; Spilker, 2000; Yannas, 2001). The variable crosslinking densities were chosen to result in a wide range of degradation characteristics. Follow device fabrication, the tubes, filled only with sterile saline, were implanted into a 15 mm gap in a sciatic nerve wound model in the adult Lewis rat (See Chapter 3 and Appendix B for greater detail of these procedures). Histomorphometric analysis of cross sections taken from the midpoint of the gap following a nine week period of implantation was performed to determine the quality of peripheral nerve regeneration and to determine a fundamental understanding of the degradation characteristics of each device.

4.2. Materials and Methods

4.2.1. Peripheral Nerve Regeneration Devices and Animal Model

This experiment examining the effect of tubular device degradation rate on the quality of peripheral nerve regeneration is part of the work detailed in Chapter 3. The experimental and control devices, the surgical and animal models, and the raw data are those described in Chapter 3. The difference is that the data will be sorted not by device identifier (A - F), but rather by degradation rate. The five experimental and one control group of devices (Table 4.1) were tested using a single-anastomosis wound model in the adult, female Lewis rat with a gap length of 15 mm.

Device	Crosslinking
A	Collagen tube; Not crosslinked
B	Collagen tube; DHT 90°C, 24 hours
C	Collagen tube; DHT 90°C, 48 hours
D	Collagen tube; DHT 120°C, 48 hours
E	Collagen tube; EDAC crosslinked
F	Integra NeuraGen; gaseous formaldehyde

Table 4.1. Devices used for remaining mass experiment. Fabrication and characterization details provided in Chapter 3.

The devices were implanted for a period of 9 weeks; at the end of this period, the animals were sacrificed by carbon dioxide inhalation, and the regenerate as well as any remaining device was removed from each animal and fixed for histological preparation and analysis.

4.2.2. Remaining Mass Analysis Methods

Following sacrifice, the whole regenerated nerve and remaining tube were fixed in Yanoff's fixative and then stored at 4°C in 70% EtOH. A complete protocol for the methodology used in this process is provided in Appendix A. A 2 - 3 mm segment of the regenerated nerve and surrounding tube was removed from the midpoint of the gap, fixed in 1% osmium tetroxide, embedded in Epon plastic, sectioned at 1 μm thickness, mounted on glass slides and stained with Toluidine Blue. In addition to these preparations at the gap midpoint, cross-sectional segments of the regenerated nerve trunk and remaining tube were taken from the proximal and distal section of the gap for analysis of the remaining mass.

An approximation of the remaining volume of each device can be generated by optical observation of the series of cross-sections of the tissue regenerate and the remaining tube taken from the proximal, medial, and distal areas of each device. In order to calculate the total volume of remaining tube, the cross sectional area measurements were combined with measurements of the total length of the implanted tube as well as the position along the tube where cross sectional area measurements were made. Combined together, these measurements yielded an approximation of the volume of the remaining tube. To generate the cross-sectional area measurements, low

magnification (2 - 5x) images were taken of the proximal and distal segments using a digital camera (Nikon, Japan) attached to a stereo-microscope (Nikon, Japan). In addition, low magnification images were taken of the Epon embedded gap midpoint tissue using the same procedure described in Chapter 3 and Appendix C. The cross sectional area of the remaining mass of the tube was calculated using the public domain software Scion Image in a manner similar to that described in Appendix C for calculating the average morphological characteristics of the axons.

After determining the total volume of the remaining tube per implant, the remaining mass of the device was calculated using the swollen device density calculated in Chapter 2. Percent remaining mass, the ratio of remaining mass to the original swollen mass of the 25 mm implant was then used as a new criteria for comparing device performance. The axon characteristics determined for the experimental and control devices were reclassified in accordance with the percent remaining mass of each device in order to understand the relationship between device degradation rate and quality of regeneration.

4.2.3. Statistical Methods

One-factor analyses of variance (ANOVA) were performed to determine the affect of crosslinking treatment on the morphology of the regenerate. If ANOVA indicated statistical significance, subsequent multiple comparisons were made using the Fisher's PLSD post-hoc test to determine the differences between pairs of experimental groups. The StatView v5.0 (SAS Institute, Inc.) statistical software package was used for all analyses. For all analyses, statistical significance was accepted for $p < 0.05$. All graphical representations are presented with the average value of the data for each group ± the standard error of the means (SEM).

4.3. Results

4.3.1. General Observations

Upon sacrifice at the end of the nine week implantation period, tissue was observed to have bridged the 15 mm gap between the proximal and distal stumps in all experimental and control devices. In addition, it was noted that there was an obvious difference in the amount of the tubular

device that remaining surrounding the regenerated tissue between the different device groups. The EDAC crosslinked collagen tube (device E) and the Integra NeuraGen control device (device F) did not appear to have degraded significantly, with both devices retaining their structural integrity. The dehydrothermally crosslinked devices were in various stages of degradation. No remaining tube was visible for either the non-crosslinked (device A) and the lightest DHT crosslinked (device B) tube, and only a small portion of the tube was visible for devices C and D, the more strongly dehydrothermally crosslinked devices. Prior morphological analysis of the regenerates (Chapter 3) revealed a significant difference in the structure (specifically diameter and N-Ratio) of these regenerates. As the devices were part of a homologous series, varying only in crosslink density and hence degradation rate, the effects of the tube degradation rate on the process of regeneration will now be discussed.

4.3.2. Remaining Mass of Collagen Devices

Gross examination of the regenerates revealed a difference in the remaining volume (and hence mass assuming the steady-state swelling condition identified in Chapter 2 has been reached) of the experimental and control devices (Table 4.2).

Device	Swollen Volume of Intact Tube [mm^3]	Swollen Volume of Degraded 25 mm Long Tube [mm^3]	Percent Remaining Mass [%]
A	230.6 ± 12.2	No Tube Remaining	0
B	124.1 ± 16.2	No Tube Remaining	0
C	115.0 ± 1.4	Small Portions of Tube Remaining	5 ± 5
D	90.7 ± 2.6	11.3 ± 1.4	12.5 ± 1.6
E	134.8 ± 5.0	126.3 ± 4.9	94 ± 3.6
F	116.5 ± 3.5	104.4 ± 3.6	90 ± 3.1

Table 4.2. Calculation of the percent remaining mass of each device following 9 week implantation period. Calculation of remaining mass made using ratio of device volumes. The swollen volume of an intact, 25 mm long tube was calculated from the swelling kinetics and steady state swelling analyses in Chapter 2. The density of the devices was neglected because within the device group, the swollen density remains constant.

This analysis showed that devices A and B had completely degraded within 9 weeks. It is

impossible to identify more precisely the relationship between the degradation characteristics of these devices because remaining mass of the device was not assessed at any time point prior to 9 weeks. In addition, only a small portion of Device C remained visible following explantation and histological analysis. Device C no longer maintained a tubular geometry and existed primarily as small portions of the collagen tube distributed around the outside of the regenerated tissue. For purposes of this qualitative comparison of device degradation, device C was considered to have approximately 5% remaining mass. A much larger portion of the collagen tube was observed for device D at 9 weeks. The tube appeared to have lost a great deal of structural stability, collapsing down around the regenerated tissue, but in many cases along the regenerated nerve still completely ensheathed the tissue. Approximately 12.5% of device D remained intact following the 9 week implantation period. The Integra control (F, ~90% intact) and EDAC crosslinked collagen tube (E, ~94% intact) remained relatively intact following implantation (Figure 4.1). These devices maintained full structural stability and completely ensheathed the regenerating tissue. Comparing the percent remaining mass for devices D, E, and F, one-factor ANOVA followed by post-hoc testing indicated that significantly greater portions of devices E and F remained compared to device D ($p < 0.0001$), but no significant difference in the percentage of remaining device between device E and F ($p > 0.495$) (Figure 4.1).

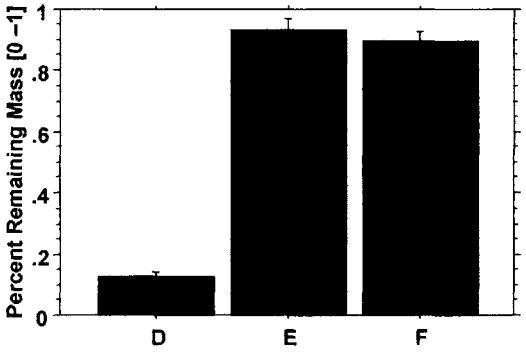

Figure 4.1. Comparison of percent remaining mass for devices D, E, F (Mean ± SEM).

The observed degradation of the experimental and control devices met predictions based on the device crosslink density, where the devices with the lowest crosslink density (and highest swelling ratio) degraded the fastest, while those with the highest crosslink density (and lowest swelling ratio) degraded the slowest.

The remainder of the analyses presented in this chapter will use four distinct groupings for percent remaining mass as a description of device degradation characteristics (Degradation Rate 1, 2, 3, 4) (Table 4.3). The first group is 0% remaining mass (Degradation Rate 1), and is made up of devices A and B. The second group (5% remaining mass, Degradation Rate 2) is made up of device C alone, and the third grouping (12.5% remaining mass, Degradation Rate 3) consists of device D.

The final grouping (90% remaining mass, Degradation Rate 4) consists of both device E and the control group, device F. These two devices were grouped together for the degradation rate analysis because no significant difference between the groups was found ($p > 0.495$). The degradation rate numeric goes in the direction of decreasing degradation rate.

Degradation Rate Identifier	Percent Remaining Mass [%]	Device Identifier (A - F)
1	0	A, B
2	5	C
3	12.5	D
4	90	E, F

Table 4.3. Degradation rate group of the six experimental and control devices based upon the percent remaining mass.

Increasing remaining mass correlates with decreasing degradation rate (Yannas et al., 1975), but it is not possible to identify the exact *in vivo* degradation rate of the individual collagen devices due to the complexity of *in vivo* degradation of collagen (Huang et al., 1977). For this analysis, however, degradation of the different devices will be assumed qualitatively similar, differing only in the rate at which degradation takes place. Based upon this analysis, the observed degradation characteristics of the device supported the hypothesis that increasing crosslink density leads to a decreased degradation rate:

Density of Crosslinks: $\mathbf{A > B > C > D > E, F}$

Hypothesized Degradation Rate (R) Relationship: $\mathbf{R_A < R_B < R_C < R_D < R_E, R_F}$

Observed Degradation Characteristics: $\mathbf{R_A, R_B < R_C < R_D < R_E, R_F}$

4.3.3. Histomorphometry

Four criteria were again used to assess the quality of regeneration: the density and number of myelinated axons, the average axon diameter, the percentage and total number of large axon fibers, and the N-ratio of the nerve trunk. This analysis utilizes the same data analyzed in Chapter 3, using degradation rate (Degradation Rate 1, 2, 3, 4 as the four groupings identified in 4.3.2) rather

than device identifier (A, B, C, D, E, F) as the independent variable. All data is presented, in both tables and graphs, as the mean ± the standard error of the means. This comparison will allow the effect of device degradation rate to be studied.

Number and Density of Myelinated Axons

The number of myelinated axons in a normal sciatic nerve contains approximately 6500 axons, with a myelinated axon density of approximately 0.0144 Ax/μm^2 (Chamberlain, 1998a). A study of the kinetics of peripheral nerve regeneration (Chamberlain, 1998a) indicated that the number and density of regenerated axons at the midpoint along the regenerate nerve axis very rapidly (by 6 weeks) reached a steady-state value at or near the number and density of myelinated axons in a normal sciatic nerve. The number and density of myelinated axons was observed in this study for all experimental device groups to support these previous observations (Table 4.4, Figures 4.2, 4.3).

Degradation Rate	**Number of Myelinated Axons (Mean ± SEM)**	**Density of Myelinated Axons [Ax/μm^2]**
Normal	6500	0.014
1	6370 ± 1180	0.024 ± 0.005
2	2970 ± 500	0.025 ± 0.001
3	4760 ± 370	0.029 ± 0.0018
4	5330 ± 1130	0.010 ± 0.0032

Table 4.4. Number and density [axons/μm^2] of myelinated axons at the midpoint of the regenerated nerve tissue (originally a 15 mm gap) nine weeks following transection (Mean ± SEM).

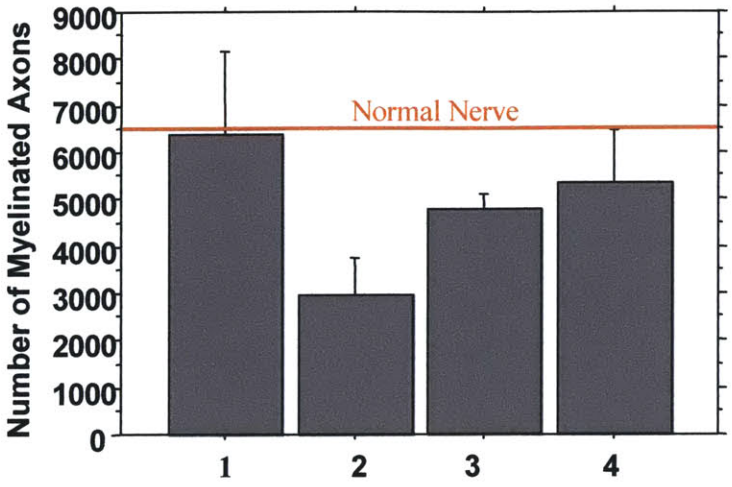

Figure 4.2. Number of myelinated axons in the regenerated nerve trunk (Mean ± SEM)

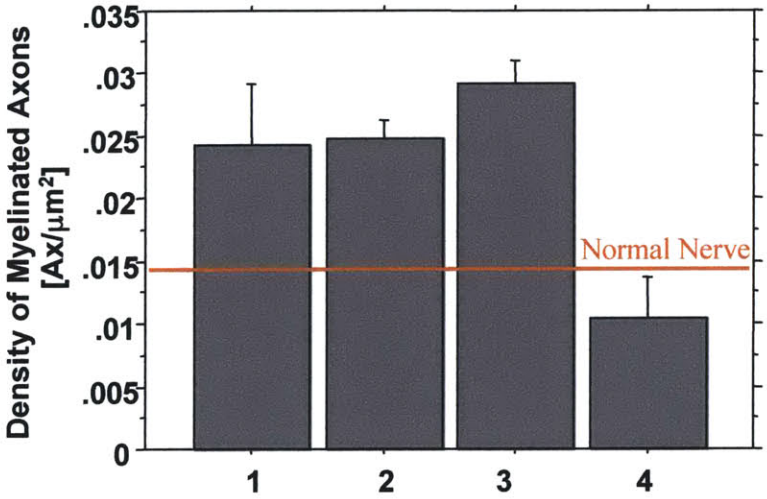

Figure 4.3. Density of myelinated axons in the regenerated nerve trunk (Mean ± SEM)

One-way ANOVA, followed by post-hoc testing revealed a significantly lower density of myelinated axons in the least degraded devices (device E and F) compared to all other devices ($p < 0.0333$); there were no other significant differences between either the number or density of myelinated axons. The significant difference in density is a result of the lack of fascicular definition, particularly in the Integra device, but also to a lesser extent in the EDAC crosslinked device as well was observed in Chapter 3. The lack of tube degradation may have obviated the need for the regenerate to develop into a densely-packed nerve trunk, as it could rely on the inner tube wall to provide the outer surface of the regenerate.

Average Axon Diameter

The average axon diameter for a normal sciatic nerve is 8.2 ± 0.2 μm (Chamberlain, 1998a). The regenerated nerve tissue, with morphological data now sorted by increasing remaining device mass (decreasing degradation rate) show a range of mean axon diameter from 2.0 - 3.2 μm (Table 4.5, Figure 4.4).

Degradation Rate	Mean Axon Diameter [μm]
Normal	8.2 ± 0.2
1	2.05 ± 0.22
2	3.14 ± 0.09
3	3.21 ± 0.10
4	2.43 ± 0.05

Table 4.5. Mean axon diameter for the four groupings of degradable tubes, from highest degradation rate (1) to lowest degradation rate (4).

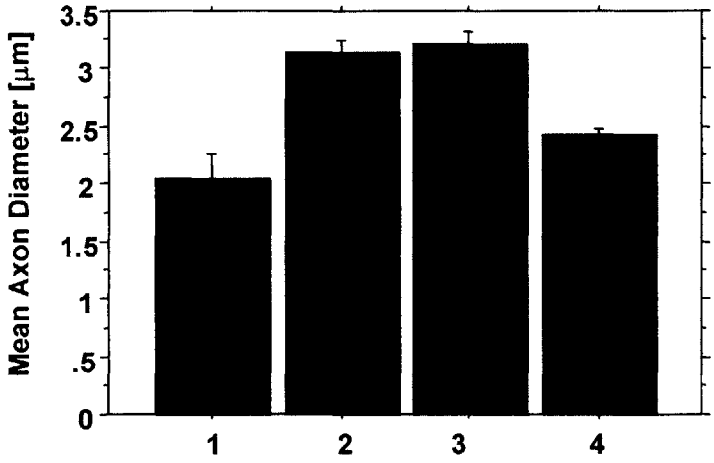

Figure 4.4. Mean axon diameter observed in the four degradation groups (Mean ± SEM)

The mean axon diameter between groups were significantly different (ANOVA, $p = 0.0001$). Post-hoc testing revealed that the devices which degraded rapidly (0% remaining mass, Degradation Rate 1) or very slowly (90% remaining mass, Degradation Rate 2) had significantly smaller mean axon diameters ($p < 0.0125$) than the other devices (5%, 12.5% remaining mass, Degradation Rate 2 and 3). All values reported for mean axon diameter were significantly smaller than those observed in a normal sciatic nerve, but past studies of the kinetics of nerve regeneration suggest that remodeling will result in a significant increase in axon size over an extended period of time (greater than 1 year post-injury).

Percentage of Large Diameter Fibers

The normal sciatic nerve is characterized by the existence of large diameter fibers (A-fibers), with an axonal diameter greater than 6 μm. These axons are responsible for the majority of motor control, and exhibit the fastest conduction velocities. Reappearance of A-fibers is critical for

functional recovery following peripheral nerve injury. The kinetics of axonal regeneration suggest that small diameter axons first attempt to bridge the gap between the transected nerve stumps; if bridging successfully occurs, the axons undergo remodeling where the axons grow in size and definition. Increased motor functionality is observed with time for regenerating axons as a greater portion of the axons become A-fibers. For a normal sciatic nerve, approximately 68.4% of all axons are A-fibers, corresponding to almost 4500 axons per nerve trunk (Chamberlain, 1998a). At 9 weeks post-injury, a range in the number and percentage of A-fibers is observed, where in all cases, the regenerates display significantly smaller numbers and percentages of A-fibers (Table 4.6, Figures 4.5, 4.6).

Degradation Rate	Number of A-Fibers	Percentage of A-Fibers [%]
Normal	4500	68.4
1	12.4 ± 5.1	0.13 ± 0.06
1	83.1 ± 39.5	2.33 ± 0.68
2	100.8 ± 18.4	2.25 ± 0.52
4	7.5 ± 4.0	0.12 ± 0.05

Table 4.6. Number and percentage of regenerated axons per nerve trunk that are A-fibers (Mean ± SEM), sorted by device resistance to degradation.

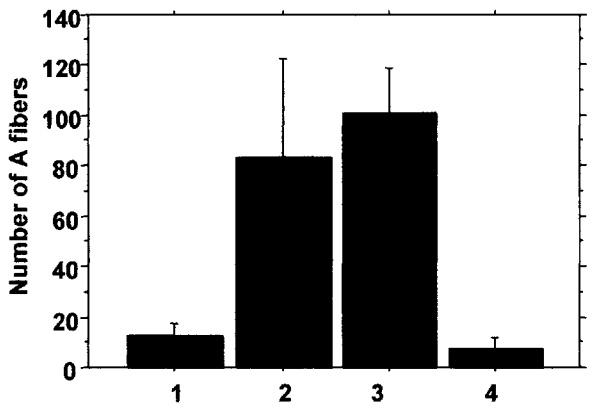

Figure 4.5. Number of A-fibers in each regenerated nerve trunk, sorted by degradation rate (Mean ± SEM).

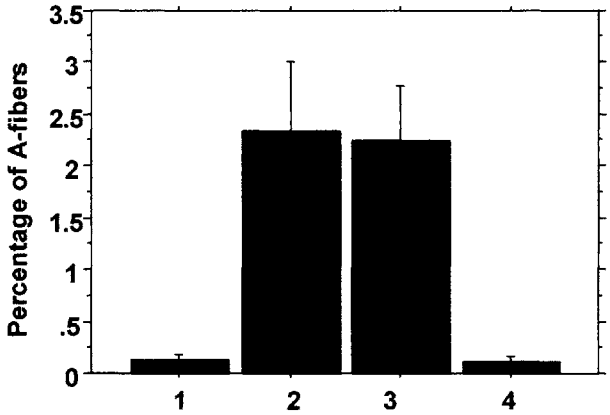

Figure 4.6. Percentage of A-fibers in each regenerate nerve trunk, sorted by degradation rate (Mean ± SEM).

There was a significant difference in the number and percentage of regenerate A-fibers between devices with different degradation characteristics (One-factor ANOVA, $p < 0.002$). Post-hoc testing indicated that there was a significantly lower number and percentage of A-fibers in the devices that degraded either rapidly (Degradation Rate 1, devices A and B) or slowly (Degradation Rate 4, devices E and F) compared to devices which exhibited more moderate degradation characteristics (Degradation Rate 2 and 3, devices C and D) ($p \leq 0.0087$).

N-Ratio

The final morphological criteria examined is the N-Ratio, the ratio of the regenerated neural tissue (axons and myelinated sheath) to the total cross-sectional area of the nerve trunk. This relationship provides a description of the relative maturity of regenerating axons (den Dunnen et al., 1996); the N-Ratio of a normal sciatic nerve is 0.76 (Chamberlain, 1998a), due to the large diameter of the individual axon and the relatively small amount of endoneurial tissue separating the axons. The experimental groups sorted by percent remaining mass were observed to have N-Ratios ranging from 0.06 to 0.32, all significantly lower than that observed in a normal sciatic nerve (Table 4.7, Figure 4.7). The N-Ratio would be expected to increase over time as the regenerated axons and nerve trunks were remodeled.

Degradation Rate	N-Ratio
Normal	0.76
1	0.13 ± 0.03
1	0.28 ± 0.02
1	0.32 ± 0.02
4	0.06 ± 0.02

Table 4.7. N-Ratio for regenerated nerve trunks, sorted by device degradation characteristics.

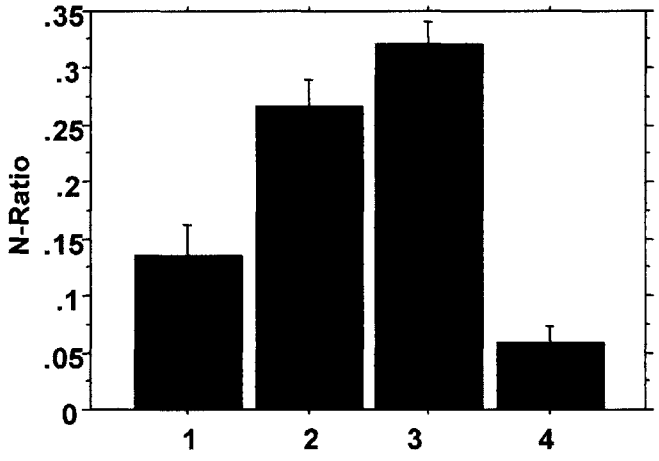

Figure 4.7. N-Ratio of the regenerated sciatic nerve, 9 weeks following injury (Mean ± SEM), sorted by device degradation characteristics.

There was a significant difference in the N-Ratio of the different degradation groups (ANOVA, $p < 0.0001$). Post-hoc testing indicated that, like the analysis of the average axon diameter and the number and percentage of A-fibers, the devices that degraded the fastest (Degradation Rate1, 0% remaining mass, devices A and B) and the slowest (Degradation Rate 4, ~90% remaining mass, devices E and F) performed significantly worse than those device with more moderate degradation characteristics (Degradation Rate 2 and 3, 5%, 12.5% remaining mass, devices C and D); in this case, the devices with moderate degradation characteristics showed significantly larger ($p < 0.001$) N-Ratios. However, as with the comparison offered in Chapter 3.3.2, the N-Ratios of devices C (Degradation Rate 2) and D (Degradation Rate 3) were not significantly different.

4.4. Discussion

Previous work has described an inverse relationship between the crosslink density and the degradation rate of collagen (Yannas et al., 1975). This relationship was again found for collagen tubes used for peripheral nerve regeneration. A homologous series of experimental collagen devices was prepared, where the devices differed only in crosslink density (density of crosslinks for six device configurations: A < B < C < D < E, F). These devices were implanted into a sciatic nerve wound model in a Lewis rat, with a 15 mm gap between transected stumps. After nine weeks, the devices were removed and the quality of peripheral nerve regeneration assayed through morphological analysis (Methodology described in Chapter 3 and in Appendix A and C). In addition, the degradation characteristics were assayed by determining the percentage of the implanted tube that was still surrounded the regenerated tissue. The six experimental and control device configurations could be grouped by percent remaining mass into four sub-populations. The devices displayed degradation kinetics consistent with past observations of crosslink density and degradation rate (Degradation rate of devices: A, B > C > D > E, F). While the *in vivo* degradation rate of the devices cannot be quantified based upon analysis of remaining mass at a single time point, it is possible to qualitatively sort device degradation.

The morphological characteristics of the regenerated axons were quantified based upon the degradation characteristics of the crosslinked collagen tube. There were four grouping describing the percent remaining mass of the device after nine weeks of implantation (Degradation Rates 1, 2,

3, 4: 0%, 5%, 12.5%, and 90% remaining mass, respectively). This work identified the devices that degraded the fastest (device A and B) and the slowest (device E and F) as having significantly smaller average axon diameter, smaller numbers and percentages of A-fibers in the nerve trunk, and smaller N-Ratios compared to those devices with a more moderate degradation rate (device C and D). There was no significant difference ($p > 0.05$) observed between the two devices with moderate degradation characteristics (Degradation Rates 2 and 3). However, comparison of N-Ratios for devices C and D suggested a difference between devices with device D showing a slight increase in performance over device C, even though the difference was not significant.

Degradation of collagen devices used for peripheral nerve regeneration significantly affects the quality of peripheral nerve regeneration. Those devices that degrade rapidly (no tube remaining after 9 weeks) and slowly (~90% of device remaining after 9 weeks implantation) perform significantly worse that those devices with a more moderate degradation rate (5 - 12.5% remaining mass after 9 weeks). There was not a significant difference in any morphological criteria for regeneration between the device groups exhibiting more moderate degradation rate (device C and D), although differences in the N-Ratio suggested that device D was at a higher level of maturity at 9 weeks. This difference was also apparent through gross examination of the axonal and myelin sheath structure of the regenerate, where devices C and D had larger regenerated axons with more a well-defined myelin sheath.

Chapter 5
Conclusions

5.1. Introduction

In this study of peripheral nerve regeneration, I set out to accomplish three objectives: (1) fabricate and characterize a homologous series of high solids-content collagen tubes that vary gradually in crosslink density and hence *in vivo* degradation rate, (2) evaluate these devices to determine their effects on the mechanisms of peripheral nerve regeneration, and (3) use these results to evaluate the effect of implant degradation rate on the mechanisms of peripheral nerve regeneration.

5.2. Collagen Tube Characteristics

The fabrication of the high solids-content collagen tubes and the physical characterization of the devices was described in Chapter 2. The new collagen tubes had a highly porous structure that showed significant differences from the previous industrial grade collagen tube used in our laboratory (Integra LifeSciences Corp.'s NeuraGen tube). The new device had an average pore diameter of 80 - 100 μm, with a pore volume fraction of approximately 90%. The pore size was significantly larger than the pore diameter of the industrial device (~22 nm), and was large enough to be permeable to soluble regulators, proteins, and cells. The pore structure was uniform through the thickness of the tube wall, presenting a consistent ligand environment for integrin-mediated cell binding and migration throughout the device. In addition, variation in crosslink density, mediated by dehydrothermal treatment of the tubes, did not affect the pore average diameter.

The swelling kinetics and the steady-state swelling ratios for the homologous series of collagen tubes and the Integra control tube showed that all devices rapidly reached a steady-state swollen condition when kept in a liquid environment at 37°C; an asymptotic relationship described the kinetics of swelling for all devices, with a time constant of less than 24 hours. The steady-state swelling ratio was also used as a qualitative comparison tool to determine relative crosslink

densities; a more highly crosslinked, and therefore stiffer, collagen matrix swelled less than a matrix with a lower density of crosslinks. As a result of the crosslinking treatments and exposure times (detailed in Chapter 2), the five experimental devices (A - E) were prepared to exhibit gradually increasing crosslink density from device A to device E. Finally, the swelling ratios (both mass and volume ratios) of the devices were used to calculate the swollen density of collagen tubes. The density of collagen tubes significantly increased with crosslink density.

Future studies are necessary to further investigate the use of high solids-content collagen tubes to induce peripheral nerve regeneration. Because the fabrication process can be controlled, these collagen tubes can be further modified to optimize the tubular device for peripheral nerve regeneration. When combined with the previously optimized nerve regeneration template (NRT), an active ECM analog, this composite device is expected to significantly improve the capacity for peripheral nerve regeneration, increasing both the quality of regeneration and the critical gap length. In addition, future studies are necessary to more closely monitor cellular interaction with and migration through the porous collagen tubes. This laboratory has the ability to study cell-matrix interactions with a Cell Force Monitor (CFM) that allows *in vitro* quantification of cell-mediated contraction of the tube material. These observations of cellular interactions with the tube may be critical to understanding the processes of peripheral nerve regeneration.

5.3. Peripheral Nerve Regenerative Capacity of High Solids-Content Collagen Tubes

The peripheral nerve regeneration capacity of the high solids-content collagen tubes fabricated and characterized *in vitro* in Chapter 2 were assayed *in vivo* in Chapter 3. It was determined that the homologous series of collagen tubes showed the ability to regenerate peripheral nerves over a 15 mm gap in the rat sciatic nerve within a nine week experiment; the control used in this experiment was the Integra NeuraGen tube, currently an FDA-approved device that is used clinically and has previously been the laboratory standard. Regardless of the crosslink density, all rats treated with the collagen tube showed tissue bridging of the proximal and distal stumps. Bridging a 15 mm gap was a significant accomplishment for the new collagen tubes; the critical gap length for silicone tubes, a common device used for peripheral nerve regeneration, is only 10 mm

in the rat sciatic nerve, and the majority of gap lengths in the literature is 10 mm due to the decreased performance of many devices over longer gaps. Further morphologic analysis determined that the quality of the regenerated axons varied significantly between tubes with different crosslink densities and the Integra control. The collagen tubes crosslinked dehydrothermally at 90°C for 48 hours (device C) and at 120°C for 48 hours (device D) resulted in regeneration of axonal structure that, while still inferior to the characteristics of the normal sciatic nerve, was significantly better that the other devices in the homologous series and significantly better than the Integra NeuraGen control. As a group, the high solids-content devices regenerated axons significantly better than the Integra control, suggesting that the difference in pore structure and permeability described in Chapter 2 significantly affected the quality of regeneration. In addition, the quality of regeneration varied significantly within the homologous series of devices, suggesting that the crosslink density of the devices (the only parameter varied in the homologous series) significantly affects regeneration.

The Integra device becomes permeable after a long time period due to degradation while the high solids-content collagen tube is cell permeable at implantation. Future studies are necessary in order to follow the migration of cells into and out of the wound site during the process of regeneration in order to gain a better understanding of how device permeability affects the mechanism of peripheral nerve regeneration.

5.4. Effect of Device Degradation of Peripheral Nerve Regeneration

The study described in Chapter 4 revealed significant effects of tube degradation rate on the quality of nerve regeneration. The degradation rate of the devices was determined by quantifying the percent remaining mass of the implanted devices at explantation after nine weeks. While the data were insufficient to calculate a degradation rate per se, the devices could be compared qualitatively. Tubes with a higher percentage of remaining mass were assumed to have a slower degradation rate. Devices with very high (0% remaining mass) and very low (~90% remaining mass) degradation rates were observed to have significantly inferior axon morphology compared with devices that had a moderate (5-12.5% remaining mass) degradation rate. As degradation rate decreased, the morphology of the regenerate was observed to increase in quality towards that of a normal nerve; when the degradation rate was decreased significantly, however, a decrease in quality of regeneration

was observed. The data suggests an optimal tube degradation rate for peripheral nerve regeneration, and this experiment has identified some bounding values for this optimal degradation rate (percent remaining mass of tube at 9 weeks must be between 12.5% and 90%), but this experiment has not illuminating the exact rate that maximizes regeneration. Since tube degradation leads to increased permeability during the process of regeneration, it is suggested that the data are consistent with a conclusion pointing to the existence of both an optimal tube permeability and optimal tube degradation rate for maximizing peripheral nerve regeneration.

Although the high solids-content collagen tube performed significantly better than the Integra control, the nerves regenerated in all tubes remained inferior to normal sciatic nerve. Future studies are needed to assess the regenerative capacity, both through morphologic and functional assays, of these newly fabricated collagen tubes over longer time periods (1 year). While remodeling during that time would result in improved morphology and functionality, future experiments should also continue to assess the impact of cellular permeability on the process of regeneration.

Appendix A
Nerve Conduit Fabrication and Characterization

A.1

Collagen-Glycosaminoglycan (CG) Slurry Protocol

Adapted from Spilker 2000

SUPPLIES

3.6 gm Type I microfibrillar bovine tendon collagen (Integra LifeSciences, Inc., Plainsboro, NJ)
3000 ml distilled, deionized water
8.7 ml Glacial Acetic Acid
0.32 gm chondroitin 6-sulfate (Sigma-Aldrich)

PROCEDURE

1. Turn on cooling system for blender (Granco overhead blender, Granco Co., Kansas City, MO) and allow to cool to 4°C (Brinkman cooler model RC-2T, Brinkman Co., Westbury, NY)

2. Prepare 0.05 M acetic acid (HOAc) solution: add 8.7 ml HOAc (glacial acetic acid, Mallinckrodt Chemical Co., Paris, KY) to 2991.3 ml of distilled, deionized water. This solution has a shelf life of approximately 1 week.

3. Blend 3.6 gm of microfibrillar bovine tendon collagen with 600 ml of 0.05 M acetic acid on HIGH speed setting for 90 minutes at 4°C.

4. Prepare chondroitin 6-sulfate solution: dissolve 0.32 gm chondroitin 6-sulfate (from shark cartilage: Cat. No. C-4384, Sigma-Aldrich Chemical Co., St. Louis, MO) in 120 ml 0.05 M acetic acid.

5. Calibrate peristaltic pump (Manostat Cassette Pump, Cat. No. 75-500-0.00, Manostat, New York, NY) to 40 ml per 15 minutes.

6. Add 120 ml of chondroitin 6-sulfate solution dropwise to the blending collagen dispersion over 15 minutes using the peristaltic pump, while maintaining the blender at HIGH speed setting and 4°C.

7. Blend slurry an additional 90 minutes on HIGH speed at 4°C.

8. Degas the slurry in a vacuum flask for 60 minutes in 1500 ml vacuum flask, until bubbles are no longer present.

9. Store slurry in capped centrifuge bottle at 4°C. Slurry will keep for up to four months.

10. If slurry has been stored for more than one week, reblend the slurry for fifteen minutes on LOW speed setting at 4°C, and degas again.

A.2

Collagen-Glycosaminoglycan Nerve Matrix Manufacture

Adapted from Chamberlain 2000

SUPPLIES

PVC Tubing: 0.25 inches O.D., 0.125 inches I.D.
Silastic silicone tubing: 0.077 inch O.D., 0.058 inch I.D.
Collagen-Glycosaminoglycan Slurry (A.1)
Luer-lock Male adapter plug
Luer-lock x barb tube fitting: 0.0625" tube I.D.
Barb x bard fitting coupling: 0.125 tube I.D.

PROCEDURE

ONE TO TWO DAYS BEFORE FREEZING:

1. Prepare PVC jackets by cutting off 7-cm sections of flexible PVC tubing (0.125 inches ID, 0.25 inches OD) and straighten at 105°C for 2 hours. Puncture the tube with a 20 gauge needle at 90° intervals around the tube and spaced 1 cm apart for the length of the tube.

2. Flush silicone prostheses tubing (Dow-Corning model 602-235 medical grade Silastic 0.058 inch ID, 0.077 inch OD, Dow-Corning Co., Midland, MI) with deionized water (Deionizing Organic Adsorption System, Hydro Services and Supplies, Inc., Durham, NC) and cut off 15-cm lengths.

3. Order a 160-liter liquid nitrogen tank from the MIT Cryogenic lab.

4. Autoclave luer-lock tube fittings (Polypropylene female luer x hose barb, 0.625" I.D., Cat. No. 51525K261, McMaster-Carr Supply Co., New Brunswick, NJ; Polypropylene barbed tube fitting coupling, Cat. No. 5121K13, McMaster-Carr Supply Company).

THE DAY OF FREEZING:

5. Dearate 100ml CG suspension in a 250 ml Erlenmeyer flask at -28mmHg for 30 minutes with agitation or until bubbles are no longer visible.

6. Turn on the uniaxial freezing bath (Loree, 1988) and set the temperature to -80°C. It will take approximately 45 minutes for the bath to reach this temperature.

7. Turn on the freeze drier (VirTis Genesis, Gardiner, NY), and set the temperature to -20°C. Follow the manual freeze-dryer steps below. Place the freeze drier tray in the freezer to cool.

8. Assemble nerve ECM analog mold. Insert female luer x barb coupling (Cat. No. 51525K261) into one end of Silastic tubing. Thread barb x barb fitting (Cat. No. 5121K13) down outside of the Silastic tubing from the end not attached to the luer x barb fitting. Slide barb x bard fitting over end of Silastic tube around luer-lock x barb fitting. This will form a tight seal around the Silastic tubing at that end. Slide PVC tubing down the Silastic tube until it pushes over the end of the barb x barb fitting, also forming a tight seal between the barb and the PVC tubing. Fasten the Locking luer male adapter plug (Cat. No. 5396-02, Abbott Laboratories, N. Chicago, IL) to the female luer-lock x barb coupling. See Figure A.1 for a schematic of assembly and final product.

9. Draw 10 ml of the CG suspension into a 10 ml syringe (Cat. No. 309604, Becton Dickinson & Co., Franklin Lakes, NJ). Expel air bubbles. Attach a 20 gauge needle (Cat. No. 305176, Becton Dickinson & Co., Franklin Lakes, NJ) to the syringe. Insert needle through the resealable membrane of the locking luer male adapter plug. This will allow the needle to be removed after filling the mold without suspension escaping.

10. Inject CG suspension until a few drops come out the free end of the Silastic tubing. Plug the end of the PVC tube opposite the needle with a pipette tip. Inject additional slurry until the silicone tube is pressurized and expands to fill the entire PVC jacket. When the tube is pressurized, **carefully** remove the needle, keeping pressure on the syringe to prevent backflow. Check to make sure the tube is still pressurized (Figure A.2).

11. Attach the large gear to either motor on the freezing apparatus. Tape four prepared PVC jackets to the PVC hanger and place it on the gear train. Lower manually until the pipette tips are just touching the bath. Start the appropriate motor and let the tubes lower into the bath at a velocity of 10^{-4} m/s (Figure A.3). Watch to make sure the tubes are lowering and that they do not stick to any of the parts of the freezing apparatus.

12. When PVC jackets are fully immersed in the bath, turn off the motor and remove the tubes from the bath. Quickly separate the tubes and remove the pipette tips. Cut off the luer lock end of the silicone tube and remove the pipette tip from the opposite end (Be sure to have plenty of new blades handy). Place the tubes on the cooled freeze drier tray (Figure A.3) and put the tray either in the freezer, or in the freeze drier if it has reached -20°C. This step must be done as quickly as possible to ensure that the tubes stay completely frozen.

13. Place the tray containing the frozen tubes in the freeze-drier. Seal the chambers on the freeze drier and close the vacuum outlet tube. Check that the door is sealed shut when the vacuum comes on. After the program is finished, clear the chamber and allow the vacuum to totally release before opening the chamber door. Turn off the unit and remove the tray.

14. Prepare aluminum foil packets for the matrices and place each PVC tube along with the matrix in a packet. Leave one end of the packet open. Place the packets in the dehydrothermal treatment (DHT) at 105°C . Seal the chamber and turn on the vacuum pump. DHT the matrices for 24 hours. Remove the packets and quickly close them. The matrices are now sterile and

must be handled using sterile procedure from this point forward. Store the matrices in a dessicator.

MANUAL FREEZE DRIER STEPS:

1. Turn on the freeze switch and set the shelf temperature to -20˚C.

2. Turn on the condenser (at the same time as step 1) and let it cool until it reaches -45˚C.

3. When the shelf reaches -20˚C, insert the tray containing the frozen tubes.

4. If the condenser is already below -45˚C, turn on the vacuum switch and wait for the vacuum to reach 100mTorr. Make sure that the chamber door seals. It sometimes requires assistance in sealing.

5. Once the vacuum reaches 100 mTorr, turn on the heat switch and set the temperature to 0˚C. Leave the product in the freeze drier for 17 hours at this temperature and pressure.

6. Set the temperature to 20˚C; when the chamber has reached this temperature, turn off the vacuum and turn on the chamber release to release the vacuum. When the vacuum is released, remove the product from the freeze drier. Turn off the freeze drier.

SCHEMATICS

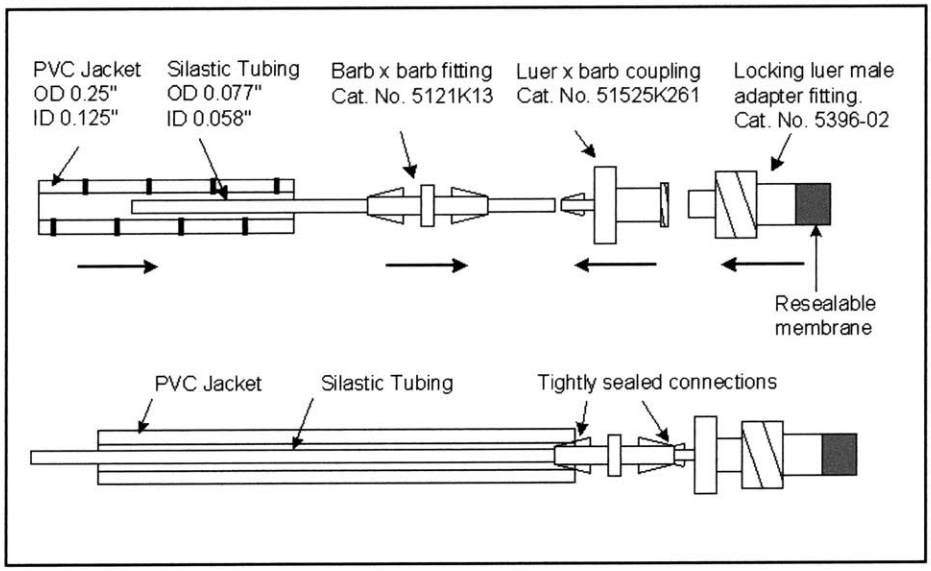

Figure A.1. Assembly and final schematic of mold for fabrication of an ECM analog to enhance peripheral nerve regeneration.

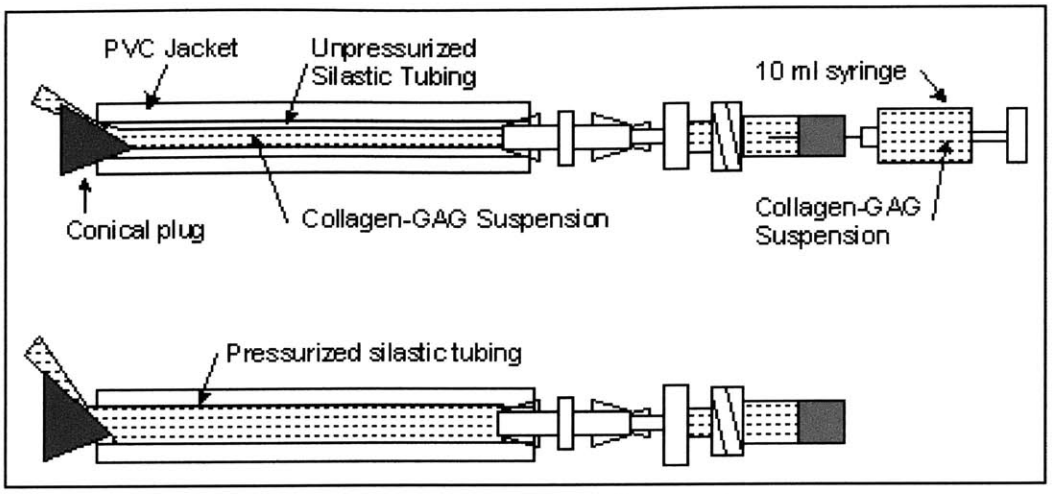

Figure A.2. Pressurizing mold for nerve regeneration template.

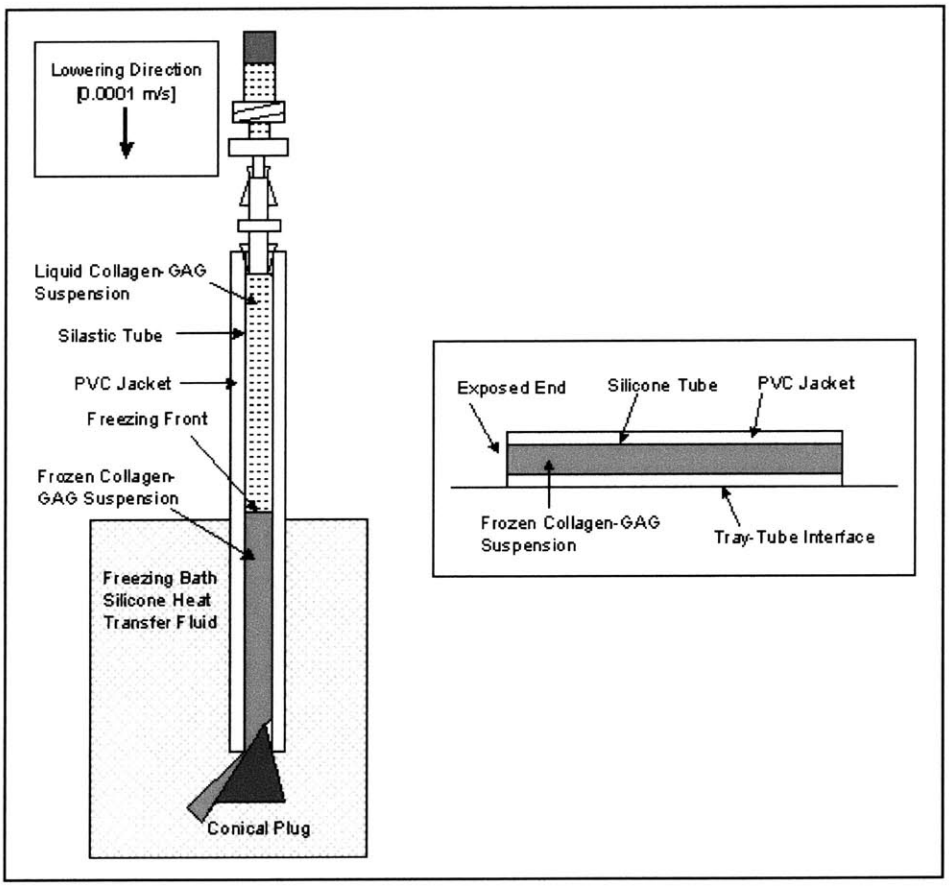

Figure A.3. Freezing and sublimation step orientation of mold to produce nerve regeneration template.

A.3

5% Collagen Tube Fabrication Protocol

SUPPLIES

0.25 gm Type I Collagen
150 µl Glacial Acetic Acid
10 ml Degassed, Distilled Water
0.032" Dia. Stainless Steel Wire
Teflon tubing, O.D. 0.125", I.D. 0.065"
Teflon Tubing, O.D. 0.056", I.D. 0.032"

PROCEDURE

1. Degas 10 ml distilled water for 10-15 minutes

2. In centrifuge tube, mix 150 µl Glacial Acetic Acid [GAA, Mallinckrodt Chemical Co., Paris, KY] with 850 µl degassed, distilled water [ddH_2O], forming 3.0M acetic acid. Draw solution into 3 ml syringe with 22 gauge needle (Cat. No. 309574, Becton Dickinson & Co., Franklin Lakes, NJ).

3. Weigh 0.25 g Type I Collagen (Integra Life Sciences, San Diego, CA). Place collagen into 10 ml syringe (Cat. No. 309604, Becton Dickinson & Co., Franklin Lakes, NJ) that has Parafilm covering luer-lock end. Add 4 ml ddH_2O and mix thoroughly with forceps.

Insert plunger into syringe and invert syringe, allowing collagen mixture to fall away from the syringe tip. Remove Parafilm and mix collagen slurry by moving stopper up and down. Purge air out from tip, bringing plunger up so that slurry comes up to the tip.

4. Slowly inject 1 ml 3.0M acetic acid into collagen, placing the needle from the 3 ml syringe through the tip of the 10 ml syringe with collagen-water suspension. Add the 1 ml acetic acid slowly while mixing with needle tip and pulling back on the 10 ml syringe plunger.

5. Blend slurry well until a homogenous mixture is achieved. Attach 10 ml syringe with collagen slurry to another 10 ml syringe with a female-female Luer-lock assembly (Stainless steel luer lock tube fitting, female luer x female luer, Cat. No. 5194k12, McMaster-Carr Supply Company, New Brunswick, NJ), and mix by injecting collagen slurry from one syringe to another. Mix back and forth 10-15 times, until collagen fibers begin to hydrate and solution appears uniform.

6. After mixing, remove empty syringe and Luer-lock fitting. Cover syringe tip with multiple layers of Parafilm to seal the syringe so that the collagen does not escape during centrifugation.

Do not remove plunger, and let slurry mixture sit for 3 hours at room temperature to allow for the collagen fibers to swell.

After 3 hours, remove plunger, but keep Parafilm over syringe tip.

7. Set Freeze-Drier to -40°C (it takes ≥ 1 hr for freeze-drier to reach set temperature).

8. Centrifuge the collagen slurry in the syringe in order to degas the collagen so that a homogenous collagen slurry without any macroscopic air bubbles if formed. Place the syringe into a 50ml conical tube, using paper towel to brace syringe along the central axis of the conical tube. The centrifugation step may be accomplished using either of the following techniques, depending on the availability of centrifuges:

i) **High speed centrifuge with high g-force rated swinging bucket motor:**
Centrifuge the syringe in a 50 ml Falcon tube at 6000xG for 20 minutes at 25°C.

ii) **Low speed centrifuge with low g-force rated swinging bucket rotor:**
Centrifuge the syringe in a 50 ml Falcon Tube at 4500 rpm (maximum angular velocity) at 25°C in the Heraeus Labofuge 400R in the lab. This angular velocity translates to 3940xG.

9. Inject centrifuged (degassed) collagen slurry into Teflon and aluminum molds (Mold Diameter 3.00 mm; See Figures A.4 and A.5). Inject slurry (~0.25 ml per tube) into closed molds until slurry is apparent on other side. Insert steel and Teflon mandrel into slurry, rotating mandrel during insertion so as to keep the mandrel centered and to maintain a uniform deposition of collagen throughout the mold. Cap the free end of the mandrel with the centering tube after mandrel is fully inserted. Repeat for each mold.

The mandrel is manufactured using a stainless steel wire core (0.032" Dia., Cat. No. GWXX-320-30, Small Parts, Inc., Miami Lakes, FL), surrounded by Teflon tubing (PTFE Tubing, Cat. No. 06417-31, Cole-Parmer Instrument Company, Vernon Hills, IL). Teflon tubing is used at the ends of the mandrel to space the mandrel in the center of the mold (PTFE Special Tubing, O.D. 0.125", I.D. 0.065", Cat. No. 06407-42, Cole-Parmer Instrument Company). Both the mandrels and spacers are autoclaved before use.

10. Place molds in freeze-drier for 1 hour. After freezing, remove the molds from the freeze-drier and split them, gently removing the tubes. Keep the mandrels inside the tubes. Place tubes with mandrels back into the freeze-drier (at -40°C).

11. Pull vacuum in freeze-drier until both readouts are below 100 mTorr (~30-60 minutes).

12. Raise temperature to 0°C and leave overnight under vacuum in freeze-drier (17 hours).

13. Raise temperature to 20°C and release vacuum.

2. Remove tubes (Figure A.6 for final dimensions) with mandrels from freeze-drier and place into aluminum foil bags for storage.

ALUMINUM-TEFLON MOLD SCHEMATIC

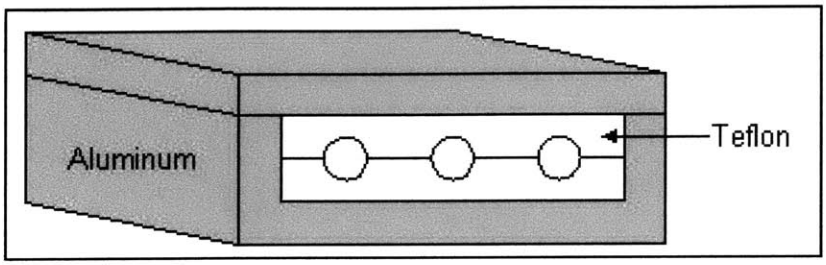

Figure A.4. Basic mold schematic.

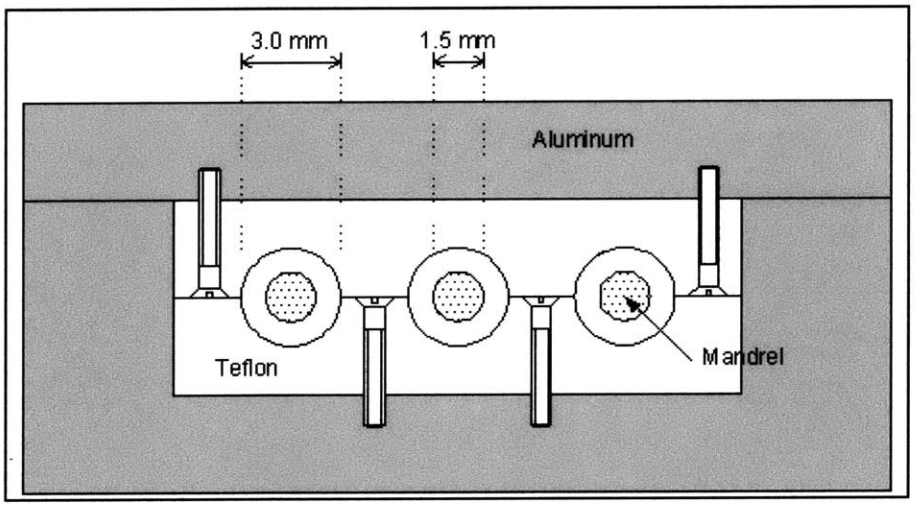

Figure A.5. Schematic of assembly of outer mold leaves and placement of mandrels to form tubular geometry.

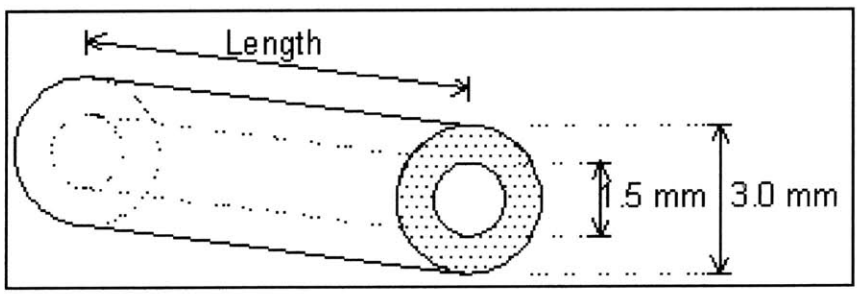

Figure A.6. Final tube dimensions.

A.4

Dehydrothermal Crosslinking Protocol

PROCEDURE

1. Place collagen material in aluminum foil packet. Leave packet open at top.

2. Place packet in vacuum oven (Isotemp Model 201, Fisher Scientific, Boston, MA) at established set temperature. The following settings are for both the collagen-glycosaminoglycan (CG) matrices and for 5% collagen tubes (multiple settings possible).

Matrix	Set Temperature	Exposure Time
CG matrix	105°C	24 hours
5% Collagen Tubes	90°C, 120°C	24 hours, 48 hours

3. Turn on vacuum. The vacuum oven should reach a final pressure of approximately -29.7 mmHg.

4. At the end of the exposure period, turn off the vacuum and cent the chamber. Open the vacuum door and immediately seal the aluminum foil bags. The matrix is now cross linked and considered sterile, so the matrix should only be handled under sterile conditions from now on.

5. Store the matrix in a dessicator. Crosslinked matrices can remain indefinitely in a dessicator prior to testing or use.

A.5

EDAC Crosslinking Protocol

SUPPLIES

0.276g EDAC, [1 ethyl 3-(3dimenthyl aminopropyl)carbodiimide]
0.064g NHS [N-hydroxysuccinimide]

SOLUTIONS

EDAC/NHS Solution

2x Solution: 0.276g EDAC, (Catalog No.E-7750, Sigma-Aldrich Chemical Co., St. Louis, MO)
0.064g NHS, (Catalog No. H-7377,Sigma-Aldrich)
5 ml distilled, deionized H_2O (ddH_2O)

PROCEDURE

1. Sterile filter EDAC solution using 0.2 μm filter (Cat. No. 4192, Pall Gelman Laboratories, Ann Arbor, MI) attached to a 10ml syringe.

2. Incubate the collagen materials in 5 ml sterile ddH_2O in order to hydrate the material.

3. Add 5ml 2x EDAC solution and incubate for 3.5 hours at room temperature.

4. Rinse matrix1x in sterile PBS (Catalog No. P-3813, Sigma-Aldrich), and incubate in fresh, sterile PBS for three hours at room temperature.

5. Rinse matrix twice in sterile ddH_2O.

Note: EDAC is hazardous waste and must be disposed of using the appropriate waste bottle located in the fume hood.

A.6

Sterile Procedure and Implant Assembly Protocols

Adapted from Spilker 2000

PROCEDURE

ONE TO TWO DAYS BEFORE GRAFT PREPARATION:

1. Sterilize the necessary implements:

In Autoclave Bags:

Tool Pack:
- 1 jewelers forceps
- 2 regular forceps
- 1 large forceps
- 1 surgical blade holder
- 1 needle holder

1 glass specimen jar for each prosthesis (Put a small piece of autoclave tape on each jar for labeling purposes later)

1 500 ml glass bottle

(Always keep an extra tool pack and an extra set of specimen jars sterile in case of an emergency. It's easiest to rotate the packs so that they don't sit unused for too long)

Wrap in Autoclave Paper:

1 Teflon sheet for working area (Tape a ruler to the sheet with autoclave tape. This makes cutting easier in the sterile environment)

Dehydrothemally Treat (DHT):

Appropriate tubes for graft preparation. Procedure is the same as with the matrix (see section A.4 for details).

Sterilize Liquid Using ZapCap and autoclaved 500-ml bottle:

Phosphate Buffered Saline Solution (PBS)

2. Turn on the HEPA hood, at least 1 hour before working, preferably 24 hours prior.

GRAFT PREPARATION:

3. Bring necessary sterile implements to workbench:
    All items sterilized in step 1.
    Envelopes with CG matrices
    Envelopes with tubes
    1 ring stand
    4 #10 surgical blades
    1 sterile pipette
    1 sterile pen
    Whirl-Pak bags (1 per prosthesis plus 3; 1 for extra tubes, 1 for extra matrix, 1 for the pen)

4. Put on latex gloves, a cap, a mask and a clean, disposable lab coat. Wipe bench, metal frames and ring stand with 70% ethanol.

5. Using sterile technique, set up sterile field with Teflon pad. Open all tool packs and pour onto sterile field, including prostheses, scalpel blades, etc. Fill each jar with sterile PBS using the sterile pipette (if the prostheses are not going to be implanted for a week or two, fill jar with 70% ethanol for storage. Before surgery, rinse in two rinses of sterile saline solution immediately before surgery). Carefully open Whirl-Pak bags and stand on metal frames in hood.

6. Trim prosthesis tubes to the desired length using scalpel. Remove the matrix from the silicone processing tube by making a careful slit with the scalpel down the length of the silicone and gently pulling out the matrix with the forceps. Trim off any crushed or otherwise damaged matrix and cut remaining portion to the desired length to be inserted into the center of the trimmed tubes. The length of the matrix is 8-mm shorter than the length of the tube.

7. Place prostheses into specimen jars with PBS, close jars tightly, label, place in Whirl-Pak bags, and close bags. Label each prosthesis by type: silicone tube or CG device.

A.7

Collagen Tube Swelling Analysis Protocol

PROCEDURE

1. Sterilely prepare 5% collagen tubes crosslinked as those in the *in vivo* degradation assay (See protocol, Spilker Ph.D. Thesis, 2000). Crosslinked tubes to prepare:

Experimental Devices (High Solid-Content Collagen Tubes):
- Not Crosslinked (Device A)
- DHT Crosslinked, 90°C for 24 hrs (Device B)
- DHT Crosslinked, 90°C for 48 hrs (Device C)
- DHT Crosslinked, 120°C for 48 hrs (Device D)
- EDAC Crosslinked (Device E)

Control Device:
- Integra LifeSciences Corp. NeuraGen tube (Device F)

2. Sterile filter PBS solution (Catalog No. P-3813, Sigma Aldrich Chemical Co., St. Louis, MO).

3. Determine dry weights and dimensions (length and diameter) of all tubes except EDAC tubes (EDAC crosslinking is done in a liquid environment, so the weights and dimensions will be "wet" dimensions). Prior to weighing, establigh an individual identier for each device in order to keep track of the swelling for each particulr deice. Weight collagen tubes on analytic balance in 1.5 ml Eppendorf tubes. Prior to weighing, individually sterilized (Autoclave, 30 min) labeled 1.5 ml Eppendorf tubes (Epi-tube); tare these tubes prior to use. Transfer dry collagen tubes into and out of the Epi-tube in the cell culture hood.

4. In cell culture hood, place each collagen tube into a sterile 2 ml glass vials. Place bottles into in 37°C incubator.

5. Every 24 hours, remove bottle from the incubator. In the cell culture hood:
- •Remove collagen tube from PBS, tap tube on side of a culture dish to remove excess PBS, and place into pre-weighed Epi-tube. Weigh on analytic balance (W_{wet}).
- •Measure approximate tube length and diameter at five locations along the device using a sterized set of calipers. From these measurements, calculate an approximate volume (Vol).
- •Blot collagen tube on sterile filter paper (Autoclave, 25 minutes) for 10 seconds. Place into pre-weighed Epi-tube and re-weigh on analytic balance (W_{blot})

6. Repeat this procedure until both W_{blot}, W_{wet}, and Vol plateau, so that the crosslinked collagen tube is fully swollen (mimic *in vivo* conditions and swelling).

7. Remove collagen tube from PBS-, fix in Yanoff's fixative for 24 hours at 4°C, transfer to 10% Neutral Buffered Formalin for 24 hours at 4°C, and place into 70% EtOH for long term storage (See Spilker Ph.D. Thesis, 2000).

8. Place collagen tube in pre-tared Epi-Tube, and determine weight of swollen, fixed collagen tube. Determine volume of tube by measuring the volume of distilled water displaced by collagen tube and by measuring the outer and inner diameter of the tube at 5 points along the tube's length. Calculate swollen density of crosslinked collagen.

$\rho = \mathbf{m/v}$ $\quad [\rho] \equiv kg/m^3$

$[m] \equiv mg$

$[v] \equiv \mu l\ dH_2O \qquad 1\ \mu l\ dH_2O = 1mm^3$

A.8

Linear Intercept Pore Size Analysis

Adapted from Freyman 2001

PROCEDURE

Image Editing

1. Open Scion Image. Open matrix image and prepare for pore analysis.

2. Under *Options* menu, select "Threshold." Change threshold values until optimal image of collagen struts is visible. Clean up any remaining spots using erase tool. The pore analysis macro will not count any artifact under 5 pixels across, so it is not necessary to remove every stray spot.

3. Under *Process* menu, select "Make Binary" under the "Binary" sub-menu. This will transform the thresholded image into a permanent binary image. Save the image as an edited .tif file.

Pore Analysis

1. Under *Special* menu, select "Load macros", and open the "pore characterization macros."

2. Set the scale for the analysis using the "Set Scale" option under the *Analyze* menu. In addition, under the *Analyze* menu, choose "Options" and select the number of significant digits to be displayed after the decimal point to be 5. The microscope scale is calibrated as follows when using the microscope-camera assembly in the Mechanical Behavior of Materials laboratory (Prof. Lorna Gibson), rm. 8-102:

Objective Magnification	Known Distance	Pixels
4x	1 mm	325.43
10x	1 mm	838.305
40x	1 μm	2.52787
100x	1 μm	8.3842

Table A.1. Calibration scales for Scion Image.

3. Select an area of the image to be analyzed using the oval drawing tool. Try to get as much of the viable image enclosed within the curve.

4. Under "Special" menu, run *Linear Intercept*. The distance between the pore walls along lines at various angles emanating from the center of the selected region. Next, run *Plot Intercepts* macro. This macro will plot the average pore radii into a best-fit ellipse and will calculate linear intercept coefficients C0, C1, and C2.

5. Transfer CO, C1, and C2 data to an Excel spreadsheet for each matrix sample. Calculate the minor (a) and major (b) axes of the ellipse as well as the aspect ratio using the following equations:

$$a = \frac{1}{\sqrt{C_0 + \sqrt{C_1^2 + C_2^2}}}$$

$$b = \sqrt{\frac{\sqrt{C_1^2 + C_2^2}}{C_0\sqrt{C_1^2 + C_2^2} + C_2^2 - C_1^2}}$$

$$AspectRatio = \frac{a}{b}$$

6. Calculate the average pore diameter using the following equation. The twp scaling factors are for a scaling factor associated with the analysis (1.5*) and to change from pore radius to pore diameter (2*):

$$PoreDiameter = 1.5 \times 2 \times \sqrt{\frac{a^2 + b^2}{2}}$$

Linear Intecept Macro Code:

```
macro 'Linear Intercept'
{This macro measures the linear intercept distance over a given ROI
at intervals of angle "ThetaStep"}
var
  left,top,width,height,MinDim,nx,ny,i,j,k:integer;
                ThetaStep,NSteps,PI,x1,x2,y1,y2,dy,dx:real;
  Theta,valx,valy,plength,scale,AspectRatio:real;
   IntLength,LineSum,dummy:real;
  Intercepts:integer;
   switch,indicator:boolean;
   unit:string;
begin
```

```
SetOptions('User1;User2');
GetRoi(left,top,width,height);
if width=0 then begin
  PutMessage('Selection required.');
  exit;
end;
if width<height  then MinDim:=width
  else MinDim:=height;
PI:=3.141592654;
GetScale(scale,unit,AspectRatio);
NSteps:=18;{GetNumber('Enter # steps between 0 and 90 deg.',3,0);}
ThetaStep:=PI/(2*NSteps);

{block out next line when doing cumulative measurements}

SetCounter(2*NSteps);
SetUser1Label('Theta(rad)');
SetUser2Label('Lx10^3');
for j:=0 to 2*NSteps-1 do begin
  LineSum:=0;
  Intercepts:=0;
  x1:=left;
  y1:=top;
  Theta:=j*ThetaStep;
 nx:=10*sin(Theta)*width/height;
 ny:=10*abs(cos(Theta));
  for i:=0 to nx do begin
   if Theta=0 then begin
            x1:=left;
            x2:=x1+width;
   end  else begin
            x1:=left+(width*i/(nx+1))+width/(2*(nx+1));
            x2:=x1+(height*cos(Theta)/sin(Theta));
          end;
   y2:=top+height;
   if x2>=left+width then begin
      x2:=left+width;
      y2:=y1+(x2-x1)*sin(Theta)/cos(Theta);
   end  else if x2<left then begin
                x2:=left;
                if Theta>PI/2 then   y2:=y1+(x2-x1)*sin(Theta)/cos(Theta);
               end;
    {plength is the length of the line to be drawn in pixels}
    plength:=sqrt(sqr(x2-x1)+sqr((y2-y1)/AspectRatio));
    valx:=x1;
    valy:=y1;
   dx:=(x2-x1)/plength;
   dy:=(y2-y1)/plength;
```

```
   switch:=true;
   if plength>=MinDim then begin
   LineSum:=LineSum+(plength/scale);
    for k:=0 to plength do begin
        if GetPixel(x1+k*dx,y1+k*dy)>0
            then indicator:=true
            else indicator:=false;
        if (switch=true) and (indicator=true) then begin
           Intercepts:=Intercepts+1;
           switch:=false;
        end;
        if  (indicator=false) then switch:=true;
     end;
  end;
 end;
for i:=1 to ny do begin
   if Theta<=PI/2 then begin
           x1:=left;
           x2:=left+width
     end  else begin
           x1:=left+width;
           x2:=left;
     end;
   y1:=top+height*i/(ny+1);
   y2:=y1+(width*sin(Theta)/abs(cos(Theta)));
    if y2>top+height then begin
     y2:=top+height;
     x2:=x1+((y2-y1)*cos(Theta)/sin(Theta));
    end;
    {plength is the length of the line to be drawn in pixels}
     plength:=sqrt(sqr(x2-x1)+sqr((y2-y1)/AspectRatio));
   valx:=x1;
    valy:=y1;
   dx:=(x2-x1)/plength;
   dy:=(y2-y1)/plength;
   switch:=true;
   if plength>=MinDim then begin
   LineSum:=LineSum+(plength/scale);
   for k:=0 to plength do begin
        if GetPixel(x1+k*dx,y1+k*dy)>0
            then indicator:=true
            else indicator:=false;
        if (switch=true) and (indicator=true) then begin
           Intercepts:=Intercepts+1;
           switch:=false;
        end;
        if  (indicator=false) then switch:=true;
     end;
```

```
      end;
    end;{i}
   IntLength:=LineSum/Intercepts;
  dummy:=rUser2[j+1];
   rUser1[j+1]:=180*Theta/PI;

{to do cumulative measurements, type in 'dummy+ before Intlength in the next line}

   rUser2[j+1]:=IntLength*1000;
  end; {j}
  ShowResults;
end;

Macro 'Plot Intercepts'
{This macro plots the linear intercept distance as a function of angle
in cylindrical coordinates
It then finds the best-fit ellipse to a set of linear intercept distance vs. angle data
using multiple linear regression of the equation Y=C0+C1*X+C2*Z, where
Y=1/L^2 ,  where L is one half  the linear intercept distance at Theta
X=cosine(2*Theta),    Z=sine(2*Theta)
C0=(Mii+Mjj)/2 , C1=(Mii-Mjj)/2 , C2=Mij.
The objective is to solve for M11, Mjj, and Mij
The best-fit ellipse it then plotted on top of the linear intercept measurements}

var
   left,top,width,height,X0,Y0,X1,Y1,i,n:integer;
   pscale,aspectRatio,dx1,dx2,dy1,dy2,maxdim:real;
   unit:string;
  sumX,sumY,sumZ,sumXZ,sumXY,sumYZ,sumZsqr,sumXsqr:real;
  C0,C1,C2,Mii,Mjj,Mij,Y,X,Z,PI,Theta1,Theta2,L1,L2:real;

begin
  PI:=3.141592654;
 SaveState;
  SetForegroundColor(255);
  SetBackgroundColor(0);
  width:=400;
  height:=400;
  maxdim:=0;
  for i:=1 to rCount do begin
    if rUser2[i]>maxdim then maxdim:=rUser2[i];
  end;
  pscale:=.8*(width+height)/(2*maxdim);
  SetNewSize(width,height);
  MakeNewWindow('Linear Intercepts vs. Theta');
  SetLineWidth(1);
  X0:=(width/2);
  Y0:=(height/2);
```

```
  MakeLineROI(0,Y0,width,Y0);
  Fill;
  MakeLineROI(X0,0,X0,height);
  Fill;
   for i:=1 to rCount do begin
    dx1:=pscale*0.5*rUser2[i]*cos(rUser1[i]*PI/180);
    dy1:=pscale*0.5*rUser2[i]*sin(rUser1[i]*PI/180);
    if i<rCount then begin
      dx2:=pscale*0.5*rUser2[i+1]*cos(rUser1[i+1]*PI/180);
      dy2:=pscale*0.5*rUser2[i+1]*sin(rUser1[i+1]*PI/180);
    end else begin
      dx2:=-pscale*0.5*rUser2[1]*cos(rUser1[1]*PI/180);
      dy2:=-pscale*0.5*rUser2[1]*sin(rUser1[1]*PI/180);
    end;
    MoveTo(X0+dx1,Y0+dy1);
    LineTo(X0+dx2,Y0+dy2);
    MoveTo(X0-dx1,Y0-dy1);
    LineTo(X0-dx2,Y0-dy2);
  end;
  n:=rCount;
  sumX:=0;
  sumY:=0;
  sumZ:=0;
  sumXY:=0;
  sumYZ:=0;
  sumXZ:=0;
  sumZsqr:=0;
  sumXsqr:=0;
  for i:=1 to n do begin
    Y:=1/(sqr(rUser2[i]/2));
    X:=cos(2*PI*rUser1[i]/180);
    Z:=sin(2*PI*rUser1[i]/180);
    sumX:=sumX+X;
    sumY:=sumY+Y;
    sumZ:=sumZ+Z;
    sumXY:=sumXY+(X*Y);
    sumYZ:=sumYZ+(Y*Z);
    sumXZ:=sumXZ+(X*Z);
    sumZsqr:=sumZsqr+sqr(Z);
    sumXsqr:=sumXsqr+sqr(X);
  end;
  C1:=((sumXY*sumZsqr)-(sumXZ*sumYZ))/((sumXsqr*sumZsqr)-sqr(sumXZ));
  C2:=((sumYZ*sumXsqr)-(sumXY*sumXZ))/((sumXsqr*sumZsqr)-sqr(sumXZ));
  C0:=(sumY/n)-C1*(sumX/n)-C2*(sumZ/n);
NewTextWindow('Results');
writeln('C0 = ',C0);
writeln('C1 = ',C1);
writeln('C2 = ',C2);
```

```
  for i:=1 to rCount do begin
    Theta1:=rUser1[i]*PI/180;
    if i<rCount then Theta2:=rUser1[i+1]*PI/180
     else Theta2:=rUser1[1]*PI/180;
    L1:=1/sqrt(C0+C1*cos(2*Theta1)+C2*sin(2*Theta1));
    L2:=1/sqrt(C0+C1*cos(2*Theta2)+C2*sin(2*Theta2));
    dx1:=pscale*L1*cos(Theta1);
    dy1:=pscale*L1*sin(Theta1);
    if i<rCount then begin
      dx2:=pscale*L2*cos(Theta2);
      dy2:=pscale*L2*sin(Theta2);
     end else begin
      dx2:=-pscale*L2*cos(Theta2);
      dy2:=-pscale*L2*sin(Theta2);
    end;
    MoveTo(X0+dx1,Y0+dy1);
    LineTo(X0+dx2,Y0+dy2);
    MoveTo(X0-dx1,Y0-dy1);
    LineTo(X0-dx2,Y0-dy2);
  end;
end;
```

Appendix B
Implantation and Removal Protocols

B.1

Surgical Protocol

Adapted from Spilker 2000

SUPPLIES

1. Order animals: Adult, female Lewis rats, 150 - 175 grams, from Charles River Laboratories. Animals must arrive at least one week in advance of surgery to reduce the stress placed on the animal due to travel.

2. Sterilize the necessary items:

- 1 metal bowl
- gauze
- 1 surgical blade holder
- 1 micro-needle holder
- 1 micro-scissors
- 2 jewelers forceps
- 1 large forceps
- 1 large scissors
- 1 surgical (tenotomy) scissors
- 2 paper clip retractors
- 2 forceps
- 1 needle holder
- animal skin staples
- wooden rods (cotton swabs)

3. Ready other sterile items:

- sterile table covering
- scalpel blades (4 #15 blade, 1 #11 blade)
- 1 bottle of PBS
- iodine sponge
- sterile draping
- Implants (sterilized and prepared as in section A.3)
- 1 bottle pentobarbital (Nembutal Sodium Solution), 50mg/ml
- sterile pen
- 10-0 sutures
- 4-0 sutures
- 1 ml syringes
- 1 bottle Lidocaine, 1%

4. Ready other non-sterile items:

- surgical board
- 4 rubber bands
- rat ear tagging tool
- numbered ear tags
- microsurgery glasses (loops)
- hair clippers

PROCEDURE

1. Weigh animal on an appropriately sized balance. Record the weight and determine anesthetic dosage based on the pre-operative weight.

2. Anesthetize animal with injection of sodium pentobarbital (50 mg of solution per kg of animal). Allow 10-15 minutes for anesthesia to take effect. Each animal reacts differently to the

anesthetic and in some cases, more time may be required.

3. Meanwhile, arrange the surgical area so that the table is at a comfortable level for the surgeon, and the tools are conveniently located.

4. The surgeon should be sterilely dressed in scrub shirt and pants, hat and mask.

5. When ready, shave the animal using the animal hair clippers from the base of the tail up to the middle of the back. The leg receiving the prosthesis should be shaved carefully and completely.

6. Place the animal on the surgical board in the prone position and secure the fore and hind limbs to the board using rubber bands. The hind legs should be in 30° abduction. Place a piece of gauze under the appropriate thigh to elevate the leg slightly.

7. Clean the shaved portion of the animal vigorously with the iodine sponge to disinfect the area. At this point, the surgeon should put on the sterile gloves and remain sterile for the rest of the procedure. Cut a hole in the sterile draping small enough so that only the leg is exposed. Place the draping over the animal.

8. Using the #15 scalpel, make a 4 cm incision along the leg of the animal. Separate the skin from the muscle along the incision by cutting through the connective tissue with the surgical scissors.

9. Using the surgical scissors, separate the muscles until the sciatic nerve is visible. Carefully cut back the muscle along the skin incision line exposing the sciatic nerve.

10. Place the paper clip retractors inside the muscle to separate the wound edges. Anesthetize the nerve by placing a few drops of Lidocaine directly on the area. Cut away the fascia surrounding the sciatic nerve carefully so that the nerve is free from constraint.

11. Transect the nerve midway between the proximal nerve trunk and the distal bifurcation using microscissors. Measure the prosthesis and make a mark 5 mm in on each end. Place the tube in the gap and insert the proximal nerve stump 5 mm into the tube end, as marked. Secure the nerve in place by using two 10-0 sutures which travel through the epineurium and then through the tube. Tie the sutures with four single knots. Insert the distal nerve end 5 mm into the other end of the tube and secure in the same manner.

12. In the case of the cross-anastomosis procedure, the sciatic nerve in the opposite hind limb is similarly exposed and transected. The two skin incisions are then joined across the rat's back using a scalpel blade.

13. The dorsal spinous processes are removed using bone rongeurs to create a trough to make space for the tube implant to be routed over the back.

14. The proximal left sciatic nerve stump is bridged to the distal right nerve stump with a tube

implant over the back.

15. For both single-leg and cross-anastomosis procedures, the paper clip retractors are removed. Close the muscle using three 4-0 sutures. Close the skin using two 4-0 sutures and three skin staples.

16. Place the animals back in the cage and observe frequently until they are awake.

B.2

Post-Operative Care and Supervision Protocol

SUPPLIES

Buprenorphine, 0.15mg/ml
1 ml syringe
27 gauge needle

PROCEDURE

1. Monitor rats immediately following surgery. Analgesic is to be started immediately following surgery while the rat is still under anesthesia. Inject 0.1 ml 0.15mg/ml Buprenorphine (approx. 0.1 mg/kg, Cat. No. 40182C, Lyphomed, Deerfield, IL) subcutaneously.

2. Place rats into individual cages for first week following surgery. Place food and gel-packs for hydration onto floor of cage for rat for the period immediately after the surgery.

3. Repeat analgesic injections twice a day for 48 hours following surgery. Continue to monitor eating and drinking and general condition of animals.

4. Monitor rats twice a day for one week following surgery. At 7 days post-operation, combine rats two to a cage, and switch to observing once a day for length of experiment.

B.3

Animal Sacrifice and Tissue Processing Protocol

Adapted from Spilker 2000

EQUIPMENT

Surgical instruments
15-ml Falcon tubes (1 for each animal)
Digital camera to take gross photographs
Container with ice

SOLUTIONS

Yanoff's Fixative

Stock Solutions

Stock A: 1.67 grams Monobasic Sodium Phosphate NaH_2PO_4
8.95 grams Dibasic Sodium Phosphate Na_2HPO_4
960 ml Distilled H_2O
40 ml 25% Glutaraldehyde

Stock B: 4.0 grams Monobasic Sodium Phosphate NaH_2PO_4
8.95 grams Dibasic Sodium Phosphate Na_2HPO_4
900 ml Distilled H_2O
100 ml 38-40% Formaldehyde

Yanoff's fixative is 1:1 mixture of stock A and stock B

10% Neutral Buffered Formalin

Stock B of Yanoff's Fixative is 10% Neutral Buffered Formalin.

70% EtOH

SACRIFICE PROCEDURE

1. Sacrifice animals by placing in carbon dioxide chamber for 3-5 minutes.

2. Open the original wound with a #15 scalpel blade The wound can be located by identifying the dermal scar or original suture marks.

3. Open the fascia and muscle to locate the tube implant and the adjacent nerve stumps.

4. Remove the entire tube implant as well as at least 10 mm of proximal and distal nerve tissue including the nerve branches at the distal end.

TISSUE PROCESSING PROCEDURE

1. Place tissue into Yanoff's fixative for 24 hours at 4˚C.

2. Transfer tissue into 10% neutral buffered formalin solution for 24 hours at 4˚C.

3. Remove tissue from formalin and rinse 1x in 70% EtOH.

4. Photograph the nerve to capture the gross morphology of the tissue.

5. Section the nerve into segments according to Figure 2.3.

6. Place each small nerve segment into an individual vial containing 70% EtOH. Each tissue segment will be either embedded in Epon or stored in 70 EtOH for future use.

Appendix C
Histological Analysis Protocols

C.1

Epon Embedding Protocol

Adapted from Spilker 2000

SOLUTIONS

Cacodylate Buffer (pH 7.4)

Stock Solutions:

Stock A (0.2 M Sodium Cacodylate - mw 214):	4.28 grams Sodium Cacodylate 100 ml of Distilled Water
Stock B (0.2 M HCl - mw 36.46):	1.7 ml HCl 100 ml of Distilled Water

Composition of Buffer:
25 ml of Stock A + 1.4 ml of Stock B (for pH 7.4)* + 73.6 ml Distilled Water
* = Volume of Stock B changes for different pH levels

Final Molar Composition of Buffer:
0.05 M Sodium Cacodylate
0.0028 M HCl

Cacodylate Buffered Glutaraldehyde

2% Solution:	8 ml 25% Glutaraldehyde 92 ml Cacodylate Buffer (pH 7.4)

Cacodylate Buffered Sucrose Solution

0.2 M Solution:	6.846 grams Sucrose - mw 342.3 100 ml Distilled Water

Osmium Tetroxide (Catalog No. 251755, Sigma-Aldrich, St. Louis, MO)

1% Solution:	2 ml 4% Osmium Tetroxide 6 ml Distilled Water

Poly/Bed 812 Embedding Kit (Catalog No. 08792, Polysciences, Inc., Warrington, PA)
Half Portion:

	Catalog #	Standard Formula	Slightly Harder
Poly/Bed 812	08791	24 ml	23.5 ml
DDSA	00563	15.5 ml	14.3 ml
NMA	00886	10.5 ml	12.0 ml
DMP-30*	00553	1.0 ml	1.0 ml

DMP-30* = The hardener component. Added just before use in final stages (step 9 and 10) only, not for initial infiltration stages.

EMBEDDING PROCEDURE

1. Soak nerves in 2% cacodylate buffered glutaraldehyde overnight at 4°C.

2. Soak nerves in 0.2 M cacodylate buffered sucrose solution overnight at 4°C.

3. Rinse nerve 1 time in cacodylate buffer for 10 minutes at 4°C.

4. Fix in 1% osmium tetroxide for two hours at room temperature (in the hood).

5. Dehydrate nerves in EtOH:

30%	5 minutes
50%	5 minutes
70%	5 minutes
80%	5 minutes
90%	7 minutes
95%	10 minutes
100%	10 minutes
100%	10 minutes
100%	10 minutes

6. Clear nerves in acetone 2 times, 5 minutes for first exposure, 10 minutes for second.

   BEWARE: Use fresh acetone for procedure. Acetone tends to pick up water overtime, resulting in the formation of micro-pockets of water along surface of nerve, impeding Epon infiltration.

7. Infiltrate in 1:1 acetone/Epon* mixture overnight at room temperature.

   Place extra Epon at 4°C overnight for storage and reuse for Step 8 only. Remove Epon from refrigerator and warm in hands before opening to minimize potential condensation problems leading to addition of water to the Epon. Remake Epon

for Steps 9 and 10 with the hardener.

8. Infiltrate in 1:3 acetone/Epon* mixture for 5 hours at room temperature.

9. Infiltrate in 100% Epon with hardener overnight at rom temperature.

10. Embed with fresh 100% Epon with hardener in TEM molds. Make all labels on computer (Times New Roman, 6 pt font)

11. Let cure 24 hours at 60°C in vacuum oven (standard pressure).

* = During infiltration, the Epon mixture should NOT contain the hardener.

C.2

Paraffin Embedding Protocol

Adapted from Chamberlain 2000

SOLUTIONS

Eosin Y (Cat. No. E-511, Fisher Scientific, Fair Lawn, NJ)
Eosin Stock: 1 gram, Eosin Y
1 Liter, 70% EtOH

Paraplast Plus Paraffin (Cat. No. 5159-464, VWR Scientific, Boston, MA)

PROCEDURE

1. Stain nerves in Eosin for 1 minute. This makes the sections easier to identify during embedding and sectioning.

2. Dehydrate nerves in EtOH:

70%	5 minutes
70%	5 minutes
80%	5 minutes
90%	5 minutes
95%	5 minutes
100%	5 minutes
100%	5 minutes
100%	5 minutes

3. Clear nerves in xylene 2 times for 5 minutes each.

4. Put nerves in tissue cassettes, sandwiched by two blue sponges, and label the cassettes with the appropriate information in pencil.

5. Infiltrate in paraffin bath 2 times for 30 minutes each.

6. Embed in paraffin.

7. Cool and store in refrigerator.

C.3

JB-4 Embedding Protocol

SUPPLIES

JB-4 Embedding Kit (Polysciences, Inc., Warrington, PA)
- JB-4 Embedding Solution A (Cat. No. 0226A)
- JB-4 Embedding Solution B (Cat. No. 0226B)
- JB-4 Catalyst (Cat. No. 02618)

SOLUTIONS

Catalyzed Solution A

100 ml Solution A
1.25 gm catalyst

Equilibration Solution

50:50 solution of Catalyzed A Solution and 100% Ethanol

Embedding Solution

25:1 solution of Catalyzed Solution A and JB-4 Solution B.

PROCEDURE

1. Place pieces of matrix to be embedded into 24 well plate

2. Collagen matrix samples should be dehydrated by hand. Water and alcohol solutions are pipetted in an out of 24 well plate and left at room temperature for 30-60 minutes per step.

Sequence of Solutions
Distilled Water (dH_2O)
dH_2O
dH_2O
50% EtOH
70% EtOH
80% EtOH
95% EtOH
95% EtOH
100%EtOH
100% EtOH
100% EtOH

3. Following dehydration, samples are equilibrated for 12 hours in Equilibrium Solution at 4°C.

4. Infiltrate samples in 100% catalyzed JB-4 solution A at 4°C for 24-96 hours. Change solution every 12 hours. To insure a high degree of infiltration (especially with larger samples), this step should be carried out under house vacuum.

5. Embed samples in Embedding Solution. Mix the solution well and pipet into plastic molds. Place samples face down into plastic molds, ensuring that sample orientation os maintained. The solution begins to harden in approximately 30 minutes. After the JB-4 mixture becomes viscous enough that the samples do not float, place labeled metal or plastic block holders into each well, and place the plastic mold tray in a refrigerator at 4°C overnight.

C.4

Epon Microtome Protocol

PROCEDURE

Epon Microtome - Yannas Lab, 3-315

Trimming Epon Block

1. Place Epon block into sample holder, and screw holder into the baseplate. Place baseplate onto microtome such that it is directly in view when using binocular magnifier.

2. Using a razor blade, remove the excess Epon from around the embedded sample (viewing procedure through binocular magnifiers). For pyramidal structure with flat top (the cut depth need only be approx. 0.3 cm)

3. Using a new razor blade, trim the top such that the Epon is trimmed down to the top of the sample. Take care to avoid creation of nicks or divots in the top surface.

Making Glass Blades

1. The glass cutter is located in the King Lab electron microscopy facility, 66-316

2. Set glass cutter to center score setting (four non-parallel lines on dial). Clamp down glass rod and score the glass. Break glass with pressure to produce square glass prism.

3. Rotate prism 45° and clap in place both horizontally and verticaly. Change scorer setting to **"25"** and score glass. Break glass again with pressure and inspect the triangular prisms for good and/or bad edges. Discard bad blades.

Microtome Procedure

1. Turn on hot plate to 100°C (Fisher Scientific, Boston, MA).

2. Paint nail polish line across angled face of the glass blade, approximately 7-9mm below the blade edge. This creates a hydrophobic surface below the lip of the blade, allowing a water droplet to remain at the blade edge.

3. Fabricate tool using toothpick and individual strand of hair, affixing the hair to the end of the toothpick with nail polish.

4. Using a syringe with a 25 gauge needle, place a water droplet on the knife face and put two large water drops on a labeled microscope slide (separate slide for each sample).

5. Follow the printed direction in the microtome's manual (Sorvall MT-2 Porter Blum Ulteramicrotome, Sorvall Inc,m Norwalk, CT) in order to cut samples at a thickness of 1μm.

6. Use the eyelash tool to pick up individual sections from water droplet below the blade edge. For complete samples, place them onto one of the two water droplets on each microscope slide. After filling both droplets on each slide with approximately 5-8 sections, place the slide onto the hotplate to evaporate the water. The individual Epon slices should stick to the glass slide as evaporation occurs. When the slide is dry, store the slides for staining and coverslipping.

C.5

Toluidine Blue Staining Protocol

Adapted from Spilker 2000

SOLUTIONS

Toluidine Blue Solution (Cat. No. BP107-10, Fisher Scientific, Boston, MA)

1% Solution: 1 gram, Toluidine Blue Powder
1 gram, Sodium Borate Powder
100 ml, distilled, deionized water

Solution should be filtered and stored in a bottle

PROCEDURE

1. Heat the slides on the hot plate to 60 - 80°C (setting about 4.5 on blue VWR 320 plates).

2. Stain with Toluidine Blue Solution for 30 - 60 seconds. Thicker sections will take less time. Use a 10ml syringe (Cat. No. 309604, Becton Dickinson & Co., Franklin Lakes, NJ) with a 0.2μm Acrodisk filter (Cat. No. 4192, Pall Gelman Laboratories, Ann Arbor, MI) to deliver stain onto the slide.

3. Rinse slides in distilled water and allow to dry on hot plate for 2 - 3 minutes. Let slide cool

4. Mount slides using Permount mounting medium (Cat. No. SP15-100, Fisher Scientific, Boston, MA) and let dry overnight.

C.6

Analine Blue Staining Protocol

SOLUTIONS

Analine Blue (Catalog No. 02570, Polysciences, Inc., Warrington, PA)
2.5 g aniline blue
2 ml glacial acetic acid
100 ml distilled, deionized water (ddH_2O)

Filter before use

Acetic Acid
1% Solution: 1 ml glacial acetic acid
99 ml ddH_2O

95%, 100% Ethanol

PROCEDURES

1. All sections to be stained should be embedded in JB-4, sectioned at a thickness of 5 μm, and mounted on standard slides.

2. Dip slides into aniline blue solution for 2-4 minutes (generally 2).

3. Dip in 1% aceti acid solution for 1 minute.

4. Dip 5-10x in 95% ethanol to wash the slide, until most of the background staining disappears.

5. Dip 5-10x in 100% ethanol to complete wash.

6. Allow slides to dry in the hood. Mount with Cytoseal 60 mounting medium (Cat. No. 8310-16, Stephens Scientific) (4 drops) and coverslip. Try not to get any air bubbles under the coverslip.

7. Dry in hood for at least 1 hour. Let dry for two more days on benchtop before use (rather arbitrary).

C.7

α-Smooth Muscle Actin Immunohistochemical Staining Protocol

Adapted from Chamberlain 2000

SOLUTIONS

Phosphate Buffered Saline (Cat. No. P-3813, Sigma-Aldrich Chemical Co., St. Louis, MO)
1 Phosphate Buffered Saline (PBS) packet
1 Liter distilled, deionized Water (ddH_2O)

Trypsin (Cat. No. T-7409, Sigma-Aldrich)
Store trypsin powder in refrigerator.
0.1% Solution: 0.01 grams Trypsin
10 ml Phosphate Buffered Saline

Hydrogen Peroxide (30% Stock, Cat. No. H-1009, Sigma-Aldrich)
Store stock solution in refrigerator.
3% Solution: 1 ml 30 % Hydrogen Peroxide
9 ml ddH_2O

Goat Serum (Cat. No. G-9023, Sigma-Aldrich)
Freeze in 1 ml aliquots.
20% Solution: 2 ml Goat Serum
8 ml Phosphate Buffered Saline

Primary Antibody, Anti-α Smooth Muscle Actin (Cat. No. A-2547, Sigma-Aldrich)
Freeze in 25 µl aliquots.
1:400 concentration: 25 µl Primary antibody
10 ml Phosphate Buffered Saline

Mouse Serum (used as Negative Control) (Cat. No. M-5905, Sigma-Aldrich)
Freeze in 20 µl aliquots.
1:200 concentration: 20 µl Mouse Serum
10 ml Phosphate Buffered Saline

Secondary Antibody, Goat Anti-Mouse IgG (Cat. No. B-0529, Sigma-Aldrich)
Freeze in 33 µl aliquots.
1:300 concentration: 33 µl Secondary Antibody
10 ml Phosphate Buffered Saline

ExtrAvidin Peroxidase Reagent (Cat. No. E-2886, Sigma-Aldrich)
Store in 100 µl aliquots in the refrigerator - DO NOT FREEZE!
1:50 concentration: 200 µl ExtrAvidin Peroxidase
10 ml Phosphate Buffered Saline

AEC Staining Kit (Cat. No. AEC-101, Sigma-Aldrich)
Mix up 8 ml according to the package instructions.

Mayer's Hematoxylin Solution (Cat. No. MHS-16, Sigma-Aldrich)

Glycerol Gelatin (Cat. No. GG-1, Sigma-Aldrich)

PROCEDURE

1. Put slides in green dipping rack. Hang rack from the side of a 2 liter beaker with enough xylene to cover the slides. Add stir bar and stir gently for 1 hour.

2. While slides are deparaffinizing, remove antibodies from the freezer:

25 µl	Primary Antibody
33 µl	Secondary Antibody
20 µl	Mouse Serum
2 ml	Goat Serum

Also, remove trypsin from the refrigerator and allow to come to room temperature before opening to avoid adding moisture to the desiccated compound.

3. Mix up PBS in glass beaker with stir bar. Add 1 packet of PBS to 1 liter of distilled water. Stir for several minutes to mix (a total of 3L of PBS will be needed for this procedure).

4. Mix up trypsin with PBS. Fabricate bench-top incubators. Place Kim Wipes in bottom of large plastic trays. Wet with distilled water and cover. Bench-top incubators to be used for the remainder of the staining steps as noted.

5. After 1 hour of xylene, remove the slides and deparaffinize as follows:

100% EtOH	2 minutes
100% EtOH	2 minutes
95% EtOH	2 minutes
80% EtOH	2 minutes
70% EtOH	2 minutes
ddH_2O	2 minutes
PBS	2 minutes
PBS	2 minutes

6. Gently dry slides, but not sections with Kimwipes. Circle sections to be stained with PAP pen. Add trypsin solution to circled sections. Do not let sections dry out between steps!!!

7. Incubate in trypsin solution (0.1%) for 1 hour at room temperature. Tip trypsin off slides into waste container.

8. PBS wash twice, 2 minutes each. Change PBS after use

9. Dry slides but not sections.

10. Incubate in hydrogen peroxide (3%) for 10 minutes.

11. Repeat steps 8 & 9.

12. Incubate with goat serum (20%) for 10 minutes.

13. Tip off excess serum, do NOT wash slides.

14. Incubate with primary antibody or mouse serum (negative control) for 2 hours at room temperature.

15. Tip off excess antibody. Be careful not to contaminate your negative control with the primary antibody. To avoid contamination in the rinse bath, use a transfer pipette to gently rinse sections individually before washing.

16. Repeat steps 8 & 9.

17. Incubate with the secondary antibody for 1 hour at room temperature.

18. Repeat steps 8 & 9.

19. Incubate with ExtrAvidin Peroxidase for 20 minutes at room temperature.

20. Begin warming glycerol gelatin.

21. Repeat steps 8 & 9.

22. Rinse slides in dH_2O. While slides are in the dH_2O, mix up AEC according to instructions on the staining kit.

23. Dry slides and begin incubating in AEC solution. Begin timing after the first slide started. Watch how long it takes to dry the slides and apply the AEC solution. Try to keep that pace when you stop the development so that all slides stain similarly.

24. Incubate in AEC solution for 15 minutes.

25. Stop development by tipping AEC off slides into an appropriate waste container (AEC is a carcinogen!) and place the slides in a slide holder in dH_2O. Rinse in dH_2O x2, 2 minutes each. Check slides for development. If some slides are not developed enough, repeat the AEC step for 2-5 minutes as needed.

26. Place slides in Mayer's hematoxylin solution for 15 minutes.

27. Running water bath for 15 minutes to develop the hematoxylin.

28. Coverslip with the warmed glycerol gelatin. If the gelatin hardens too early, place slides on 40 degree surface (like water bath edge) or in 57° oven for a few minutes to re-melt the gelatin.

C.8

Image Capture Protocol

Adapted from Spilker 2000

SUPPLIES

100x Objective (Nikon)
Immersion Oil (Nikon Immersion Oil, MVI, Inc, Avon, MA)
70% Ethanol

PROCEDURE

1. Bring the 100x objective, immersion oil, 70% ethanol, a zip disk, and the sample slides to the Mechanical Behavior of Materials Laboratory (Prof. Gibson), rm. 8-102.

2. Open Snappy program on computer attached to the microscope. In the Setup page, select te following options:

Video Source: *Live camera*
Snap Type: *High quality*
Image Type: *Black and white*
New Image: *Current window*
Image Size: *640*480*
Video thru for TV: *Connected*

3. Put the sample slide on microscope stage and focus with eyepiece. Check the image on the TV display, because this is the image that will be taken using Snappy. If the image is blurry, adjust the microscope focus until it becomes clear.

4. Pick a sample on the slide with the smallest number of wrinkles and tears and is vertically or horizontally oriented on the slide (the orientation will help in the later steps, but is not absolutely necessary). Circle the sample with a water resistant marker on the back of the slide.

5. Use the function keys and the up and down arrow keys on the keyboard to adjust the quality of the TV image such as sharpness, brightness and contrast. If the image is too bright decrease the light intensity on the microscope.

6. Take a low magnification image of the whole nerve trunk (usually at 4x or 10 x objective) in order to determine the fascicle area of the chosen sample. If the nerve cable is much larger than the fascicle, choose the highest magnification that includes all fascicles. However, if the nerve cable area is not significantly larger than the fascicle area, incorporate the whole nerve cable in the image.

7. Click on "Snap" key in the Snappy program window to capture the image. The captured image is then shown on the computer screen. Double click on the image and the Snappy control panel will return. If the image quality is acceptable, click on "Save" in the Snappy program window.

8. Open Scion Image. Use the low magnification image taken in step 7 and the procedures in the Image Analysis protocol to determine the area of the fascicle. In some cases the boundary of the fascicle is readily visible from the image. For samples with more than one fascicle, each fascicle should be circled, and the sum total of all fascicles calculated.

9. Determine how many images are necessary to adequately sample the nerve (Table C.1).

Fascicle Area Range [mm^2]	Fascicle Area Range [μm^2]	Number of Images Necessary	Image Area Divided by Total Fascicle Area
$A < 0.25$	$A < 250{,}000$	3	$\geq 10\%$
$0.25 < A < 0.4167$	$250{,}000 < A < 416{,}700$	5	10% - 16%
$0.4167 < A < 0.75$	$416{,}700 < A < 750{,}000$	9	10% - 18%
$0.75 < A < 1.08$	$750{,}000 < A < 1{,}080{,}000$	13	10% - 14%
$1.08 < A < 1.417$	$1{,}080{,}000 < A < 1{,}417{,}000$	17	10% - 13%
$1.417 < A < 1.75$	$1{,}417{,}000 < A < 1{,}750{,}000$	21	10% - 12%
$A > 1.75$	$A > 1{,}750{,}000$	21	<10%

Table C.1 Number of images necessary to describe nerve trunks of different cross-sectional area. Capturing the appropriate number of images results in sampling of at least 10% of the total tissue area, except when the area is larger than 1.75 mm^2. If tissue filled the entire inside diameter of the implant tubes, the area would be 1.77 mm^2; therefore, in the majority of cases sampling is greater than 10%.

10. Place a drop of immersion oil on the slide above the selected section, then move the focus in and out a little so that the oil is completely spread between the lens and the sample. Position the sample so that the long axis of the nerve is along the Y-axis.

11. Divide the nerve into four quadrants (see Figure C.1). Count the number of full-screen images from the top-center of the nerve trunk to the bottom-center of the trunk (**Y-Length**). Count the number of full-screen images from the left-center of the nerve trunk to the right-center (**X-Length**).

12. Begin imaging the cross-section using the chart in Figure C.1. as a guide. Begin with image 5, the geometric center of the image. Capture all images from Quadrant 1, and then Quadrant 2, etc. Use the values of **X-Length** and **Y-Length** calculated in Step 11 to locate the position for each image. For example, Image 5 is ½*(**Y-Length**) down from the top-center or ½*(**X-Length**) to the right of the left-center of the nerve trunk; Image 11 is 1/4*(**Y-Length**) down from the top-center and 1/4 *(**X-Length**) to the left.

13. Capture the appropriate number of images. Refer to Table C.2. to determine images to be taken and Figure C.1. to determine the location of images.

Number of Images to be Taken	Image Location
1	5
3	5, 11, 41
5	5, 11, 21, 31, 41
9	5, 11, 12, 21, 22, 31, 32, 41, 42
13	5, 11, 12, 13, 21, 22, 23, 31, 32, 33, 41, 42, 43
17	5, 11, 12, 13, 14, 21, 22, 23, 24, 31, 32, 33, 34, 41, 42, 43, 44
21	5, 11, 12, 13, 14, 15, 21, 22, 23, 24, 25, 31, 32, 33, 34, 35, 41, 42, 43, 44, 45

Table C.2. Images to be taken for each combination of number of required images.

14. When more than one fascicle is present in the nerve, divide the quadrants between the fascicles in proportion to the area of each fascicle. Redistribute the image capturing to reflect the fasciclular size and orientation.

15. Clean the emergent oil on the 100x objective and the sample slide using 70% ethanol. Return the objective and the emergent oil to 3-333.

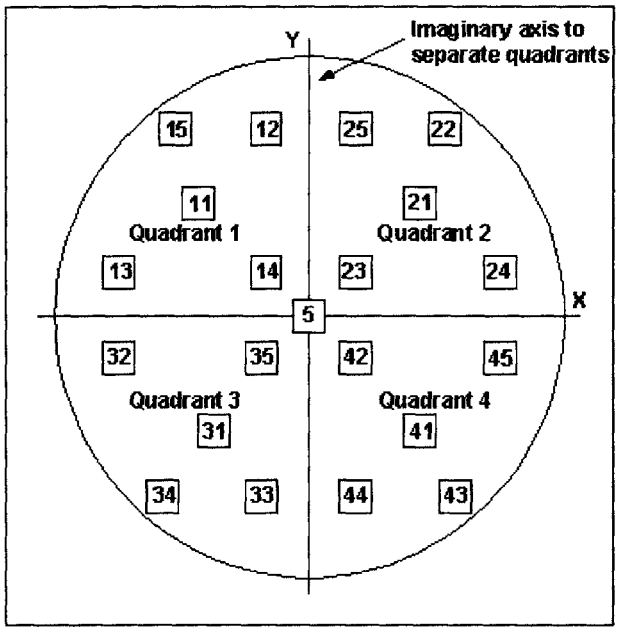

Figure C.1. Schematic showing the location of images around the nerve section

C.9

Image Analysis Protocol

PROCEDURE

1. Open Scion Image.

2. Open image file.

3. Go to the *Analyze* menu and select *Set Scale*. Select the appropriate unit of measure for the magnification of the image (*i.e.,* millimeters for low magnification images and micrometers for high magnification images). Use Table C.3. to fill in the *Known Distance* and the *Pixels* entries. Table C.3. is calibrated for the microscope assembly in the Mechanical Behavior of Materials laboratory (Prof. Gibson) in rm. 8-102, with images captured using Snappy.

Magnification Power	Known Distance	Pixels
4x	1 mm	325.4302041
10x	1 mm	838.305
40x	1 μm	2.52787
100x	1 μm	8.3842

Table C.3. Calibration values to set the scale for the appropriate magnifications on Scion Image. The magnification power refers to the objective that was used on the microscope the in Gibson Lab, Rm. 8-102 (Nikon E600 Microscope, Nikon, Japan).

4. Use *Smooth* and/or *Sharpen* from the *Enhance* menu to improve the quality of the image if needed. If you do not like the effect of these, choose *Undo* from the *Edit* menu before doing anything else.

5. From the *Enhance* menu, choose *Arithmetic, Subtract*. Subtract 3.

6. From the *Options* menu, select *Density Slice*. Threshold all the way to black so that no red is showing in the image.

7. Select the pencil from the toolbar. Move the cursor over the red portion of the color scale and choose red as the color. (The paintbrush will appear red when the appropriate color has been selected).

8. Circle the axons with the pencil on the OUTSIDE perimeter of the myelin sheath.

9. When all axons have been circled, go to the *Analyze* menu and select *Options*. Choose *Area, Perimeter/Length, Include Interior Holes*, and *Headings*. Set the number of significant digits

after the decimal point to 5.

10. Choose SAVE AS from the *File* menu and save the image as an edited file.

11. In the *Analyze* menu choose *Analyze Particles*. Enter the following:

Minimum particle size:	5 pixels
Maximum particle size	30000 pixels
Ignore particles touching edge	
Include Interior Holes	
Reset Measurement Counter	

12. Each axon will become darkened and numbered as it is counted. Make sure that all axons are filled in. If an axon is not darkened, part of the perimeter is not complete, therefore, it has been measured inappropriately. Fix and repeat step 11.

13. Choose *Show Results* from the *Analyze* menu. Copy the results (keystroke: Control-C) and paste them directly into Excel for analysis (keystroke: Control-V).

14. Close the image. Do not save the changes to your edited file.

C.10

Nerve Data Analysis Protocol

Adapted from Chamberlain 1998

The following is a stepwise procedure for analyzing the data obtained via image analysis. The protocol for obtaining images and the basic image analysis technique was outlined in section C.7. This section details how the numerical values were calculated from the raw data.

1. Measure the tissue area (A_{tissue}) and capture the appropriate number of images as described in section A.9.

2. Use image analysis program (NIH Image) to count the number of myelinated axons per image and measure the diameters. For each axon, the program will determine the area of the axon and the perimeter. Paste the raw data for all of the axons into a Microsoft Excel spreadsheet (as described in section A.9).

3. Calculate the diameter of each myelinated fiber using the following formula:

$$D = \frac{P}{\pi}$$

where D is the fiber diameter and P is the perimeter.

4. Calculate a diameter histogram for the axons of each image using Microsoft Excel. Highlight the column containing the fiber diameters. Select *Data Analysis* from the *Tools* menu. Select *Histogram* from the list of data analysis tools. Enter the *Input Range, Bin Range, and Output Range*. The *Bin Range* should be a separate column from the data and should contain integers from 1-12. Excel will output the number of axons in each diameter bin in the *Output Range* location.

5. Repeat steps 2 through 4 for all images captured for the nerve (from 3 - 21 images).

6. Once all images have been analyzed, calculate the myelinated axon density using the following formula:

$$AxonDensity = \frac{\sum_{i=1}^{N} (\#axons)_i}{N * Area_{Image}}$$

where N is the total number of images, $(\#axons)_i$ is the number of axons in image i, and $Area_{image}$ is the area of each digitized image. When images are captured according to the protocol

in section A.9, the $Area_{image} = 8.334 \times 10^{-3}$ mm^2.

7. Calculate the total number of myelinated axons per nerve using the following formula:

$$\frac{Axons}{Nerve} = AxonDensity * A_{Tissue}$$

where *AxonDensity* is as calculated in step 6 and A_{tissue} is the total tissue area measured in step 1.

8. Determine the percentage of axons in each of the 12 size bins using the following formula for each bin:

$$Perventage_x = \frac{\sum_{i=1}^{N} (\#axons_x)_i}{\frac{Axons}{Nerve}}$$

where $(\#axons_X)_i$ is the number of axons in size bin X for image i, N is the total number of images, and *Axons/Nerve* is as calculated in step 7.

9. Calculate the total number of large diameter myelinated fibers (D ≥ 6 μm) using the following formula:

$$\frac{LgAxons}{Nerve} = \left(\sum_{X=6}^{12+} Percentage_X \right) * \frac{Axons}{Nerve}$$

where $Percentage_X$ is as calculated in step 8, and *Axons/Nerve* is as calculated in step 7.

10. To calculate an diameter distribution, multiply each $Percentage_X$ by the *Axons/Nerve* to obtain the values for each bin.

Literature Cited

Aebischer P., Guenard V., Winn S.R., Valentini R.F., Galletti P.M., (1988). Blind-ended semipermeable guidance channels support peripheral nerve regeneration in the absence of a distal stump nerve. *Brain Res.*, 454:179-187.

Aidley D.J., (1971). The Physiology of Excitable Cells. Cambridge, U.K.: Cambridge University Press.

Aitken J.T., Sharman M., Young J.Z., (1947). Maturation of regenerating nerve fibres with various peripheral connexions. *J. Anat.* 81:1-22.

Aitken J.T., (1949). The effects of peripheral connexions on the maturation of regenerating nerve fibres. *J. Anat.* 83:32-43.

Aldini N.N., Perego G., Cella G.D., Martarello M.C., Fini M., Rocca M., Giardano R., (1996). Effectiveness of a bioabsorbable conduit in the repair of peripheral nerves. *Biomaterials.* 17:959-962.

Arbuthnott R., Boyd A., Kalu K.U., (1980). Ultrastructural dimensions of myelinated peripheral nerve fibers in the cat and their relation to conduction velocity. *J. Physiol. (Lond).* 308:125-157.

Archibald S.J, Krarup C., Shefner J., Li S.-T., Madison R.D., (1991). A collagen-based nerve guide conduit for peripheral nerve repair: An electrophysiological study of nerve regneration in rodents and nonhuman primates. *J. Comp. Neurol.* 306:685-696.

Archibald S.J., Shefner J., Krarup C., Madison R.D., (1995). Monkey median nerve repaired by nerve graft or collagen nerve guide tube. *J. Neurosci.* 15:4109-4123.

Bailey S.B., Eichler M.E., Villadiego A., Rich K.M., (1993). The influence of fibronectin and laminin during Schwann cell migration and peripheral nerve regeneration through silicon chambers. *J. Neurocytol.* 22:176-184.

Billingham R.E., Medawar P.B., (1951). The technique of free skin grafting in mammals. *J. Exp. Biol.* 28:385-394.

Billingham R.E., Medawar P.B., (1955). Contracture and intussusceptive growth in the healing of expensive wounds in mammalian skin. *J. Anat.* 89:114-123.

Bradley J.L., Abernathy D.A., King R.H.M., Muddle J.R., Thomas P.K., (1998). Neural architecture in transected rabbit sciatic nerve after prolonged nonreinnervation. *J. Anat.* 192:529-538.

Brau R.R., (2002). Mechanisms of Peripheral Nerve Regeneration and Neuroma Formation. M. Eng. thesis, Massachusetts Institute of Technology, Cambridge, MA.

Brushart T.M.E., (1988). Preferential reinnervation of motor nerves by regeneration. *Plast. Reconstr. Surg.* 92:927-940.

Bryan D.J., Miller R.A., Costas P.D., Wang K.-K., Seckel B.R., (1993). Immunohistochemistry os skeletal muscle basal lamina grafts in nerve regeneration. *Plast. Reconstr. Surg.* 92:927-940.

Burke J.F., Yannas I.V., Quincy W.C., Bondoc C.C., Jung W.K., (1981). Successful use of a physiologically acceptable artificial skin in the treatment of extensive burn injury. *Ann. Surg.* 194:413-428.

Buti M., Verdu E., Labrador R.O., Vilches J.J., Fores J., Navarro X., (1996). Influence of physical parameters of nerve chambers on peripheral nerve regeneration and reinnervation. *Exp Neurol.* 137(1):26-33.

Carr M.M., Best T.J., Mackinnon S.E., Evans P.J., (1992). Strain differences in autotomy in rats undergoing sciatic nerve transection or repair. *Ann. Plast. Surg.* 28:538-544.

Chamberlain L.J., (1998a). Influence of implant parameters on the mechanisms of peripheral nerve regeneration. Ph.D. thesis, Massachusetts Institute of Technology, Cambridge, MA.

Chamberlain L.J., Yannas I.V., Hsu H.P., Strichartz G., Spector M., (1998b). Collagen-GAG substrate enhances the quality of nerve regeneration through collagen tubes up to level of autograft. *Exper. Neurol.*, 154:315-329.

Chamberlain, L.J., Yannas, I.V., (1998c). Preparation of collagen-glycosaminoglycan copolymers for tissue regeneration. In Methods in Molecular Medicine, Vol. XX: Tissue Engineering Methods and Protocols, Chapter 1. (J.R. Morton and M.L. Yarmush, Eds.), pp. 3-17. Towona, NJ: Humana Press.

Chamberlain L.J., Yannas I.V., Hsu H.-P., Spector M., (2000a). Connective tissue response to tubular implants for peripheral nerve regeneration: The role of myofibroblasts. *J. Comp. Neuro.* 417:415-430.

Chamberlain L.J., Yannas I.V., Hsu H.-P., Strichartz G.R., Spector M., (2000b). Near terminus axonal structure and function following rat sciatic nerve regeneration through a collagen-GAG matrix in a 10-mm gap. *J. Neurosci. Res.* 60:666-677.

Chang A.S., Yannas I.V., Perutz S., Loree H., Sethi R.R., Krarup C., Norregaard, Zervas N.T., Silver J., (1990). Electrophysiological study of recovery of peripheral nerves regenerated by a collagen-glycosaminoglycan copolymer matrix. In Progress in Biomedical Polymers (C.G. Gebelin and R.L. Dunn, Eds.), pp.107-119. New York: Plenum Press.

Chang A.S., Yannas I.V., (1992). Peripheral Nerve Regeneration. In Encyclopedia of Neuroscience (B. Smith and G. Adelman, Eds.), pp. 125-126. Boston: Birkhauser.

Compton C.C., Butler C.E., Yannas I.V., Warland G., Orgill D.P., (1998). Organized skin structure is regenerated in vivo from collagen-GAG matrices seeded with autologous keratinocytes. *J. Invest. Dermatol.* 110:908-916.

Cordeiro M.F., Occleston P.T., Khaw P.T., (1997). New concepts: manipulation of the wound-healing response. *Dev. Ophthalmol.* 28:242-260.

Dellon A.L., Mackinnon S.E., (1988). An alternative to the classical nerve graft for the management of the short nerve gap. *Plast Reconstr Surg.* 82:849-56.

den Dunnen W.F.A., Schakenraad J.M., Zondervan G.J., Pennings A.J., van der Lei B., Robinson P.H., (1993a). A new PLLA/PCL copolymer for nerve regeneration. *J. Mater. Sci. Mater. Med.* 4:521-525.

den Dunnen W.F.A., van der Lei B., Schakenraad J.M., Blaauw E.H., Stokroos I., Pennings A.J., Robinson P.H., (1993b). Long-term evaluation of nerve regeneration in a biodegradable nerve guide. *Microsurgery.* 14:508-515:582-587.

den Dunnen W.F.A., Stokroos I., Blaauw E.H., Holwerda A., Pennings A.J., Robinson P.H., Schakenraad J.M., (1996). Light microscopic and electron-microscopic evaluation of short term nerve regeneration using a biodegradable poly(DL-lactide-$\in$-caprolacton) nerve guide. *J. Biomed. Mater. Res.*, 31:105-115.

Ducker T.B., Hayes G.J., (1968). Experimental improvements in the use of silastic cuff for peripheral nerve repair. *J. Neurosurg.* 28:582-587.

Erlanger J., Gasser H.S., (1937). Electrical signs of nervous activity. Philadelphia: University of Pennsylvania Press.

Fawcett J.W., Keynes R.J., (1986). Muscle basal lamina: a new graft material for peripheral nerve repair. *J. Neurosurg.* 65:354-363.

Ferdman A.G., Yannas I.V., (1993). Scattering of light from histologic section: A new method for the analysis of connective tissue. *J. Invest. Dermatol.* 100:710-716.

Fields R.D., Ellisman M.H., (1986). Axons regenerated through silicone tube splices. I. Conduction properties. *Exp. Neurol.* 92:48-6

Fields R.D.,LeBeau J.M., Longo F.M., Ellisman M.H., (1989). Nerve regeneration through artificial tubular implants. *Prog. Neurobiol.* 33:87-134.

Freyman T.M. (2001). Development of an *in vitro* model of contraction by fibroblasts. Ph.D. thesis, Massachusetts Institute of Technology, Cambridge, MA.

Fu S.Y., Gordon T., (1997). The cellular and molecular basis of peripheral nerve regeneration. *Mol. Neurobiol.* 14:67-116.

Geggel H.S., Friend J., Throft R.A., (1984). Conjunctival epithelial wound healing. *Invest. Ophthalmol. Invest. Sci.* 25:860-863.

Geren B.B., (1954). The formation from the Schwann cell surface of myelin in the peripheral nerves of chick embryos. *Exp. Cell Res.* 7:558.

Glasby M.A., Gschmeissner S.E., Huang C.L.-H., de Souza B.A. (1986). Degenerated muscle grafts used for peripheral nerve repair in primates. *J. Hand Surg.* 11-B:347-351.

Guenard V., Kleitman N., Morrissey T.K., Bunge R.P., Aebischer P., (1992). Syngeneic Schwann cells derived from adult nerves seeded in semipermeable guidance channels enhance peripheral nerve regeneration. *J. Neurosci.* 12:3310-3320.

Gulati A.K., (!988). Evaluation of acellular and cellular nerve grafts in repair of rat peripheral nerve. *J. Neurosurg.* 68:117-123.

Haber R.M., Hanna W., Ramsay C.A., Boxall L.B., (1985). Cicatricial junctional epidermolysis bullosa. *J. Am. Acad. Dermatol.* 12:836-844.

Haftek J., Thomas P.K., (1968). Electron-microscope observations on the effects of localized crush injuries on the connective tissues of peripheral nerve. *J. Anat.* 103:233-243

Heimback D., Luterman A., Burke J., Cram A., Herdon D., Hunt J., Jordan M., McManus W., Solem L., Warden G., Zawacki B., (1988). Artificial dermis for major burns: A multi-center randomized clinical trial. *Ann. Surg.* 208:313-320.

Hodgkin A.L., Huxley A.F., (1952). A quantitative description of membrane current and its application to conduction and excitation in nerve. *J. Physiol.* 117:500-544.

Hodgkin A.L., (1958). Ionic movements and electrical activity in giant nerve fibres. *Proc. R. Soc. Lond.* 148:1-37.

Hsu W.C., Spilker M.H., Yannas I.V., Rubin P.A., (2000). Inhibition of conjunctival scarring and contraction by a porous collagen-glycosaminoglycan implant, *Invest. Ophthalmol. Vis. Sci.*, 41:2404-11.

Huang C., Yannas I.V., (1977). Mechanochemical studies of enzymatic degradation of insoluble collagen fibers. *J. Biomed. Mater. Res.* 11(1):137-154.

Hunt C.C., (1954). Relation of function to diameter in afferent fibers of muscle nerves. *J. Gen. Physiol.* 38:117-131.

Hursh J.B., (1939). Conduction velocity and diameter of nerve fibres. *Am. J. Physiol.* 127:131-139.

Hynes R.O., (1990). Fibronectin. New York: Springer-Verlag.

Hynes, R.O., (1992). Integrins: Versatility, modulation and signaling in cell adhesion. *Cell*, 69:11-25.

Ikeda K., Oda Y., Tomita K., Nomura S., Nakanishi I., (1989). Isolated Schwann cells can synthesize the basement membrane in vitro. *J. Electron. Microsc. (Tokyo)* 38:230-234.

Janecka I.P., Sekhar L.N., Sen C.N., (1993). Facial nerve management in cranial base surgery. *Laryngoscope.* 103:291-298.

Jenq C.-B., Coggeshall R.E., (1984). Effects of sciatic nerve regeneration on axonal popoulations in tributary nerves. *Brain Res.* 295:91-100.

Jenq C.B., Coggeshall R.E., (1985). Numbers of regenerated axons in tributary nerves following neonatal sciatic nerve crush in rat, *Neurosci. Lett.*, 61:43-8.

Jenq C.B., Jenq L.L., Coggeshall R.E., (1987). Nerve regeneration changes with filters of different pore size. *Exp. Neurol.* 97:662-671.

Kandel E.R., Schwartz J.H., Jessell T.M., (1991). Principles of Neural Science, Third Edition. Norwalk, CT: Appleton & Lange.

Keynes R.D., (1951). The ionic movements during nervous activity. *J. Physiol.* 114:119.

Kim D.H., Connolly S.E., Kline D.G., Voorhies R.M., Smith A., Powell M., Yoes T., Daniloff J.K., (1994). Labeled Schwann cell transplants versus sural nerve grafts in nerve repair. *J. Neurosurg.* 80:254-260.

Korompilias A.V., Chen L.E., Seaber A., V., Urbaniak J.R., (1999). Interleukin-1 beta promotes functional recovery of crushed peripheral nerve. *J. Orthop. Res.* 17:714-719.

Le Beau J.M., Ellisman M.H., Powell H.C., (1988). Ultrastructural and morphometric analysis of long-term peripheral nerve regeneration through silicone tubes. *J. Neurocytol.* 17:161-172.

Lee C.R., Grodzinsky A.J., Spector, M., (2001). The effects of crosslinking of collagen-glycosaminoglycan scaffolds on compressive stiffness, chondrocyte-mediated contraction, proliferation, and biosynthesis. *Biomaterials.* 22:3145-3154.

Lehv M., Fitzgerald P.J., (1968). Pancreatic acinar cell regeneration IV: Regeneration after surgical resection. *Am. J. Pathol.* 53:513-535.

Li S.-T., Archibald S.J., Krarup C., Madison S.D., (1990). Semipermeable collagen nerve conduits for peripheral nerve regeneration. *Polym. Mater. Sci. Eng.* 62:575-582.

Li S.-T., Archibald S.J., Krarup C., Madison R.D., (1992). Peripheral nerve repair with collagen conduits. *Clin. Materials.* 9:195-200.

Lisney S.J.W., (1989). Regeneration of unmyelinated axons after injury of mammalian peripheral nerve. *Q. J. Exp. Phys.* 74:757-784.

Lundborg G., Dahlin L.B., Danielsen N., Gelberman R.H., Longo F.M., Powell H.C., Varon S., (1982). Nerve regeneration in silicone chambers: Influence of gap length and of distal stump components. *Exp. Neurol.* 76:361-375.

Lundborg G., Dahlin L.B., Danielsen N., (1991). Ulnar nerve repair by the silicon chamber technique. *Scand. J. Plast. Reconstr. Hand Surg.* 25:79-82.

Madison R.D., da Silva C.F., Dikkes P., Chiu T.-H., Sifman R.L., (1985). Increased rate of peripheral nerve regeneration using bioresorbable nerve guides and a laminin-containing gel. *Exp. Neurol.* 88:762-777.

Madison R.D., da Sila C.F., Dikkes P., (1988). Entubulation repair with protein additives increases the maximum nerve gap distance successfully bridged with tubular prostheses. *Brain Res.* 447:325-334.

Madison R.D., Archibald S.J., Krarup C., (1992). Peripheral nerve injury. In Wound Healing: Biochemical and Clinical Aspects (I.K. Cohen, R.F. Diegelmann, and W.J. Lindblad, Eds.), pp. 450-487. Philadelphia: W.B. Saunders.

Madison R.D., Archibald S.J., Brushart T.M., (1996). Reinnervation accuracy of the rat femoral nerve by motor and sensory neurons. *J. Neurosci.* 16:5698-5703.

Mackinnon S.E., Dellon A.L., (1988). Surgery of the peripheral nerve. New York: Thieme Medical Publishers.

Martinez-Hernandez A., (1988). Repair, regeneration, and fibrosis. In Pathology (E. Rubin, J.L. Farber, Eds.). Philadelphia: J.B. Lippincott.

Morrissey T.K., Kleitman N., Bunge R.P., (1991). Isolation and functional characterization of schwann cells derived from adult peripheral nerve. *J. Neurosci.* 11(8):2433-2442.

Murphy G.F., Orgill D.P., Yannas I.V., (1990). Partial dermal regeneration induced by biodegradable collagen-glycosaminoglycan grafts. *Lab. Invest.* 63:305-313.

Navarro X., Verdu E., Wendelschafer-Crabb G., Kennedy W.R., (1995). Innervation of cutaneous structures in the mouse hind paw: A confocal microscopy immunohistochemical study. *J. Neurosci. Res.* 41:111-120.

Noback C.R., Husby J., Girardo J.M., Andrew C., Bassett L., and Campbell J.B., (1958). Neural regeneration across long gaps in mammalian peripheral nerves: early morphological findings. *Anat. Rec.* 131:633-647.

Ohbayashi K., Inous H.K., Awaya A. Kobayashi S., Kohga H., Nakamura M., Ohye C., (1996). Peripheral nerve regeneration in a silicone tube: effect of collagen sponge prosthesis, laminin, and pyrimidine compound administration. *Neurol. Med. Chir.* 36:428-433.

Oliver J., (1953). Correlations of structure and function and mechanisms of recovery in acute tubular necrosis. *Am. J. Med.* 15:535-557.

Orgill, D.P. et al., (1996). Behavior of collagen-GAG matrices as dermal replacements in rodent and porcine models. *Wounds*, 8:151-157.

Orgill D.P. and Yannas I.V., (1998). Design of an artificial skin. IV. Use of island graft to isolate organ regeneration from scar synthesis and other processes leading to skin wound closure. *J. Biomed. Mater. Res.*, 39(4):531-535.

Robertson J.D., (1960). The molecular structure and contact relationships of cell membranes. *Prog. Biophys.* 10:343.

Robinson P.H., van der Lei B., Hoppen H.J., Leenslag J.W., Pennings A.J., Nieuwenhuis P., (1991). Nerve regeneration through a two-ply biodegradable nerve guide in the rat and the influence of ACTH4-9 nerve growth factor. *Microsurgery.* 12:412-419.

Rodriguez F., (1996). Principles of Polymer Systems. Washington, D.C.: Taylor & Francis.

Rosen J.M., Hentz V.R., Kaplan E.N., (1983). Fascicular tubulization: a cellular approach to peripheral nerve repair. *Ann. Plast. Surg.* 11:397-411.

Rosen J.M., Padilla J.A., Nguyen K.D., Padilla M.A., Sabelman E.E., Pham H.N., (1990). Artificial nerve graft using collagen as an extracellular matrix for nerve repair composed with sutured autograft in a rat model. *Ann. Plast. Surg.* 25:375-387.

Rushton W.A.H., (1951). A theory of the effects of fibre size in medullated nerve. *J. Physiol.* 115:101-122.

Sanders F.K., Young J.Z., (1944). The role of the peripheral stump in the control of fibre diameter in regenerating nerves. *J. Physiol.* 103:119-136.

Sanders F.K., Young J.Z., (1946). The influence of peripheral connexion on the diameter of regenerating nerve fibres. *J. Exp. Biol.* 22:203-212.

Spilker M.H., (2000). Peripheral nerve regeneration through tubular devices: a comparison of assays of device effectiveness. Ph.D. thesis, Massachusetts Institute of Technology, Cambridge, MA.

Stemerman M.B., Spaet T.H., Pitlick F., Cintron J., Lejnieks I., Tiell M.L., (1977). Intimal healing. The patterns of reendothelialization and intimal thickening. *Am. J. Pathol.* 87:125-142.

Stenn K.S., Malhotra R., (1992). Epithelialization. In Wound Healing (I.K. Cohen, R.F. Diegelmann, and W.J. Lindblad, Eds.) Philadelphia: W.B. Saunders.

Stern R., McPherson M., Longaker M.T., (1990). Histologic study of artificial skin used in the treatment of full-thickness thermal injury. *J. Burn Care Rehab.* 11:7-13.

Strichartz G.S., Covino B.G., (1990). Local Anesthetics. In Anesthesia (R.D. Miller, Ed.), pp. 437. New York: Churchill Livingstone.

Sunderland S., (1990). The anatomy and physiology of nerve injury. *Muscle Nerve.* 13:771-784.

Thomas P.K., Olsson Y., (1975). Microscopic anatomy and function of the connective tissue components of peripheral nerve. In Peripheral Neuropathy (P.J. Dyck, P.K. Thomas, and E.H. Lambert, Eds.), pp. 168-189. Philadelphia: W.B. Saunders.

Tountas C.P., Bergman R.A., Lewis T.W., Stone H.E., Pyrek J.D., Mendenhall H.V., (1993). A comparison of peripheral nerve repair using an absorbable tubulization device and conventional suture in primates. *J. Appl. Biomater.* 4:261-268.

Vracko R., (1972). Significance of basal lamina for regeneration of injured lung. *Virchows Arch. (Pathol. Anat.)* 355:264-274.

Vracko R., (1974). Basal lamina scaffold: Anatomy and significance for maintenance of orderly tissue structure. *Am. J. Pathol.* 77:313-346.

Walker J.L., Evans J.M., Resig P., Guarnieri S., Meade P., Sisken B.S., (1994). Enhancement of functional recovery following a crush lesion to the rat sciatic nerve by exposure to pulsed electromagnetic fields. *Exp. Neurol.* 125:302-305.

Wall P.D., Devor M., Inbal R., Scadding J.W., Schonfeld D., Seltzer Z., Tomkiewicz M.M., (1979). Autotomy following peripheral nerve lesions: Experimental anaesthesia dolorosa. *Pain.* 7:103-113.

Weiss P., Edds M.V., Cavanaugh M., (1945). The effect of terminal connections on the caliber of nerve fibers. *Anat. Rec.* 92:215-233.

Whitworth I.H., Brown R.A., Dore C., Green C.J., Terenghi G., (1995). Orientated mats of fibronectin as a conduit material for use in peripheral nerve repair. *J. Hand Surg.* 20B:429-436.

Williams L.R., Longo F.M., Powell H.C., Lundborg G., Varon S., (1983). Spatial-temporal progress of peripheral nerve regeneration within a silicone chamber: parameters for a bioassay. *J. Comp. Neurol.* 218:460-470.

Williams L.R., Varon S., (1985). Modification of fibrin matrix formation in situ enhances nerve regeneration in silicone chambers. *J. Comp. Neurol.* 231:209-220.

Williams L.R., Azzam N.A., Zalewski A.A., Azzam R.N., (1993). Regenerating axons are not required to induce the formation of a Schwann cell cable in a silicone chamber. *Exp. Neurol.* 120:49-59.

Yannas I.V., Tobolsky A.V., (1967). Cross-linking of gelatine by dehydration. *Nature.* 215(100):509-510.

Yannas I.V., (1972). Collagen and gelatin in the solid state. *J. Macromol. Sci. Revs. Macromol. Chem.* C7:49-104.

Yannas I.V, Burke J.F., Huang C., Gordon P.L., (1975). Correlation of in vivo collagen degradation rate with in vitro measurements. *J. Biomed. Mater. Res.* 6:623-625.

Yannas, I.V., et al., (1980). Design of an artificial skin. II. Control of chemical composition. *J. Biomed. Mater. Res.*, 14:107-131.

Yannas I.V., Burke J.F., Warpehoski M., Stasikelis P., Skrabut E.M., Orgill D.P., Giard D.J., (1981). Prompt, long-term functional replacement of skin. *Trans. Am. Soc. Artif. Intern. Organs.* 27:19-22.

Yannas, I.V., Burke J.F., Orgill D.P., Skrabut E.M., (1982). Wound tissue can utilize a polymeric template to synthesize a functional extension of skin. *Science*, 215:174-176.

Yannas I.V., Orgill D.P., Silver J., Norregaard, T.V., Zervas N.T., Schoene W.C., (1987). Regeneration of sciatic nerve across 15 mm gap by use of a polymeric template. In Advances in Biomedical Polymers (C.G. Gebelin, Ed.), pp. 1-9. New York: Plenum Publishing Corporation.

Yannas I.V., Lee E., Orgill D.P., Skrabut E.M., Murphy G.F., (1989). Synthesis and characterization of a model extracellular matrix that induces partial regeneration of adult mammalian skin, *Proc. Natl. Acad. Sci. USA*, 86:933-937.

Yannas, I.V., (1998). Studies on the biological activity of the dermal regeneration template. *Wound Rep. Reg.*, 6:518-524.

Yannas I.V., (1995). Regeneration Templates. In The Biomedical Engineering Handbook (J.D. Bronsino, Ed.), pp. 1619-1635. CRC Press.

Yannas, I.V., (2000). Synthesis of organs: in vitro or in vivo? *Proc. Natl. Acad. Sci. USA*, 97:9354-9356.

Yannas, I.V., (2001). Tissue and Organ Regeneration in Adults. New York: Springer-Verlag.

Yoshii S., Ymamuro T., Ito S., Hayashi M., (1987). In vivo guidance of regenerating nerve by laminin-coated filaments. *Exp. Neurol.* 95:469-273.